NAVAL POSTGRADUATE SCHOOL

MONTEREY, CALIFORNIA

THESIS

MECHANICAL AND MICROSTRUCTURAL PROPERTIES OF AL-4008 PRODUCED BY ADDITIVE MANUFACTURING VIA LIQUID METAL PRINTING

by

William C. Kimberl V

June 2022

Thesis Advisor: Claudia C. Luhrs
Co-Advisor: Walter C. Smith

THIS PAGE INTENTIONALLY LEFT BLANK

REPORT DOCUMENTATION PAGE	*Form Approved OMB No. 0704-0188*

1. AGENCY USE ONLY *(Leave blank)*	**2. REPORT DATE** June 2022	**3. REPORT TYPE AND DATES COVERED** Master's thesis

4. TITLE AND SUBTITLE
MECHANICAL AND MICROSTRUCTURAL PROPERTIES OF AL-4008 PRODUCED BY ADDITIVE MANUFACTURING VIA LIQUID METAL PRINTING

5. FUNDING NUMBERS

6. AUTHOR(S) William C. Kimberl V

7. PERFORMING ORGANIZATION NAME(S) AND ADDRESS(ES)
Naval Postgraduate School
Monterey, CA 93943-5000

8. PERFORMING ORGANIZATION REPORT NUMBER

9. SPONSORING / MONITORING AGENCY NAME(S) AND ADDRESS(ES)
N/A

10. SPONSORING / MONITORING AGENCY REPORT NUMBER

11. SUPPLEMENTARY NOTES The views expressed in this thesis are those of the author and do not reflect the official policy or position of the Department of Defense or the U.S. Government.

12a. DISTRIBUTION / AVAILABILITY STATEMENT
Approved for public release. Distribution is unlimited.

12b. DISTRIBUTION CODE
A

13. ABSTRACT (maximum 200 words)

Additive manufacturing (AM) applications continue to gain traction as a viable and advantageous means of manufacturing compared to traditional manufacturing (TM) techniques. Liquid metal printing is an AM technique in which a metal filament is melted in a nozzle and delivered onto a heated bed, layer by layer, to build a part. This work studied the mechanical properties and microstructural features of liquid metal printed Al-4008 by performing tensile and microhardness tests, along with X-ray diffraction (XRD), optical microscopy (OM) and scanning electron microscopy (SEM) analysis. Mechanical properties of Al-4008 parts produced via liquid metal printing were compared to A356 cast aluminum parts following T6 heat treatment. Microhardness tests revealed that the hardness, tensile, and yield strength increase 2–3 times after the solution treatment and artificial aging. Print direction directly affects mechanical properties, specifically tensile strength (UTS) and yield strength.

14. SUBJECT TERMS
additive manufacturing, AM, 3D printing, Al-4008, liquid metal printing, A356, scanning electron microscopy, SEM, X-ray diffraction, XRD, optical microscopy, OM

15. NUMBER OF PAGES
113

16. PRICE CODE

17. SECURITY CLASSIFICATION OF REPORT	**18. SECURITY CLASSIFICATION OF THIS PAGE**	**19. SECURITY CLASSIFICATION OF ABSTRACT**	**20. LIMITATION OF ABSTRACT**
Unclassified	Unclassified	Unclassified	UU

NSN 7540-01-280-5500

Standard Form 298 (Rev. 2-89)
Prescribed by ANSI Std. 239-18

THIS PAGE INTENTIONALLY LEFT BLANK

Approved for public release. Distribution is unlimited.

MECHANICAL AND MICROSTRUCTURAL PROPERTIES OF AL-4008 PRODUCED BY ADDITIVE MANUFACTURING VIA LIQUID METAL PRINTING

William C. Kimberl, V
Lieutenant, United States Navy
BSME, Old Dominion University, 2016

Submitted in partial fulfillment of the
requirements for the degree of

MASTER OF SCIENCE IN MECHANICAL ENGINEERING

from the

NAVAL POSTGRADUATE SCHOOL
June 2022

Approved by: Claudia C. Luhrs
Advisor

Walter C. Smith
Co-Advisor

Garth V. Hobson
Chair, Department of Mechanical and Aerospace Engineering

THIS PAGE INTENTIONALLY LEFT BLANK

ABSTRACT

Additive manufacturing (AM) applications continue to gain traction as a viable and advantageous means of manufacturing compared to traditional manufacturing (TM) techniques. Liquid metal printing is an AM technique in which a metal filament is melted in a nozzle and delivered onto a heated bed, layer by layer, to build a part. This work studied the mechanical properties and microstructural features of liquid metal printed Al-4008 by performing tensile and microhardness tests, along with X-ray diffraction (XRD), optical microscopy (OM) and scanning electron microscopy (SEM) analysis. Mechanical properties of Al-4008 parts produced via liquid metal printing were compared to A356 cast aluminum parts following T6 heat treatment. Microhardness tests revealed that the hardness, tensile, and yield strength increase 2–3 times after the solution treatment and artificial aging. Print direction directly affects mechanical properties, specifically tensile strength (UTS) and yield strength.

THIS PAGE INTENTIONALLY LEFT BLANK

TABLE OF CONTENTS

LIST OF FIGURES

LIST OF TABLES

THIS PAGE INTENTIONALLY LEFT BLANK

LIST OF ACRONYMS AND ABBREVIATIONS

Al	aluminum
AM	additive manufacturing
AP	as printed
ASTM	American Standard for Testing and Materials
CAD	computer automated design
CNC	computer numerical control
CRADA	cooperative research and development agreement
DOD	Department of Defense
EDS	energy dispersive spectroscopy
HT	heat treated
HV	hardness according to Vickers
IAW	in accordance with
Mg	magnesium
QC	quality control
SB	sandblasted
SEM	scanning electron microscope
Si	silicon
TM	traditional manufacturing
XRD	X-ray diffraction

THIS PAGE INTENTIONALLY LEFT BLANK

ACKNOWLEDGMENTS

It takes a village…it is more than a cliché. This endeavor has encompassed more time than I could have imagined.

Renee, you are my rock and compass. I owe more to you than anyone else. Thank you for handling all of life's countless distractions throughout this process. Every duty requires unique challenges and adaptation. Your ability to empower our children and help them to navigate this world is nothing short of incredible. Emmalee, Colton, Bennett, and Liliana: you all give me more inspiration than I could ever explain. I hope you all pursue ALL your dreams and ambitions. Each of you will have such a great impact on this world.

Thank you Dr. Luhrs for teaching me so much along the way and encouraging my interests in material science. The dedication to your craft is inspirational. Thank you, Mr. John Mobley, for taking up so much of your time to machine tensile specimens, only for me to break them in mere minutes. Thank you, Dr. Chanman Park and Dr. Troy Ansell, for teaching me to use the equipment required for this research. Thank you, Dr. Emre Gunduz, for further expanding my interests and knowledge in 3D printing.

I greatly appreciate all the feedback, updates, and teamwork provided by Xerox® Elem™ Additive Solutions, especially Mrs. Miranda Moschel. Your teamwork greatly improved the analysis and understanding of the interworks of the ElemX™ printer.

THIS PAGE INTENTIONALLY LEFT BLANK

I. INTRODUCTION

A. MOTIVATION

Companies and corporations around the world seek to incorporate new technologies and implement new techniques into their business models to improve efficiency and produce better quality products for their clients. Like many of these corporations, the Department of Defense (DOD) is constantly seeking out the latest advancements in technology and evaluating if and how those products will be beneficial to the warfighter.

An area of technology the DOD has recognized as an opportunity of growth and adoption for DOD forces is additive manufacturing [1]. The Office of the Under Secretary of Defense for Research and Engineering released the Department of Defense Additive Manufacturing Strategy. In the strategy, the DOD's "Vision for the Use of Additive Manufacturing (AM)" highlighted that to AM was needed to arm a "more agile, adaptable and aligned defense supply base" to maintain an edge from adversarial threats [2]. It goes on to state that "AM will be a widely accepted manufacturing technology used across DOD and defense industrial base…Standards, specifications, and data sets will be available to rapidly qualify AM machines and materials and verify AM parts." In an effort to accomplish this outlined vision, the DOD will focus on integrating AM into its defense industries and expand proficiency in AM. Three emphasize points in the vision were to "learn, practice, and share knowledge" [2]. The research presented in this thesis focused on the learn, practice, and share knowledge goal outlined by the DOD AM Strategy.

In 2017, the Department of the Navy (DON) issued the DON AM Implementation Plan V2.0 which addressed five objectives, one of them being to "develop the capability to rapidly qualify and certify AM components" [3]. However, certification of a Metal AM process and a material is a repetitive process. The certification type will be dependent on the application of the component produced through the additive manufacturing process in question. The certification requirements will be defined by the application of the printed part [4]. Certification of the process and material are critical in ensuring confidence in the

additively manufactured part. Sharing learned information from new AM technology processes and materials helps to improve the overall certification process.

When a new technology emerges and is nearing the end of the product design cycle, it usually undergoes a series of beta testing. Beta testing is a type of test that is conducted by a customer-like user in a real-world environment to simply use the product. During this time the user will discover problems, if any, before the product is made available to the end users [5]. Generally, there is no outline requirements for beta testing, rather a continuous feedback loop of user interaction experiences and complications.

As part of a cooperative research and development agreement (CRADA), The Naval Postgraduate School (NPS) partnered with Xerox® Corporation to provided beta testing on the Xerox® ElemX™ Liquid Metal Printer.

As this research was integrated as part of the Beta Testing of the ElemX™ Liquid Metal Printer, thus, the printing and testing of tensile specimens was undertaken repeatedly throughout the study. As Xerox® received feedback, hardware and software updates were completed in an effort to improve print quality and material properties. The results represented in Chapter III for the as-printed tensile specimens was conducted in the earlier phases of this Beta Testing and prior to the completion of all updates and modifications. The testing and results presented in Chapter IV represent the mechanical properties and analysis after all updates were completed.

It is important to note that the information presented in this research is not an attempt to certify any AM process or material, but rather, it is provided for informational purposes only. The research in this thesis was developed within the framework of the CRADA between NPS and Xerox®. The focus of which was to identify mechanical properties such as ultimate tensile strength, yield strength, elongation percentage and hardness of the part printed with Al-4008 using the ElemX™ printer. This information was relayed to Xerox® in continuous feedback to implement software and hardware upgrades to improve print quality and material properties.

B. ABOUT THE ELEMX™ LIQUID METAL PRINTER

The Xerox® ElemX™ is an on-demand Liquid Metal Deposition Printer (LMP) that uses a metal wire medium to produce parts up to 300mm x300mm x120mm (11.8in x 11.8in x 4.7in) [6]. The original technology was created by Vader Systems and was later acquired by Xerox® Corporation [7]. Figure 1 is a picture of the Xerox® ElemX™ 3D printer used for this research.

Figure 1. Xerox® ElemX™ Liquid Metal Printer

Like many automated AM technologies, the Liquid Metal Printing (LMP) additive manufacturing (AM) processes consist of first creating a model of the desired part using a Computer Aided Drawing (CAD) software. The CAD drawing is then saved in an STL file, a triangulated surface representation of a solid part. This .stl file is then processed through the Xerox® ElemX™ proprietary slicer software that generates a main program file (.mpf).

The .mpf, often referred to as a G-code is layer-by-layer directions for the tool path for each layer. In addition to the path of the printer head (Z-direction) and print bed (XY-direction), the printer also requires a recipe file for the specific print [8]. The recipe file is

a set of print parameters such as layer height, print speed, flowrate/extrusion rate, hot end (nozzle) temperature, bed temperature, etc. Collectively, this G-code and recipe file will be unique to each product being 3D printed. Figure 2 illustrates the concept to printed part process.

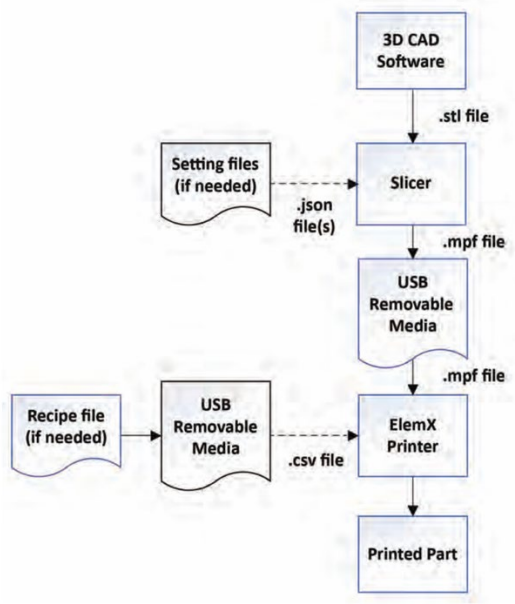

Figure 2. Drawing to Printed-Part Flow Chart. Source: [8].

a. Wire filament

A 1.575mm (0.062in) diameter Al-4008 wire filament is currently being used as the manufacturing material. Al-4008 is commonly found as commercially available welding wire in the same class of materials as Aerospace Material Specification 4181, Aluminum A356, and Alloy 4010. Al-4008 is typically used as a filler metal for gas tungsten arc weld (GTAW, also called TIG Welding) and gas metal arc welding (GMAW also called MIG Welding). Al-4008 is commonly used in sand casting and permanent mold castings. These castings are referred to as A356 cast aluminum and are widely used in the automotive industry due to its high strength applications [9]. Alloy Al 4008 is also typically more tightly controlled than Al 4010.

Al-4008 has a compositional base of Aluminum-Silicon-Magnesium which is alloyed with other metals as shown in Table 1 [10]. The addition of silicon improves the fluidity of aluminum. Also, silicon particles are much harder than aluminum and improve the wear resistance of the aluminum. The addition of magnesium in the alloy allows for the hardenability through precipitation of the Mg_2Si particles [11].

Table 1. Elemental Composition of AL-4008 and A356 Alloys. Source [10].

AL-4008 composition

Element	Al	Si	Mg	Ti	Fe	Cu	Mn	Zn	Other
wt%	Bal.	6.5-7.5	0.3-0.45	0.04-0.15	<=0.09	<=0.05	<=0.05	<=0.05	<=0.15

A356 composition

Element	Al	Si	Mg	Ti	Fe	Cu	Mn	Zn	Other
wt%	Bal.	6.5-7.5	0.25-0.45	<=0.2	<=0.2	<=0.2	<=0.1	<=0.1	<=0.15

The similarity of the composition of these metals allows for the assumption that an additively manufactured component from Al-4008 would be a viable substitute for a similar component manufactured from A356 cast aluminum. However, to consider this manufacturing process as an acceptable means of substitution, the mechanical properties from each manufacturing process would need to meet the same standards.

b. The Hot End

The hot end in additive manufacture process refers to the part or parts that make up the mechanism which heats the filament for extrusion. The hot end for the Xerox® ElemX™ printer consists of the heated reservoir and ejection chamber.

The wire filament is fed into a heated reservoir where the wire is heated to 825°C, melted and collected in a user prepared graphite nozzle within the ejection chamber. Figure 3 illustrates the hot end.

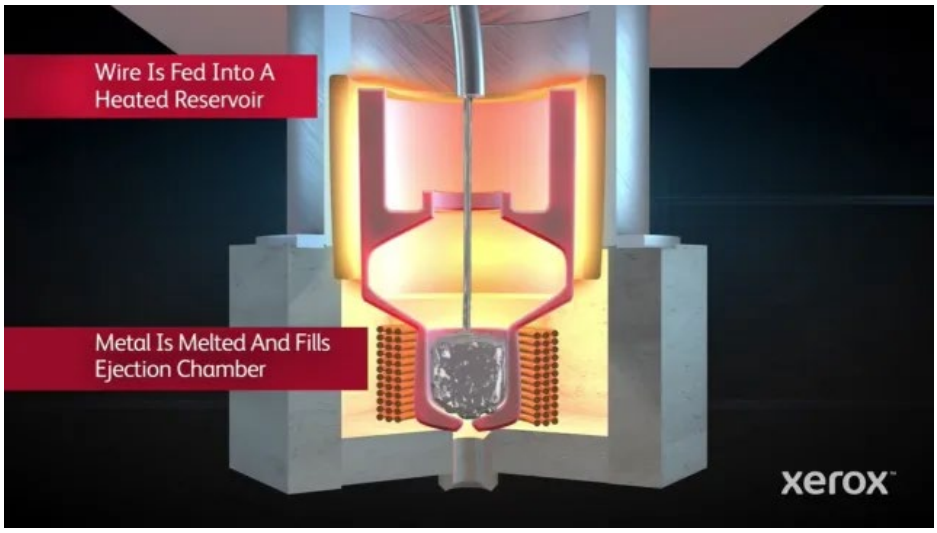

Figure 3. Illustration of ElemX^{TM} Heated Reservoir and nozzle. Source: [12].

The boron nitride upper pump connects to the graphite lower pump. The nozzle is part of the lower pump and is pre-conditioned with an argon plasma treatment wand by the user prior to printing [8]. Figure 4 illustrates the upper and lower pump components. The molten Al-4008 is protected with an Argon gas shield to prevent oxidation in the nozzle and during extrusion [13].

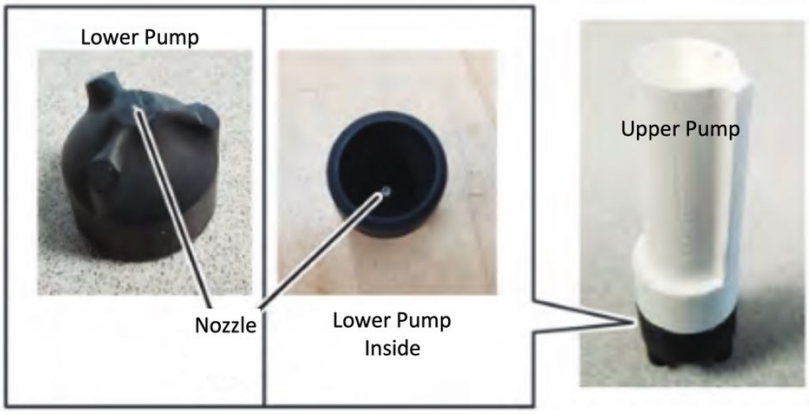

Figure 4. Upper and Lower Pump Assembly. Adapted from [8].

The 825°C nozzle temperature far exceeds the melting point of pure aluminum (660°C) and Al-4008 (up to 615°C) creating a low viscosity molten aluminum to aid in the extrusion process [10].

Pulse coil assembly consists of coils surrounding the nozzle which create perpendicular current density and Lorentz force vectors [14], [15]. These Lorentz forces create magnetohydrodynamic pressure gradients allowing for the modulation of discontinuous molten metal droplets to extrude from the nozzle at a controllable rate ranging from 100Hz to 1000Hz are generated.

The standard printing frequency of these droplets is 400Hz. Figure 5 illustrates the magnetic field created by the charged coils.

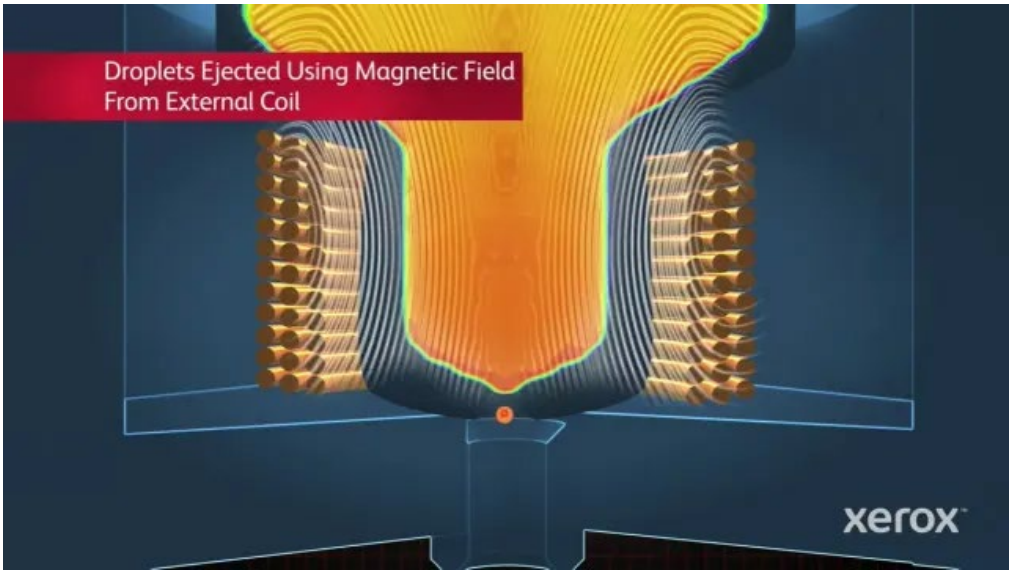

Figure 5. Illustration of Induced Magnetic Field Interaction with Metal Droplets. Source: [12].

The controlled liquid metal extrusion process ensures that independent metal droplets are precisely distributed. The height of the nozzle from the working surface is controlled by the hot end moving up and down along the z-axis. The printer uses two 3D laser line profile sensors to periodically scan the printed part to ensure better estimate that the correct amount of mass is being deposited. From this estimate, the nozzle distance from

the printing surface is optimized [8]. An illustration of the liquid metal droplet extrusion can be seen in Figure 6. It is important to note that the droplets are not an unbroken-continuous flow of the liquid aluminum, but rather individual droplets.

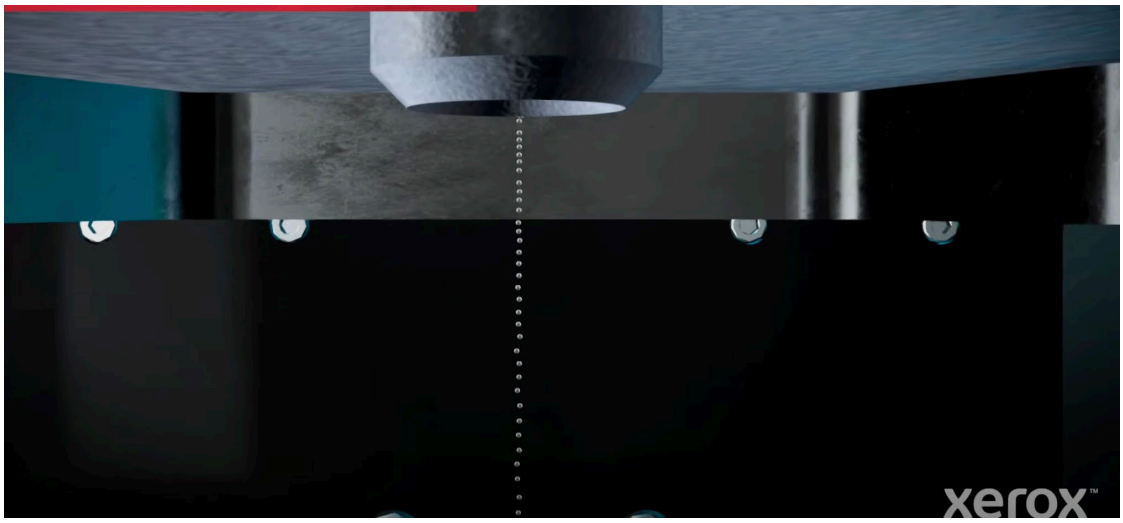

Figure 6. Illustration of Liquid Metal Droplets Extruding from Nozzle.
Source: [6].

c. The Build Plate

The metal droplets are extruded onto a nickel coated hot build plate (475°C) that moves in the XY plane to control drop location. The build plate lays on top of a ceramic heating bed to maintain build plate temperature throughout the printing process. The printed parts continue to be extruded on top of each other in a layer-by-layer fashion until the printed part is complete and influences the mechanical properties of the specimen.

Upon completion of the print, the part, still attached to the build plate must be removed from the printer and quenched in a water bath to remove the printed part from the build plate. The cooling of the build plate and the part at different cooling rates allows for the separation of the part from the build plate.

The printed part is now completed. Optional post-print processing, such as heat treatments, can be conducted to the printed part. This study will analyze the effects on the parts material properties from conducting those post-print processes.

d. Post Printing Heat Treatments

Like cast aluminum products, post-print heat treatments are an option to increase material properties for specific applications. Approved standards and specifications of heat treatment processes have been defined by the ASTM B917/B917M: Standard Practice for Heat Treatment of Aluminum-Alloy Casting from All Processes Cast [16]. The basis of heat treatment specifications will align with A356 cast aluminum as this has a similar composition to the Al-4008 wire filament, see Table 1. Two common heat treatments are T5 and T6. T5 allows for the material to naturally cool following extrusion, while T6 requires the allow to be instantaneously water cooled via quenching [17].

The T6 heat treatment is designed to ensure that finished product consists of the alpha-aluminum and silicon (α+Si) phase with minimal strain hardening after solution treatment and the emergence of the phase Mg_2Si after the ageing step. With 6.5%-7.5% Si wt% in the Al-4008 filament, the printed part must be heated up above 510°C in order to achieve a stable α+Si phase as can be seen in Figure 7. The two-step process of the T6 heat treatment will be discussed in the next chapter.

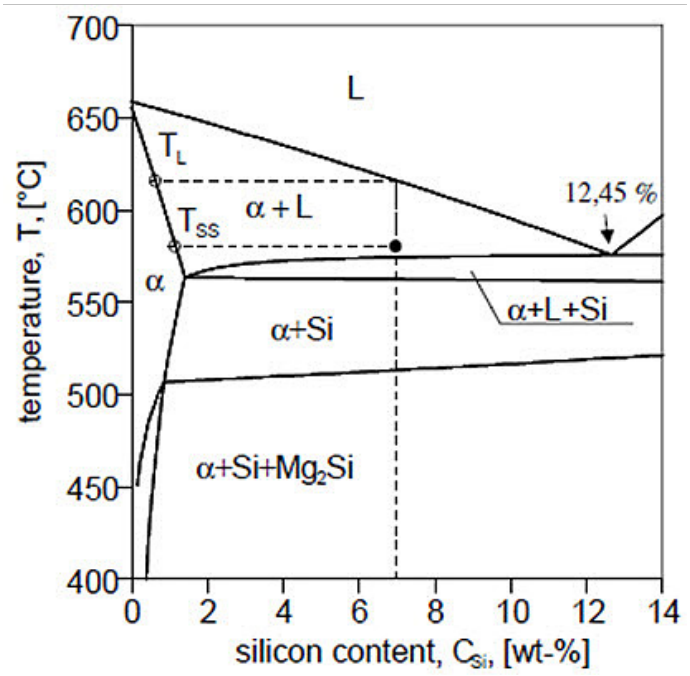

Figure 7. Pseudo-Binary Section of the System AlSiMg0.3. Source: [11].

From the magnesium weight percentage perspective, see Figure 8, a temperature of 500°C-550°C will be needed to stabilize the α +Si phase depending on the content of magnesium which can range from 0.3%-0.45%.

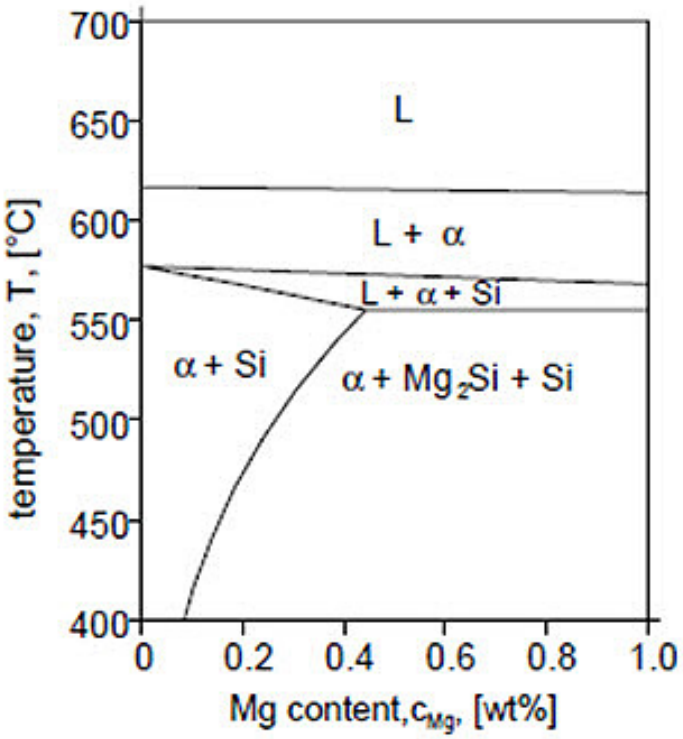

Figure 8. Pseudo-Binary Section of the System AlSi7Mg. Source: [11].

The solubility of Mg and Si in α-Al varies as a function of temperature with concurrent presence of Mg_2Si and Si in equilibrium as can be seen in Figure 9. An increase in temperature will increase the solubility of both Mg and Si. We will heat the samples up to 538°C in accordance with ASTM B917/B917M. The aging process will heat the sample to 155°C which will keep the same phases present but will remove internal stresses created when quenching the samples from the solution treatment.

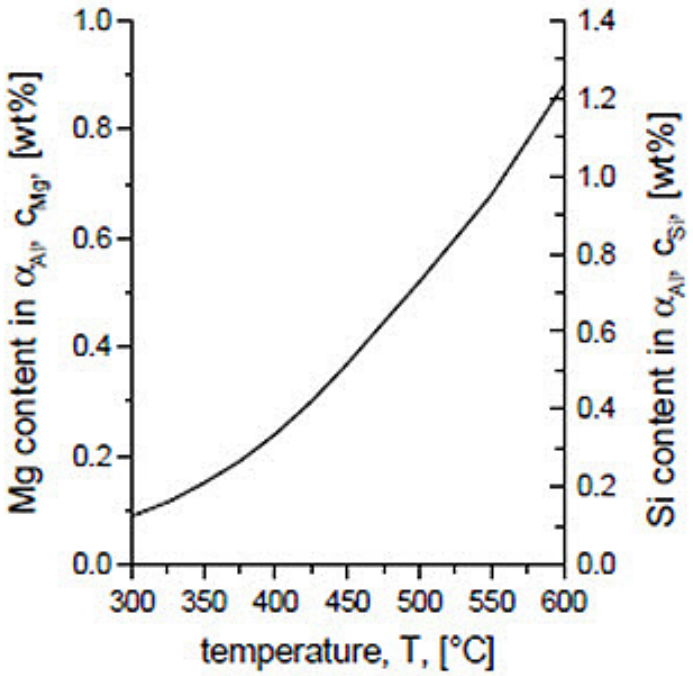

Figure 9. Solubility of Mg and Si in α_{Al} with Concurrent Presence of Mg_2Si and Si in Equilibrium. Source: [11].

C. WHY LIQUID METAL PRINTING?

Liquid Metal Deposition Printing offers many benefits over other metal AM processes. LMP uses a wire metal feedstock, similar to a spool of welding wire, instead of metal powders as the medium. Metal powders, due to their fine particle size (as small as 20μm), inherently have health and safety limitations that require additional safety measures to store, handle, and discard [18]. Additionally, special installation considerations such as non-explosive ventilation systems and additional hazardous material handling equipment such as respirators and explosion proof vacuum cleaners must be utilized.

Complex geometries, including hollow parts can be manufactured with LMP. Power based processes, including Selective Laser Melting (SLM) and Selective Laser Sintering (SLS) methods require drain holes to be designed into the part to allow for the excess powder to be removed. Additionally, post-processing techniques to remove binder and sintering is not required, unlike Printer Injection Molding (PIM) and Metal Injection Molding (MIM) techniques.

Additive manufacturing (AM) of aluminum has traditionally been unachievable except with laser powder bed fusion, which is a high-cost process. Due to its high potential for oxidation, aluminum is difficult to sinter if used in indirect processes like binder jetting. It is also difficult printing in welding-style processes like directed energy deposition (Metal BAAM) [7]. Gerdes et al. analyzed the oxidation impact on AlSi16 via the StarJet technologies liquid metal printer with conclusive results that there was no issue of oxidation from the liquid metal printer [13].

D. OBJECTIVES

During the design phase of engineering a new product, material selection is a key focus to ensure the designed components will meet the required mechanical properties for the application of the new product. These required properties are not limited to structural integrity considerations, but also thermal diffusivity, weight, and electrical conductivity. The point being that a part can be made to 'fit' the design shape, but may lack the strength, corrosive properties, or texture needed for the application. Simply printing a part to fit a repair need or a manufacturing requirement may appear as a quick solution to the problem, but it may not be the 'right' solution for the problem. By understanding the material properties of the Al-4008 products printed using liquid metal disposition printing, the end user can have the confidence the manufactured part will meet the material needs for the application.

This study will provide quantitative data on the material properties, specifically Ultimate Tensile Strength, Yield Strength, Elongation Percentage, and Microhardness, of additively manufactured Al-4008 that can be compared to the already established Military Standards of A356 cast aluminum. Once mechanical properties are determined, applicably of Aluminum 3D printed parts for use in structural, mechanical, and load-bearing components can be considered as a viable and reliable means of manufacturing and replacement. With reliable 3D printed parts, ends users will have the confidence the part will meet configuration specifications, ultimately maintaining material readiness and operational readiness.

This study does not aim to certify the process nor certify the end product as an accepted means of manufacturing new or replacement parts for any system. Rather, the goal is to present the properties found during this research to inform others. Further study, beyond the scope of this research would be needed to determine the certification of the material and manufacturing process. Ultimately, the aim of this study is four-fold:

- Evaluate the mechanical properties of the additively manufactured parts using Al-4008 filament and compare them to the established material property standards in accordance with MIL-A-21180D: Military Specification for Aluminum Alloy Castings, High Strength of A356 Cast Aluminum.

- Understand the impact of post-process heat treatment, specifically T6 heat treatments in accordance with ASTM B917/B917M: Standard Practice for Heat Treatment of Aluminum-Alloy Casting from All on the additively manufactured component's material properties.

- Understand the impact of build direction (horizontal and vertical) on the additively manufactured components material properties.

- Identify causes of premature failure in any samples and propose process changes, configuration changes, and methods to improve print quality and decrease material defects that could lead to premature failure.

Note: The term 'premature failure' refers to a part that did not perform to expectations, in this case the sample did not reach the mechanical properties established in the mentioned standard.

Chapter 2 will discuss the experimental procedures and methods, materials, and equipment used to complete the research objectives. Chapter 3 and 4 will cover the experimental results and findings to include material properties, microstructural analysis and fractography of the additively manufactured Al-4008 samples. Chapter 5 will review the research objectives and highlight the research findings to include recommendations for future research and focus.

THIS PAGE INTENTIONALLY LEFT BLANK

II. EXPERIMENTAL TESTS AND PROCEDURES

This chapter introduces the processes, materials, and equipment used in the manufacturing and testing of the additively manufactured Al-4008 samples. This chapter is broken down in three sections: sample fabrication methods, post-print processing (surface treatments and heat treatments), and tensile testing and microstructural characterization methods. A layout of the chapter is illustrated in Figure 10.

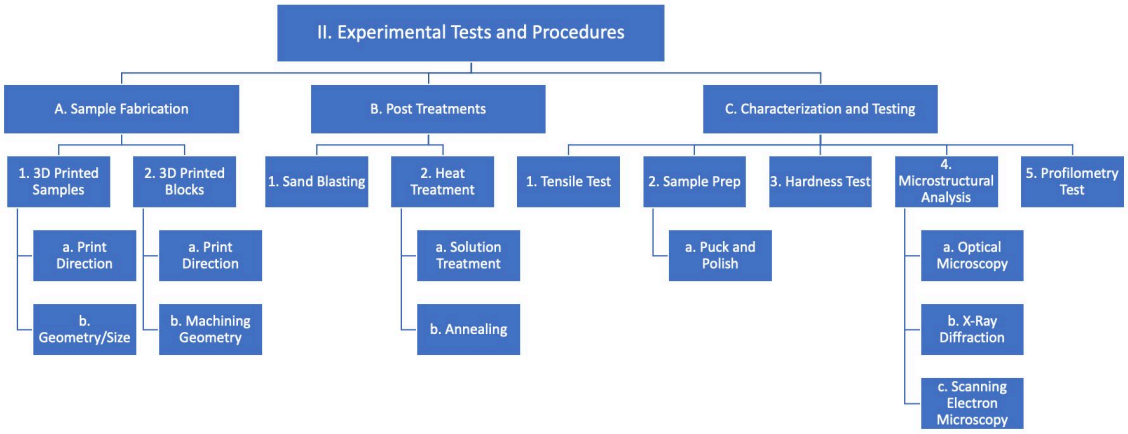

Figure 10. Experimental Procedures Layout

Through these testing methods we aim to determine and compare the ultimate tensile strength, yield strength, elongation percentage, and microhardness for additively manufactured Al-4008 both with and without post print processing to a T6 condition. These properties were determined for samples printed in various print orientations. Additionally, the microstructural characteristics (crystalline phases, grain sizes, porosity levels, etc.) of the additively manufactured Al-4008 were identified as well as the effects that heat treatments had on those microstructural features. Fractography was conducted on samples that showed properties below the ones for Class 1 defined in MIL-A-21180D: Military Specification for Aluminum Alloy Castings, High Strength for A356-T6 for A356 cast aluminum. Class 1 and Class 3 are material strength classifications defined in MIL-A-21180D to distinguish higher material properties requirements for a material. Only certain, often critical locations of the part are required to meet these properties.

A. SAMPLE FABRICATION

This section discusses the process of sample fabrication including print orientation, sample geometry and printer settings during the additive manufacturing process.

Models of the samples were designed using Solidworks CAD software. These .stl files were uploaded into the ElemX^{TM} proprietary slicer software to create a g-code file. As discussed previously, the g-code provides layer by layer printing directions for the nozzle, print head, and print bed.

The user then prepares the nozzle for use. The graphite nozzle is treated with the argon plasma etcher (Plasma Etch Inc.). Figure 11 illustrates a nozzle being plasma treated. The plasma treatment increases the wettability of the graphite with the aluminum ensuring better surface interaction between them to minimize bubble adhesion which would impact the development of the Lorenz forces. The nozzle hole itself is treated carefully from both directions (upstream and downstream, relative to droplet ejection). These treatments are done for 1 minute each. The inside cup of the nozzle is then treated in a manual circular process for an additional minute to surface treat the entire wetted area inside the nozzle. After the argon plasma etch is completed, an additional air etch process is performed. This also is manually done and lasts approximately 1 minute.

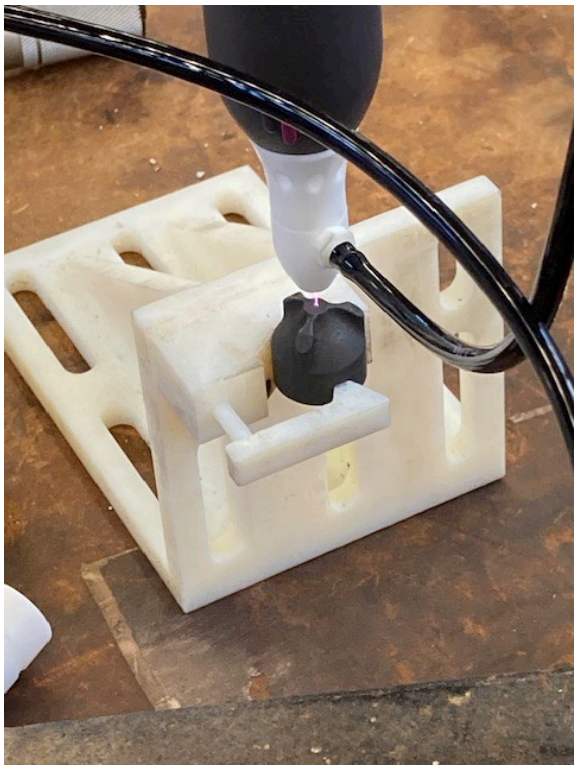

Figure 11. Nozzle Undergoing Plasma Treatment

Once the interior of the nozzle is fully surface treated, the nozzle length must be adjusted to be within specification. This process is done by sanding, with 1000-grit sandpaper, the front face of the nozzle. The sanding process is manually performed by the user and the specification requires the nozzle to be 0.5mm +/- 0.05mm (0.45mm to 0.55mm). In addition to ensuring the appropriate nozzle length, this process also effectively removes the surface treatment from the exterior "front face" of the nozzle. If the front face does wet with aluminum, then jetting will be poor, and a functional printed part may not result. This is one of the many user-controlled variables that could impact the quality of the printed parts.

The printer then goes through a 'burn-in' process which is required to ensure the liquid metal droplets are uniform and accurately dispensed. During the burn in process the droplets are extruded at 100Hz, 200Hz, 300Hz and 400Hz to bring the droplets to a steady state.

Once complete, a drop mass calibration is conducted by the user. This is another user-controlled step in the additively manufactured process. The mass of 10,000 droplets is measured to ensure they match with the programmed extrusion mass. The droplet mass is adjusted by the "high time" of the pulse train actuating the electromagnetic coil. The specification for droplet mass is 1.45g +/- 0.05g per 10,000 droplets ejected at 60% nominal rate. If needed the user adjusts the frequency output and re-calibrates the droplet mass. The calibration effects of the higher mass output compared to the lower mass output within this acceptable range were not compared during this research.

System parameters were set as shown in Table 2.

Table 2. Print Parameters for AL-4008 Samples

Nozzle Temp [°C]	Print Bed Temp [°C]	Droplet Frequency [Hz]	Infill [%]
825°C	475°C	400 Hz	100%

The analysis of samples that were printed as tensile test samples is presented in section 1 below. It was assumed that the mechanical properties of additively manufactured tensile specimens will be comparable to those of 3D printed products with a similar surface roughness, without further machining.

In contrast, section 2 covers the samples that were printed as solid blocks, then machined into tensile test specimens. The printed blocks that are machined into tensile specimens represent the printed Al-4008 in optimal testing conditions (minimal surface roughness, consistent cross-sectional area, etc.) which is in alignment with the industry standard practices of testing 3D printed metals.

1. 3D Printed Samples

The samples manufactured in the section were printed as tensile test specimens, conforming to the ASTM E8/E8M: Standard Test Methods for Tension Testing of Metallic Materials [19] dimensional requirements.

a. Print Direction

Print direction has been determined in previous studies to correlate to different material properties in additively manufactured metals and plastics [20], [21]. Printed samples were printed in either the horizontal (XY) direction or vertical (Z) direction, as defined by the coordinate system shown in Figure 12. The tensile specimens that were printed in the vertical direction had a wide base that was designed to prevent the specimens from falling over during the print process due to the rapid movement of the print bed during printing.

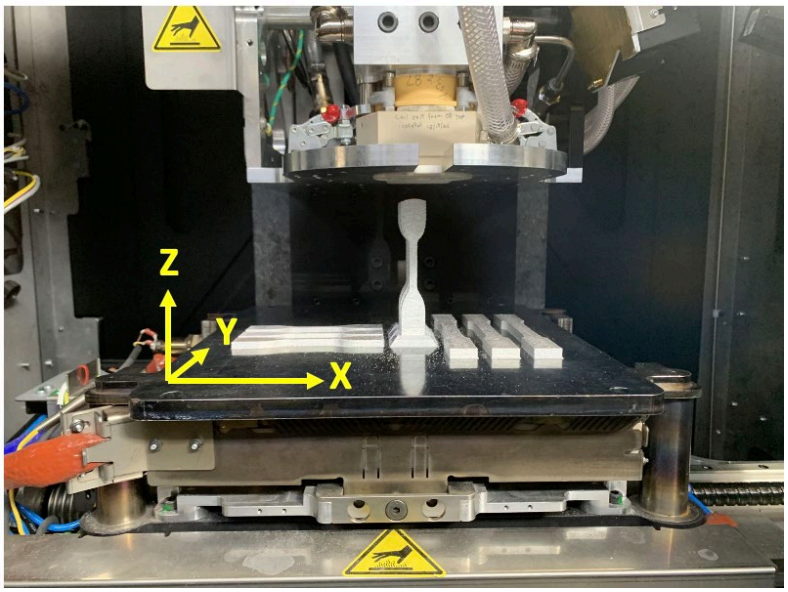

Figure 12. Coordinate System for As-Printed Tensile Specimens

b. Geometry and Size

There were two different size test specimens printed as samples. All samples were printed with dimensions consistent with ASTM E8: Standard Test Methods for Tension Testing of Metallic Materials [19]. See Figure 13 for ASTM E8 Specifications for the tensile specimens.

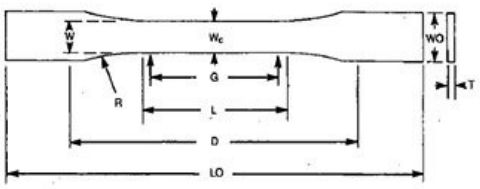

TYPES I, II, III & V

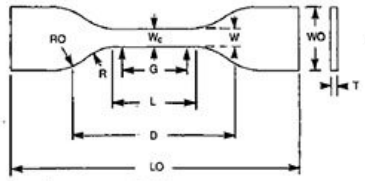

TYPE IV

Specimen Dimensions for Thickness, *T*, mm (in.)[A]

Dimensions (see drawings)	7 (0.28) or under		Over 7 to 14 (0.28 to 0.55), incl	4 (0.16) or under		Tolerances
	Type I	Type II	Type III	Type IV[B]	Type V[C,D]	
W—Width of narrow section[E,F]	13 (0.50)	6 (0.25)	19 (0.75)	6 (0.25)	3.18 (0.125)	±0.5 (±0.02)[A,C]
L—Length of narrow section	57 (2.25)	57 (2.25)	57 (2.25)	33 (1.30)	9.53 (0.375)	±0.5 (±0.02)[C]
WO—Width overall, min[G]	19 (0.75)	19 (0.75)	29 (1.13)	19 (0.75)	...	+ 6.4 (+ 0.25)
WO—Width overall, min[G]	...	...	...	...	9.53 (0.375)	+ 3.18 (+ 0.125)
LO—Length overall, min[H]	165 (6.5)	183 (7.2)	246 (9.7)	115 (4.5)	63.5 (2.5)	no max (no max)
G—Gage length[I]	50 (2.00)	50 (2.00)	50 (2.00)	...	7.62 (0.300)	±0.25 (±0.010)[C]
G—Gage length[I]	...	...	...	25 (1.00)	...	±0.13 (±0.005)
D—Distance between grips	115 (4.5)	135 (5.3)	115 (4.5)	65 (2.5)[J]	25.4 (1.0)	±5 (±0.2)
R—Radius of fillet	76 (3.00)	76 (3.00)	76 (3.00)	14 (0.56)	12.7 (0.5)	±1 (±0.04)[C]
RO—Outer radius (Type IV)	...	...	...	25 (1.00)	...	±1 (±0.04)

Figure 13. ASTM E8: Standard Test Methods for Tension Testing of Metallic Materials Dimension Requirements. Source [19].

The horizontal printed test specimens were printed as Type I (big) or Type IV (small). The vertical printed test specimens were printed as Type IV. The specific dimensions for the Type IV samples are shown in Figure 14.

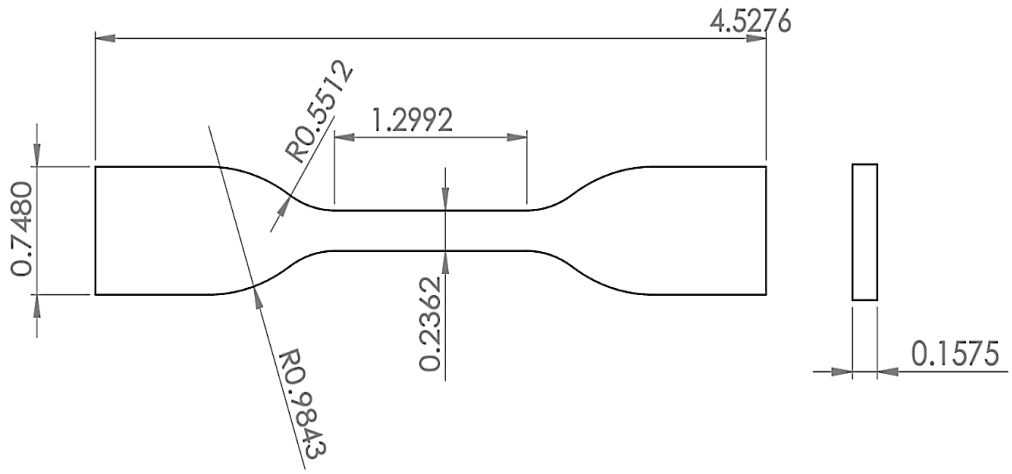

ASTM E8 Type IV, for as-printed tensile specimens (units in inches). Note: Vertical printed samples had a base under them to prevent the sample from falling during printing. This base was removed prior to testing.

Figure 14. Type IV Printed Tensile Test Sample Specifications

2. 3D Printed Blocks

This section discusses the manufacturing process of the additively fabricated printed blocks that were later heat treated and machined into tensile test specimens. As previously discussed, the industry standard for testing these material properties is to machine the samples to meet the ASTM E8 specifications. By machining these samples to the correct dimensions rather than directly printing the tensile specimen to shape surface roughness and stress concentrators are minimized to produce an optimized sample.

a. Print Direction

Printed blocks were printed in either the horizontal position or vertical position. When printing these blocks, only one block was manufactured at a time to reduce print time. The coordinate reference for these block specimens can be seen in Figure 15.

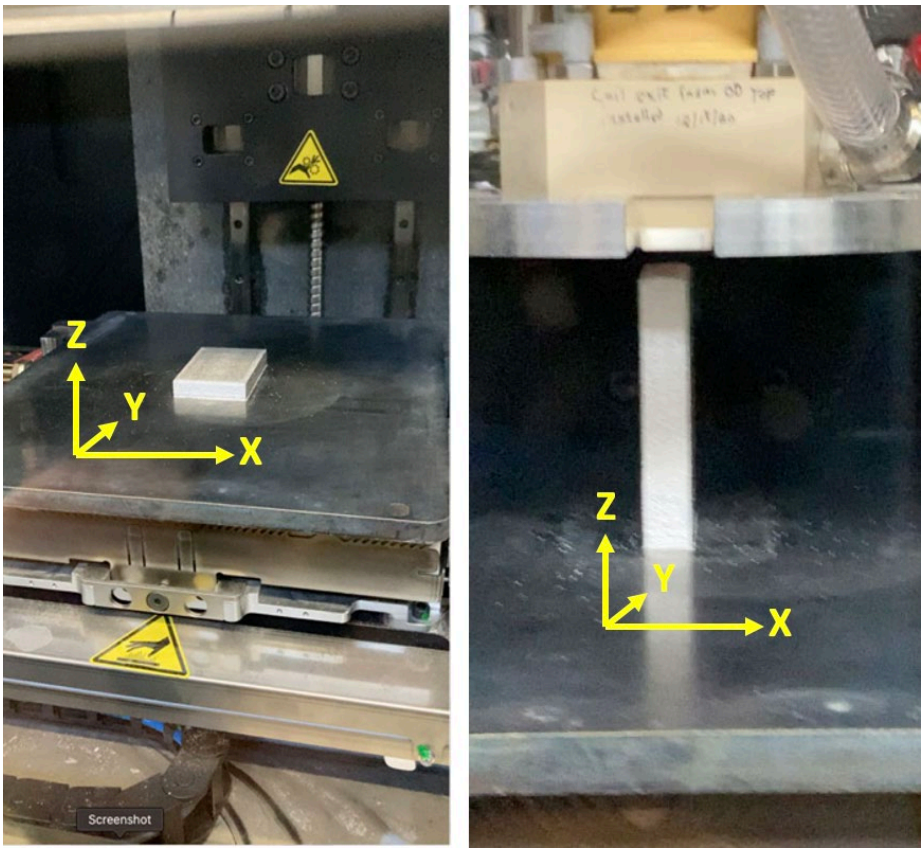

Block Specimen printed in Horizonal Position (left) and Vertical Position (right)

Figure 15. Coordinate System for Printed Blocks

b. Machining Geometry and Size

Each printed block, both vertical and horizontal print directions was machined into three ‘Specimen 3’ tensile test specimens, in accordance with ASTM E8: Standard Test Methods for Tension Testing of Metallic Materials (see Figure 16) [19]. By machining three tensile specimens from each block, materials properties could be analyzed for a larger representation of the printed block. For example, if any sample were to have materials properties which were inconsistent with the other samples produced from the same block, fractographic analysis could be compared between the samples.

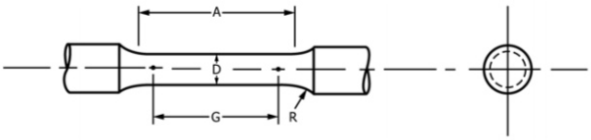

Dimensions, mm [in]

	For Test Specimens with Gauge Length Four times the Diameter [E8				
	Standard Specimen	Small-Size Specimens Proportional to Standard			
	Specimen 1	Specimen 2	Specimen 3	Specimen 4	Specimen 5
G—Gauge length	50.0 ± 0.1 [2.000 ± 0.005]	36.0 ± 0.1 [1.400 ± 0.005]	24.0 ± 0.1 [1.000 ± 0.005]	16.0 ± 0.1 [0.640 ± 0.005]	10.0 ±0.1 [0.450 ± 0.005]
D—Diameter (Note 1)	12.5 ± 0.2 [0.500 ± 0.010]	9.0 ±0.1 [0.350 ± 0.007]	6.0 ± 0.1 [0.250 ± 0.005]	4.0 ± 0.1 [0.160 ± 0.003]	2.5 ± 0.1 [0.113 ± 0.002]
R—Radius of fillet, min	10 [0.375]	8 [0.25]	6 [0.188]	4 [0.156]	2 [0.094]
A—Length of reduced parallel section, min (Note 2)	56 [2.25]	45 [1.75]	30 [1.25]	20 [0.75]	16 [0.625]

Figure 16. ASTM E8 Tensile Test Specimen Specifications for Round Cross-Section. Source [19].

The circular cross-section tensile specimens are the industry standard for testing material properties due to the minimized stress concentration areas compared to rectangular cross-section tensile specimens. The actual specifications used in the machining process can be viewed in Figure 17.

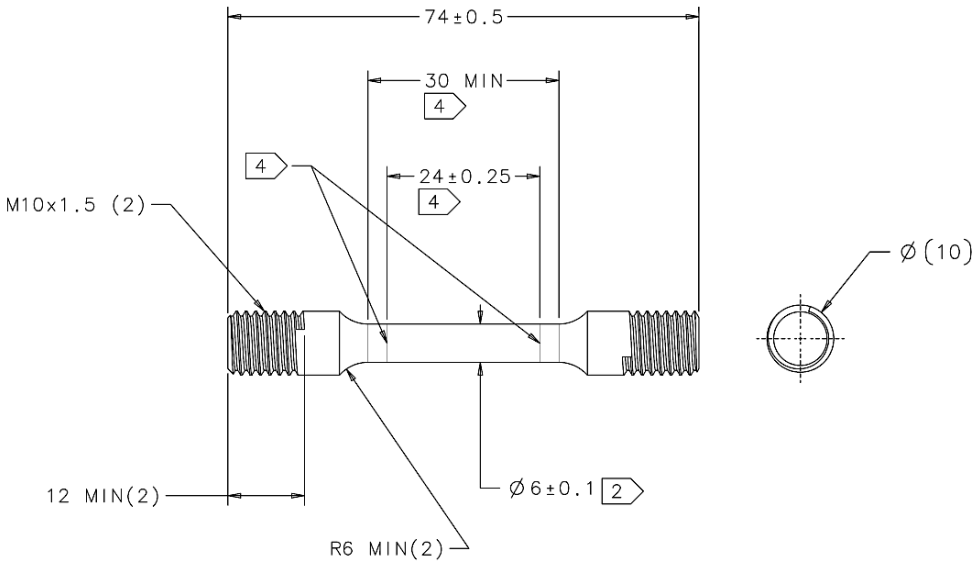

ASTM E8 Specimen 3, for machined tensile specimens with circular cross section (units in mm).

Figure 17. Machined Tensile Test Sample Specifications: ASTM E8/E8M Specimen 3: Circular Cross-Section

B. POST PROCESS TREATMENT

This section discusses materials and equipment used in the post printing process. It is important to note that not all samples had post-print processing.

1. Sand Blasting

A Universal Abrasive Blast Machine with 60–120 grit medium grade smooth glass beads was used to remove surface roughness from selected samples. Only select as-printed samples were sand blasted. The purpose of sand blasting these samples was to reduce surface roughness to compare material properties from sand blasted and non-sand blasted tensile specimens. An objective analysis of mechanical properties will determine if any reduction is surface roughness will produce large deviations in material properties.

2. Heat Treatment

Selecte samples were heat treated to meet the T6 requirements for A-356 cast aluminum [16]. Only a select few of the as-printed tensile specimens were heat treated. Each of the printed blocks were heat treated prior to machining into tensile specimens.

The T6 heat treatment process utilized for the 3D printed AL-4008 parts is the same process used for A356 cast aluminum to improve mechanical properties, increasing the ultimate tensile strength and yield strength for high strength applications. This research with utilized the T6 Heat treatment as defined in ASTM B917/B917M. The sample (less than 13mm in thickness) sized appropriate procedure utilized was:

- Four hours at 538°C
- Fresh Water Quench
- Three hours at 155°C
- Air Cooled

a. Solution Treatment

The first step in the T6 Heat treatment process is to solution treat the printed specimen. This step brings the specimen up to a specified temperature, below melting temperature) for a set duration of time to ensure the desire phases are present throughout the sample. Once the desired phases are achieved, the sample is rapidly quenched to 'lock-in' those phases.

In the case of A-356 cast aluminum and the Al-4008 filament there is a 6.5-7.5% composition of silicon present in the alloys. An average value of 7% silicon will be used as a reference. The α+Si phase offers the stronger material properties desired in high strength applications. The samples need to be heated to 538°C for four hours to allow the alloying elements to dissolve in the α-Al and allow for the spherization of eutectic Si [22]. Then it returns to the α+Si phase and the sample needs to remain at that temperature long enough for the entire sample to come to equilibrium. Once the samples reach an equilibrium state with the α+Si phase, it must be rapidly quenched to keep the α+Si phase present. If it were cooled slowly the specimen would undergo a phase change to the α+Si+Mg_2Si phase which is what is present following the completion of the printed part. Figure 18 illustrates the applicable section of the pseudo-binary phase diagram of AlSiMg0.3 during the solution treatment compared to the expected phase presence while the part is on the build plate.

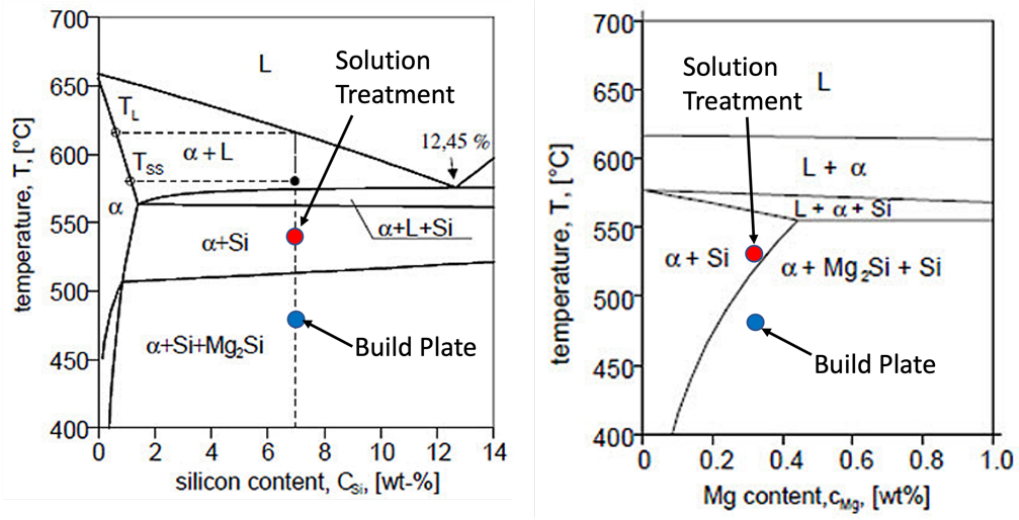

Figure 18. Pseudo-Binary Section of the System AlSiMg0.3. Adapted from Source [11].

A Thermo Scientific Lindberg Blue M Box Furnace was used to solution treat samples. the samples were heated at 538°C for four hours, then the samples were quenched in room temperature water. A step-by-step illustration of the solution treatment process can be seen in Figure 19.

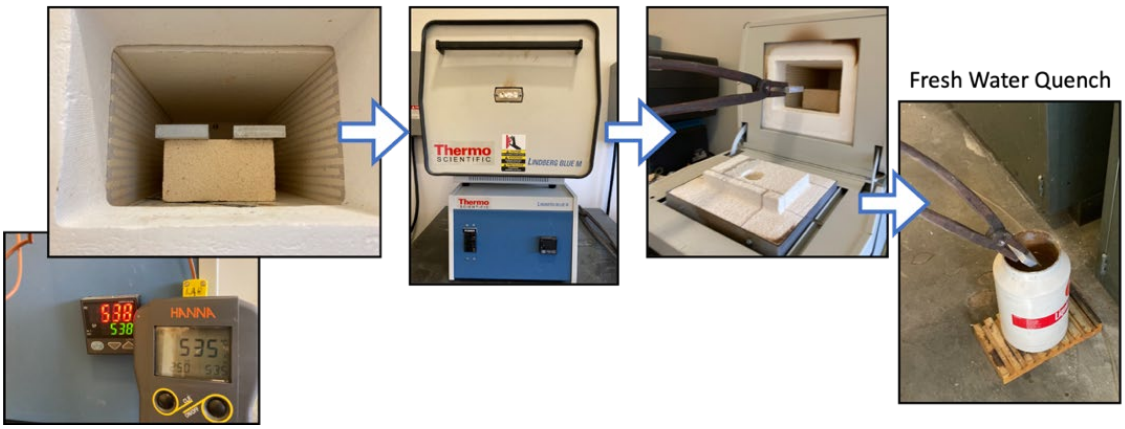

Figure 19. Solution Treatment Process

b. Aging

Aging or precipitation hardening is the second step of the post-processing heat treatment. The aging process in the T6 heat treatment is a low temperature (155°C) process used to remove any adverse properties that were created during the solution treatment process and to harden and strengthen the Al-4008 samples [23]. During this process, the Mg_2Si phase is produced. The grain size, distribution, and morphology of Mg_2Si within an aluminum alloy have been linked as the primary dependent factor in mechanical property determination in aluminum alloys [24].

A Thermo Scientific Lindberg Blue M Box Furnace was used to solution treat and artificially age the samples. the samples were heated to 155°C for three hours. After three hours, the samples were removed from the furnace and allowed to air cool at room temperature. Figure 20 illustrates the aging process used for the Al-4008.

Figure 20. Aging Process

C. CHARACTERIZATION AND TESTING

This section discusses the materials, equipment, and procedures used to measure material properties such as ultimate tensile strength, yield strength, and elongation percentage as well as microhardness. Additionally, the section covers the equipment and processes conducted in the microstructural analysis and fractography of the samples.

1. Tensile Test

Tensile properties were measured using the Instron 5982 Tensile Tester. All tests were conducted in accordance with ASTM E8: Standard Test Methods for Tension Testing of Metallic Materials [19]. Samples were tested at a rate of 2.0 mm/min. For the rectangular shaped specimens, the equipped clamps were used to hold the ends. For the circular cross section specimens, custom holders were designed and manufactured to house the threaded ends. The as-printed samples and circular machined samples can be seen in the Instron 5982 Tensile Tester in Figure 21.

Left: As-printed tensile specimen. Right: Printed block then machined circular cross-section tensile specimen.

Figure 21. Tensile Test Specimens Mounted in Instron 5982 Tensile Tester.

2. Sample Preparation

Many of the samples were used in further analysis beyond evaluation of the material properties under tensile loading. This section discusses the steps taken to cut, mount, and polish samples for further testing and analysis.

a. Cutting

Many of the samples were cut to reveal and expose the cross-sectional area of the samples or to remove the fractured surface from the tensile specimens for further microscopic analysis. A wet saw was used to cut the parts from the printed samples to analyze different sections of the samples. The size of the cuts varied for different applications. The cut off coupons were cut to fit in the X-ray Diffraction sample holder, Scanning Electron Microscope mounting trays, and epoxy pucks for various testing and analysis.

b. Epoxy Mounting

Samples were cut from the test specimens to fit inside a cylindrical mold and mounted inside the molds with Struers EpoFix Epoxy. The EpoFix transparent epoxy was mixed with 25 parts resin to 3 parts hardener and cured overnight before removal from the mold. Pictures of the samples being mounted can be seen in Figure 22.

Epoxy molds were used instead of the traditional hot pressed molded resin pucks to minimize effects of localized heating on the samples. These molded mounts were used in the polishing phases which prepared the samples for microhardness testing and to observe internal microstructures of the specimens in the optical microscope and scanning electron microscope.

Figure 22. Epoxy Sample Molds

c. Sample Polishing

The mounted samples were then ground and polished using an Ecomet4 Variable Speed Polisher/Grinder with 200/400/800/1200/2500/4000 grit paper with 4lbs force at 120 rpm for 15 minutes each grit. The samples were then polished with a 1µm Al_2O_3 for 25 minutes. A scratch free, mirror like finish was desired upon completion of polishing to ensure no self-imposed defects would be observed during the analysis. Samples undergoing polishing can be seen in Figure 23.

Figure 23. Ecomet4 Variable Speed Variable Speed Grinder/Polisher Used to Prepare the Samples for Microscopy and Microhardness Testing

3. Hardness Test

Microhardness testing was conducted using a Struers DuraScan hardness tester set to Vickers Hardness, HV to mounted and polished samples. The HV 0.1 test method was utilized. A load was applied by compressing a diamond into the surface of the sample, then measuring the size of the impression dimensions left on the sample surface. The value d is calculated by taking the average of d_1 and d_2, then d is compared a table using Vickers EN ISO 6507 to determine the hardness. Figure 24 shows and example of an indention left by the diamond tip.

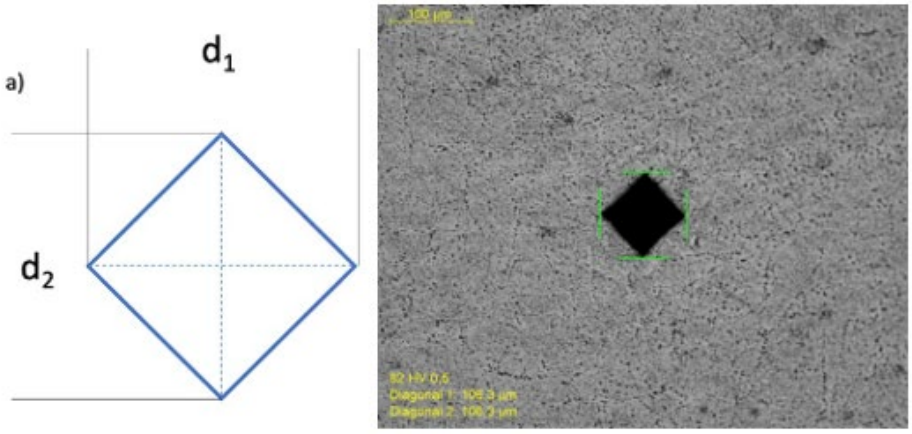

Figure 24. Vickers Hardness HV Impression Measurement

At least one sample was tested from each batch and position, with ten to twenty measurements taken from each sample. Each measurement was spaced from the others to prevent a localized bias. Additional measurements were taken for samples with outliers (greater than two standard deviations). Vickers hardness testing can be seen in Figure 25.

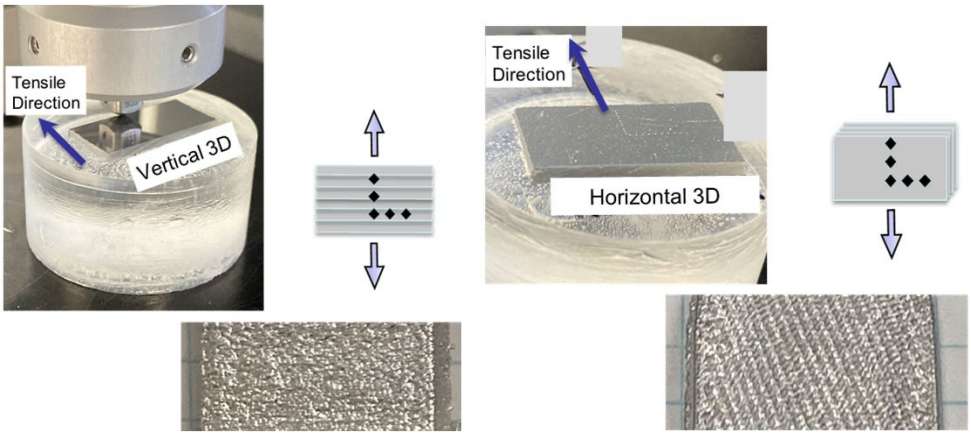

Figure 25. Vickers Hardness Testing Being Conducted on Mounted and Polished Samples

4. Profilometry Test

Profilometry was conducted on the fractured surfaces of the samples from the printed blocks. Profilometry was conducted by Xerox® Elem™ Additive Solutions as part

of the CRADA. A Keyence VR-5000 3D optical profilometer under a magnification of 40x was used to collect the images. These images to observe the method of fracture in those samples and to correlate microscopic features with their locations on the fractured surfaces.

5. Microstructural Analysis

This section discusses the equipment and procedures used during various microscopy techniques to further analyze the samples and their fractured surfaces.

a. Optical Microscopy

Optical microscopy was used to observe the microstructure within the cross-section of the samples. The observations were used to compare the phases present, pore sizes, and other defects from samples with different printing orientations and following heat treatments.

The samples were etched with Keller's Reagent (Mixture of 5 ml Nitric Acid (NHO_3) + 3 ml Hydrochloric Acid (HCl) + 2 ml Hydrofluoric Acid (HF) + 190 ml H_2O) [10] to reveal grain boundaries and their orientations and to aid in observation of phases present in the samples. The optical images were captured at various magnifications from 2.5-100x using the Nikon Epiphot 200 software. Some of the images were processed with ImageJ to measure the quantity and size of pores and defects.

b. X-Ray Diffraction

X-Ray Diffraction (XRD) was used to determine the presence of the crystalline phases within the samples. The crystalline phases were compared with samples that were not heat treated and samples that were heat treated. This analysis is critical to determine that the Heat-Treated Al-4008 had the expected crystalline phases.

Samples were prepared by cutting flat coupons from the specimens using a wet saw and were mounted to the specimen holder using a clay putty to ensure the samples were flat and flush with the specimen holding disk (see Figure 26).

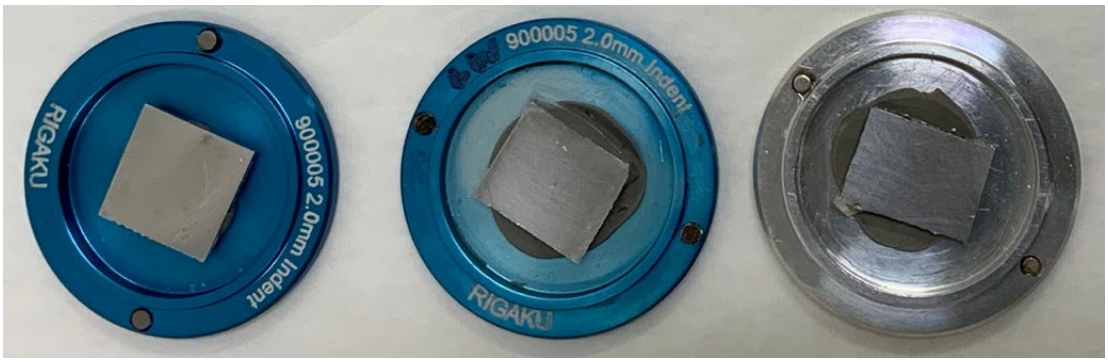

Figure 26. Mounted Coupon Samples Ready for X-ray Diffraction

The Rigaku Miniflex 600 XRD was used to determine the presence of crystalline phases. The testing parameters were set to 40mV and 15mA utilizing a scan rate of 2.0°/minute over the 2θ range of 10° to 120°.

PDF-4+ 2020 RDB, a product of the International Centre for Diffraction Data was used for a XRD database reference.

c. Scanning Electron Microscopy

Scanning Electron Microscopy was used to observe higher magnification images of the fractured surfaces and cross-sectional areas. Electrons from the incident beam interact with the surface/near surface electrons which are discharged as low energy secondary electrons and collected by the in-lens detector.

Additionally, the EDS feature was used to identify elemental presence throughout various location within the samples. In EDS operation, the incident beam interacts with the samples and the sample discharges a photon which has an energy signature which is unique to that element. During the failure analysis portion of this research, the SEM with EDS was used to identify the presence of foreign material within some samples and helped to determine the probable source of this foreign material.

Higher magnification images of the samples were captured using a Zeiss Neon 40 scanning electron microscope (SEM), see Figure 27. Samples were observed through a 30μm aperture. An accelerating voltage of 5kV to 20kV was used while working distance was set to 5mm.

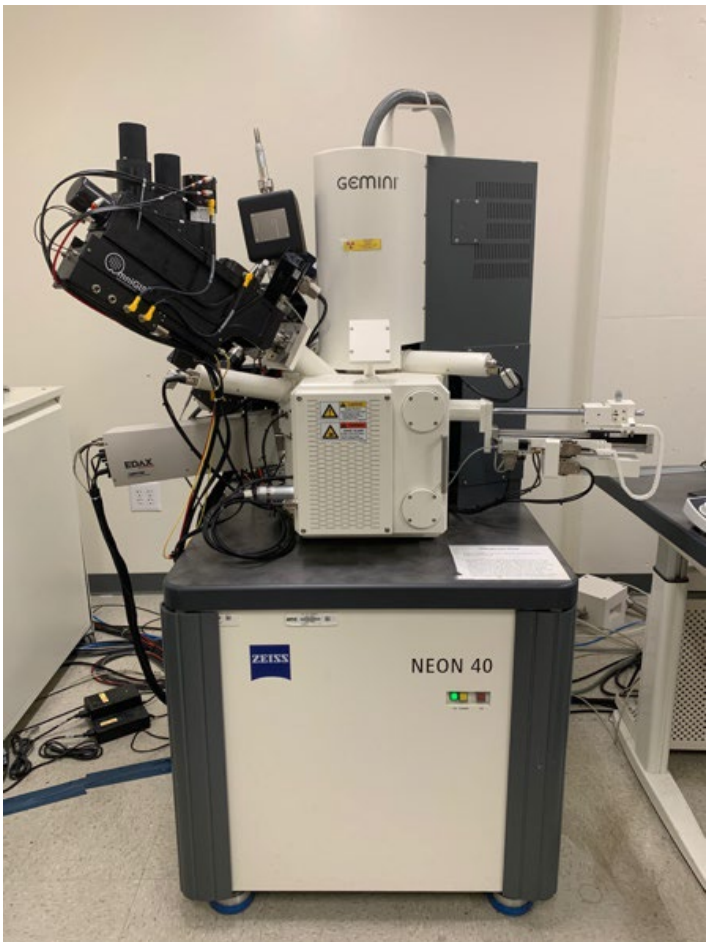

Figure 27. Zeiss Neon 40 SEM

Copper tape was used to connect the puck mounted samples to the mounting hardware to prevent charging of the sample. Fractured surface samples were mounted directly to the mounting plates with an adhesive tape. Figure 28 shows both puck mounted samples and fractured surface samples ready the SEM.

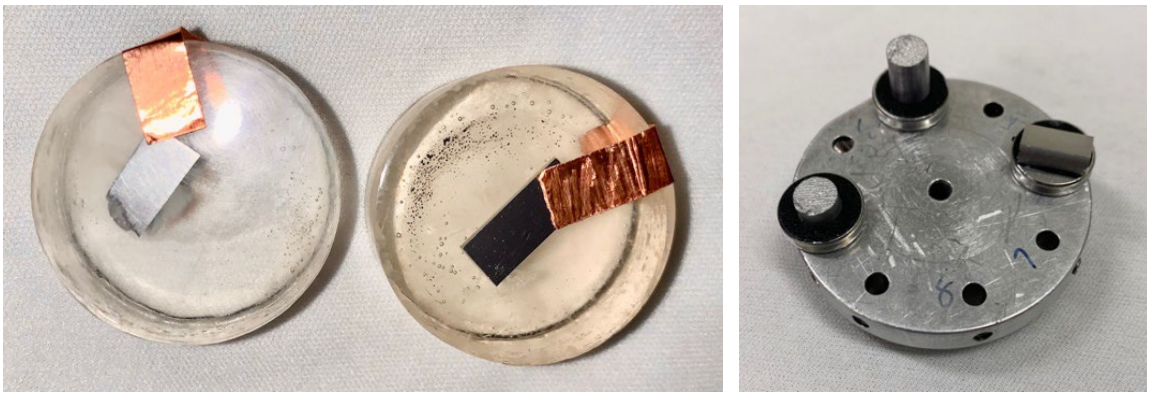

(Left) Copper Tape was used to ground the puck mounted samples. (Right) Fractured surface samples were mounted using the adhesive tape on the mounting fixtures.

Figure 28. Samples Prepared for Scanning Electron Microscope

Select samples were analyzed with Energy-Dispersive X-Ray spectroscopy (EDS). EDS was used to identify the elements present on the sample surfaces. A 60µm aperture was used with a 5kV-20kV accelerating voltage. The working distance was set to 5mm for all EDS analysis. Spot analysis as well as mapping was conducted on various samples.

III. RESULTS: 3D PRINTED TENSILE TEST SPECIMENS

This chapter presents the results and findings from the testing and analysis of the As-Printed Al-4008 tensile specimens along a discussion that compares the data with others for similar alloys found in the literature. The chapter also includes a comparison of the material properties and microstructural features for samples with and without post print processing. Figure 29 outlines this chapter.

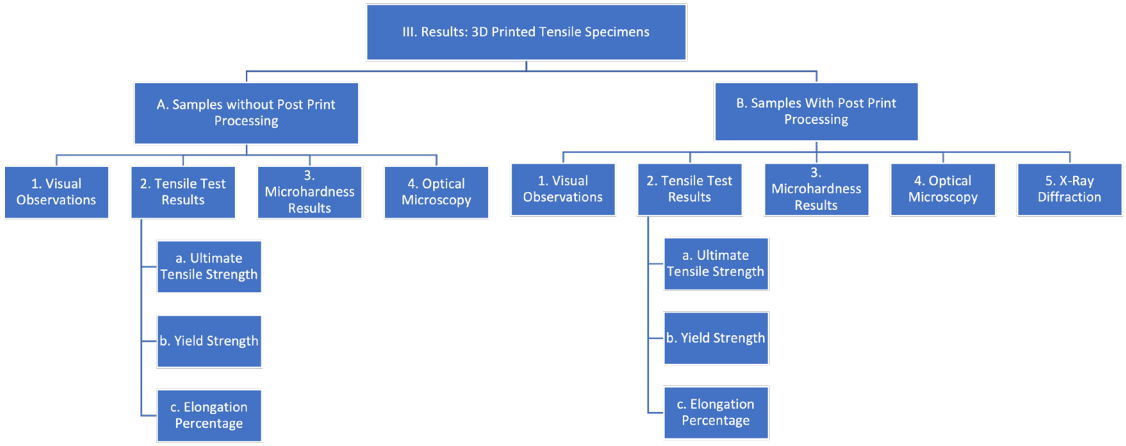

Figure 29. As-Printed Tensile Specimen Results Chapter Overview

A. SAMPLES WITHOUT POST PRINT PROCESSING

These samples were printed as tensile test specimens to compare the effects of print direction on the material yield and tensile strength, surface roughness, and hardness. None of these samples were heat treated or modified after printing with the exception of cutting the base off of the vertical samples that was required to support the samples from falling over during the printing process. The samples are compared to the material properties consistent with A356.0.F: As-Cast Aluminum [26] (green dashed line on graphs). The Class 1 and Class 3 standards established by MIL-A-21180D: Military Specification for Aluminum Alloy Castings, High Strength for A356-T6 are marked on each graph (red dashed line) as well. The different classes represent minimum material properties requirements and where on the part those requirements are required. Both Class 1 and Class

3 inspection requirements are applicable to a designated location, (likely the high-stress area of concern), whereas Class 10,11,12 require the material properties to be met at all locations of the part [27]. Class 1 has slightly lower material strength requirements compared to Class 3. However, these classes only apply only to samples which have been T6 heat treated. Figure 30 shows the tensile test specimens being printed.

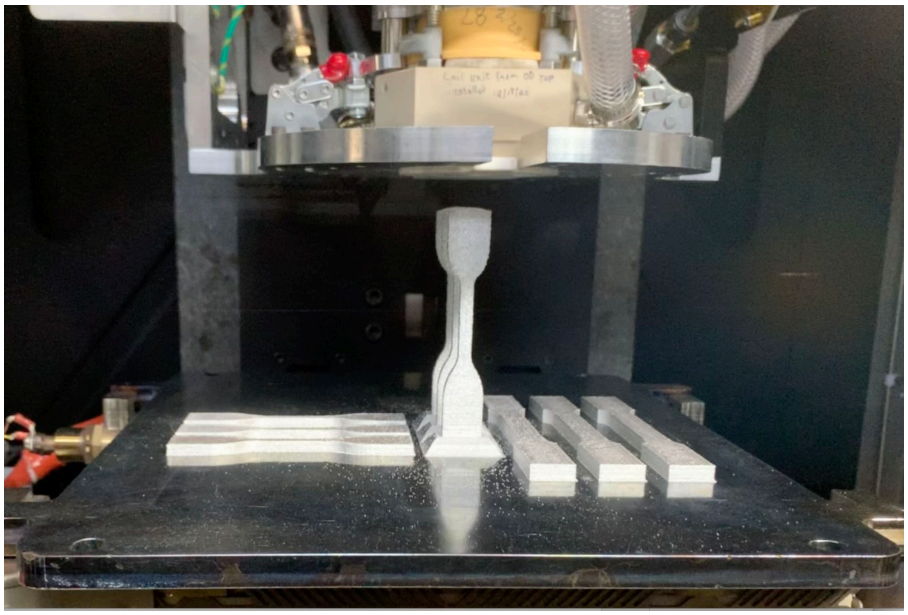

Figure 30. As-Printed Tensile Specimens

1. Visual Inspections

All three Type-IV horizontal and all three Type-I horizontal prints were relatively smooth prints with no obvious defects. Each of these prints has a very thin brim (first layer only) which exceeds the print dimension to aid in print bed adhesion, see Figure 31.

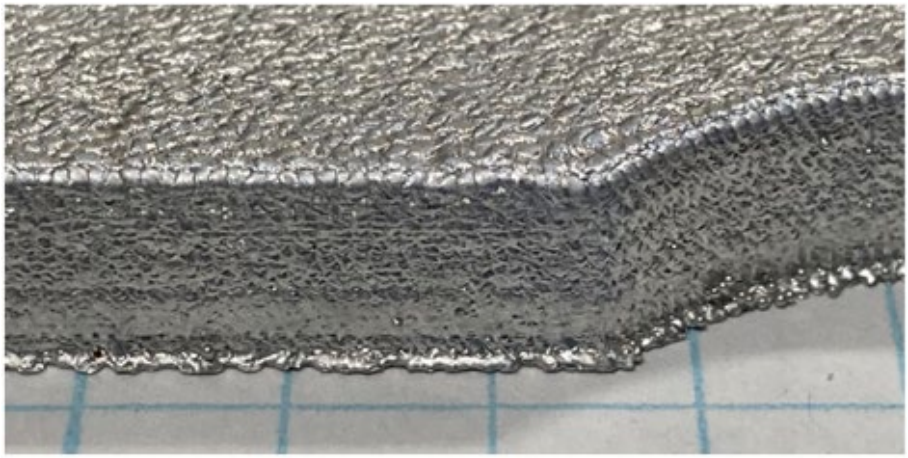

Horizontal Print- Brim can be seen at the base of the entirety of the printed specimen. The brim increases the contact surface area of the print with the print bed, increasing print bed adhesion.

Figure 31. Horizontal As-Printed Tensile Specimen: Visual Inspection

As can be seen in Figure 32, the Type-IV vertical samples started off as smooth as the horizontal samples, but surface roughness increased as the print continued along the z-axis. This was most likely related to the vibration increase of the print bed throughout the duration of the print.

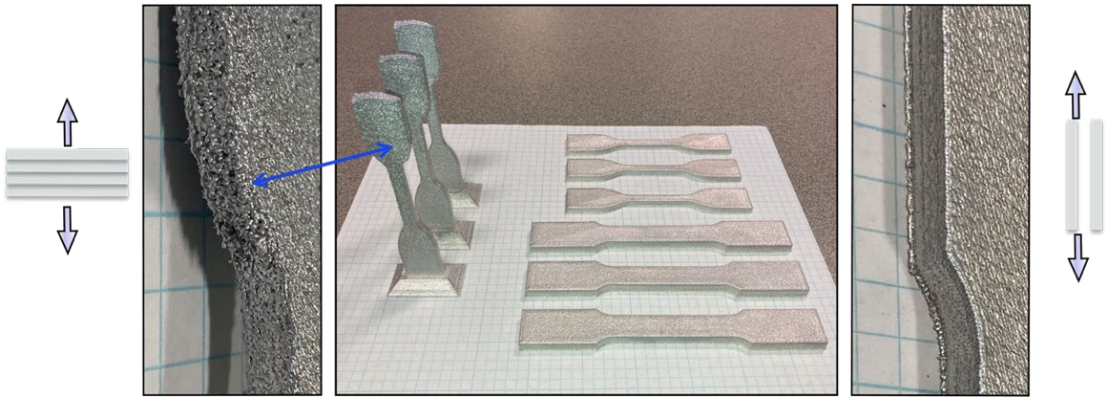

Figure 32. As-Printed Tensile Specimens: Visual Inspection

2. Tensile Test Results

This section discusses the results from the tensile testing of the as printed tensile specimens. The ultimate tensile strength, yield strength, and elongation percentage are

discussed and compared. Table 3 lists the material properties found in the as-printed tensile specimens without post-print processing.

Table 3. Material Properties: As-Printed Untreated Al-4008 Samples

	Horizontal: Type I [MPa]	Horizontal: Type IV [MPa]	Vertical: Type IV [MPa]	As Cast A356.0 [MPa]
UTS (STD)	154.81 (1.29)	139.57 (7.87)	132.79 (1.87)	160
YS (STD)	49.83 (1.00)	63.7 (3.64)	55.53 (0.49)	70
EL% (STD)	24.65 (2.65)	13.94 (1.37)	20.65 (2.20)	6

As-Cast A356.0 values taken from [26]. Standard Deviations are in parenthesis.

a. Ultimate Tensile Strength

The horizontal (XY-print direction) Type-I sized samples had a higher UTS than the horizontal (XY-print direction) Type-IV samples. We suspect this is due to the impacts of surface defects. The Type-I samples have a surface volume to cross-section area ratio of 29.34, while the Type-IV samples have a ratio of 32.45. Similar microstructure and pores were found in both sized samples. Barba et. al found similar results when comparing additively manufactured Ti-6Al-4V [20]. Samples with larger cross sections revealed a 10.91% higher UTS than the samples with smaller cross sections printed in the same direction.

Samples printed in the horizonal print direction (XY), both Type-I (large) and Type-IV (small) had higher Ultimate Tensile Strength (UTS) than the samples printed in the vertical print direction (Z), which were of Type IV geometry. This increase in UTS in the horizontal print direction is likely due to the bonding between print layers. While printing in the horizontal position the droplets are coalescing with the droplets along the same layer which haven't cooled as much as the previous layer, therefore the droplet-to-droplet bonds are stronger for the duration of the entire print layer. From the study on print bed temperature effects, Sukhotski et al. concluded cooler print beds led to a lack of strong

coalescence between layers due to the printing on a cooler substrate [28]. In the vertical print direction, the layers are smaller, therefore they print for less time within each layer.

Additionally, we suspect the vertical samples fracture due to delamination from one layer to another. The fractured surfaces of the horizontal prints exposed the shredded layers of the tensile specimens while the vertical prints had a much smoother fracture. Figure 33 shows the fractured surfaces from the two print directions.

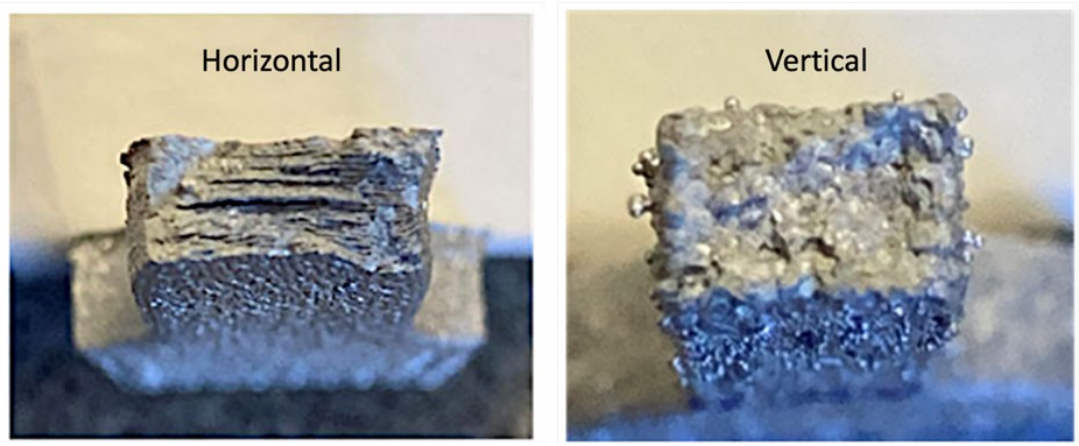

Figure 33. Fractured Surfaces of As-Printed Samples

Figure 34 shows the correlation of print direction to ultimate tensile strength when no post-print processing is conducted. The green dashed line represents A356.0 cast aluminum which is not subjected to any heat treatment [26]. We observed UTS that are similar to the published mechanical properties in the as-cast A356.0 in the Type-1 (big) samples. However, the Type-IV (small) samples in both the horizontal and vertical print directions were lower than the as-cast A356.0.

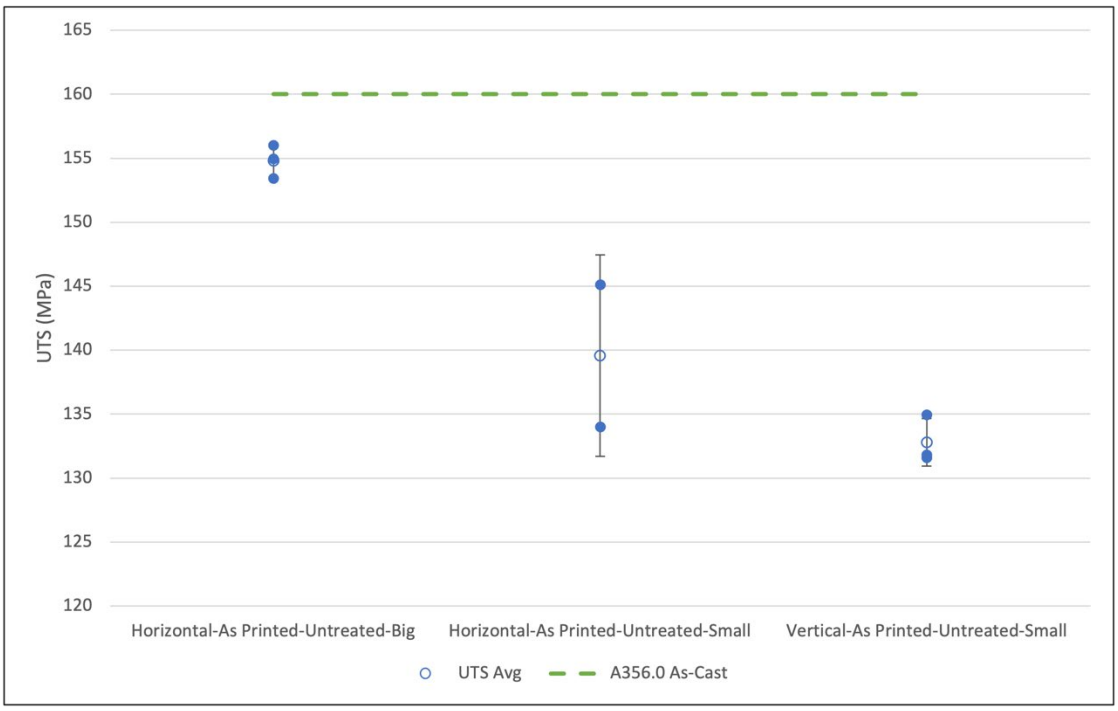

As-Cast A356.0 values taken from [26].

Figure 34. Ultimate Tensile Strength: Non-Treated Printed Tensile Specimens

b. Yield Strength

Like the UTS results, the average yield strength was higher in the horizontal (XY) print direction than in the vertical (Z) print direction for the samples which were of Type-IV (small) geometry (See Table 3). We hypothesize the yield strength for all three configurations was lower than reported values of yield strength due to the porosity within the printed samples and the effects of surface roughness. The optical microscopy finding will be discussed in the next section. The cracks and areas of voids likely led to reduced yield strengths in the as-printed tensile specimens. Figure 35 shows average yield strengths of the as-printed tensile specimens in both the horizontal and vertical print directions.

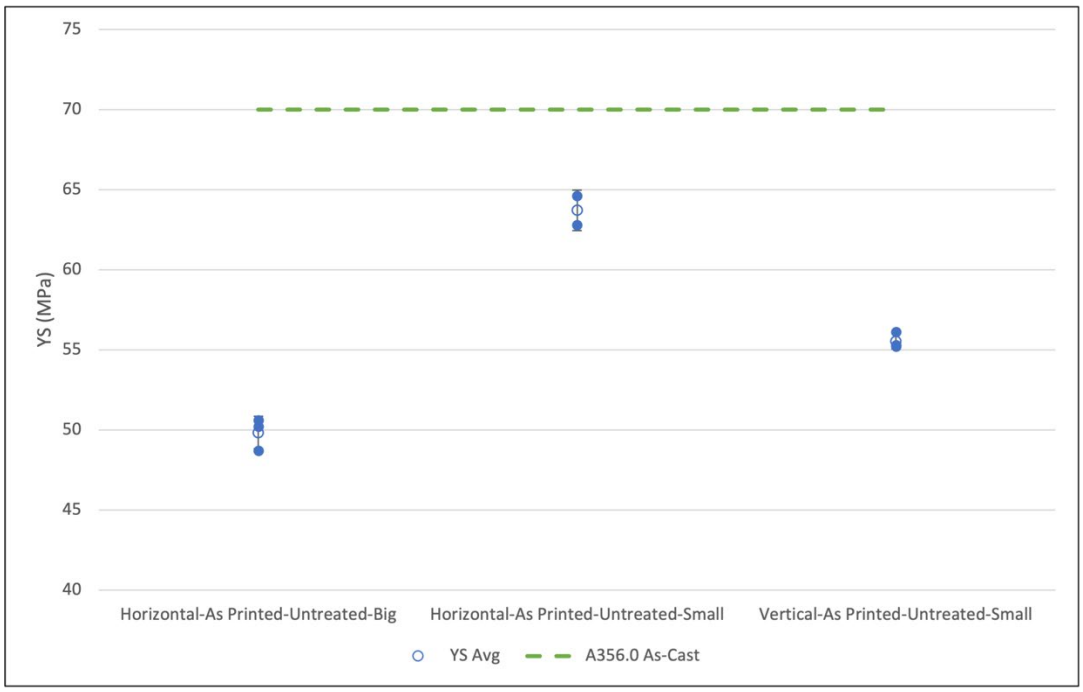

As-Cast A356.0 values taken from [26].

Figure 35. Yield Strength: Non-Treated Printed Tensile Specimens

c. Elongation Percentage

There was an increased elongation percentage between the vertical samples compared to the horizontal samples of the Type-IV geometries (See Table 3). The increased elongation percentage in the vertical samples is likely due to the intra-layer bonds yielding rather than completely separating. The larger (Type-I) horizontal printed tensile specimens had a much higher elongation percentage than those of the smaller (Type-IV) geometry printed in the horizontal direction. The lower elongation percentage is likely due to a smaller cross-sectional area with similar surface roughness and stress concentration factors of the larger samples. Figure 36 shows the elongation percentages of the different as-printed tensile specimens. All the samples exceeded the expected values of elongation percentage compared to as-cast A356.0.

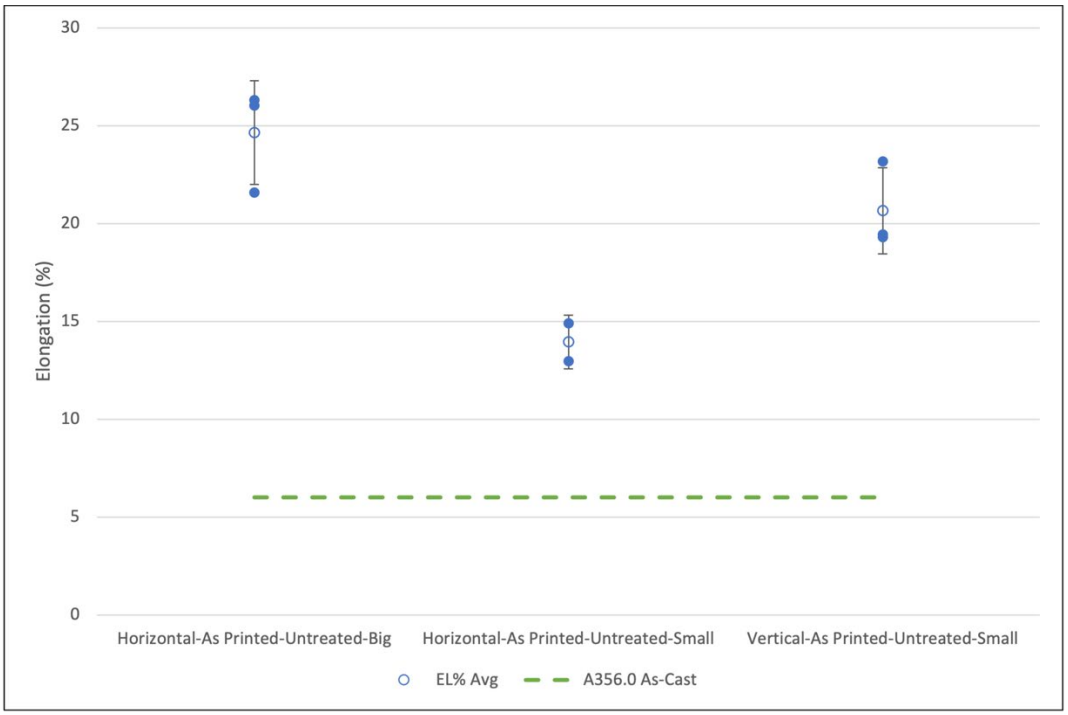

As-Cast A356.0 values taken from [26].

Figure 36. Elongation Percentage: Non-Treated Printed Tensile Specimens

3. Microhardness Results

Microhardness for Al-4008 has been observed from 60–105 HV depending on the heat treatment process. For as-cast A356.0, the Vickers Hardness has been reported to be 74.5 +/- 4.2 HV [29]. These samples, not being heat treated were expected to be near those values. The horizontally printed samples had a slightly higher microhardness when compared to the vertically printed samples, but there was no statistically significant difference in the hardness from horizontal versus vertical samples. Horizontally (XY) printed samples had an average microhardness of 54.24 HV (1.06 STD), while the vertically printed samples had an average microhardness of 53.3 HV (1.96 STD). Without heat treatment or other post-print processing, the microhardness of both the horizontally and vertically printed samples was as expected. Microhardness results can be seen in Figure 37.

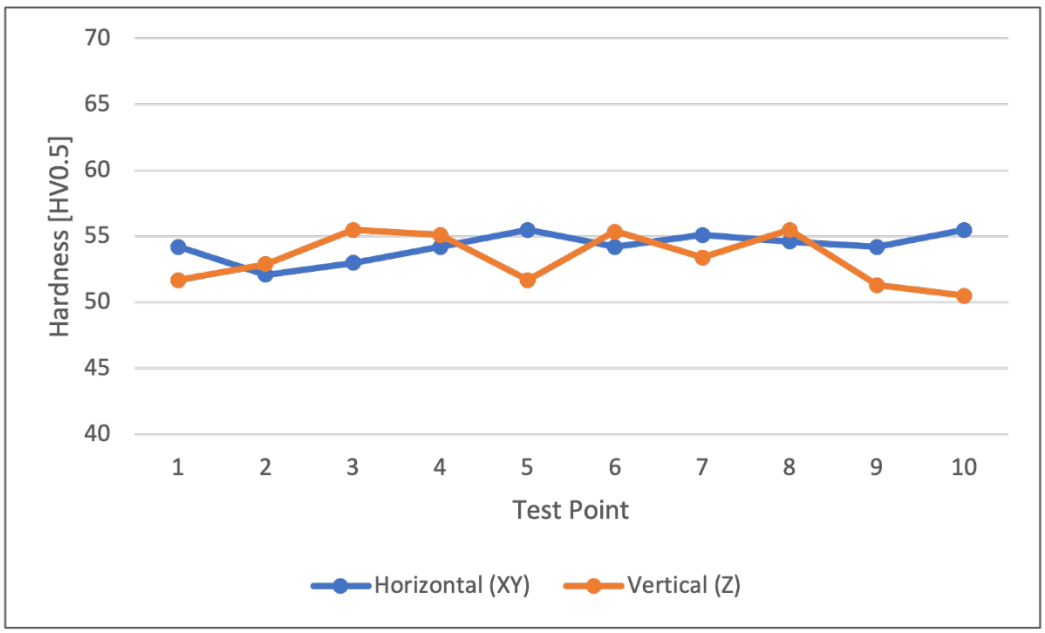

Figure 37. Vickers Hardness of As-Printed Tensile Specimens

4. Optical Microscopy

Optical microscopy highlighted the grains of the phases present in the as-printed samples. α+Si+Mg_2Si phases were observed as expected in both the horizontal and vertical print directions. Figure 17 shows the expected phases (referenced as the build plate). There was not an observable difference in the microstructure of the vertically printed samples from the horizontally printed samples, see bottom left and bottom right images in Figure 38. However, the presence of pores, cracks, and other defects were observed in both the horizontally and vertically printed samples.

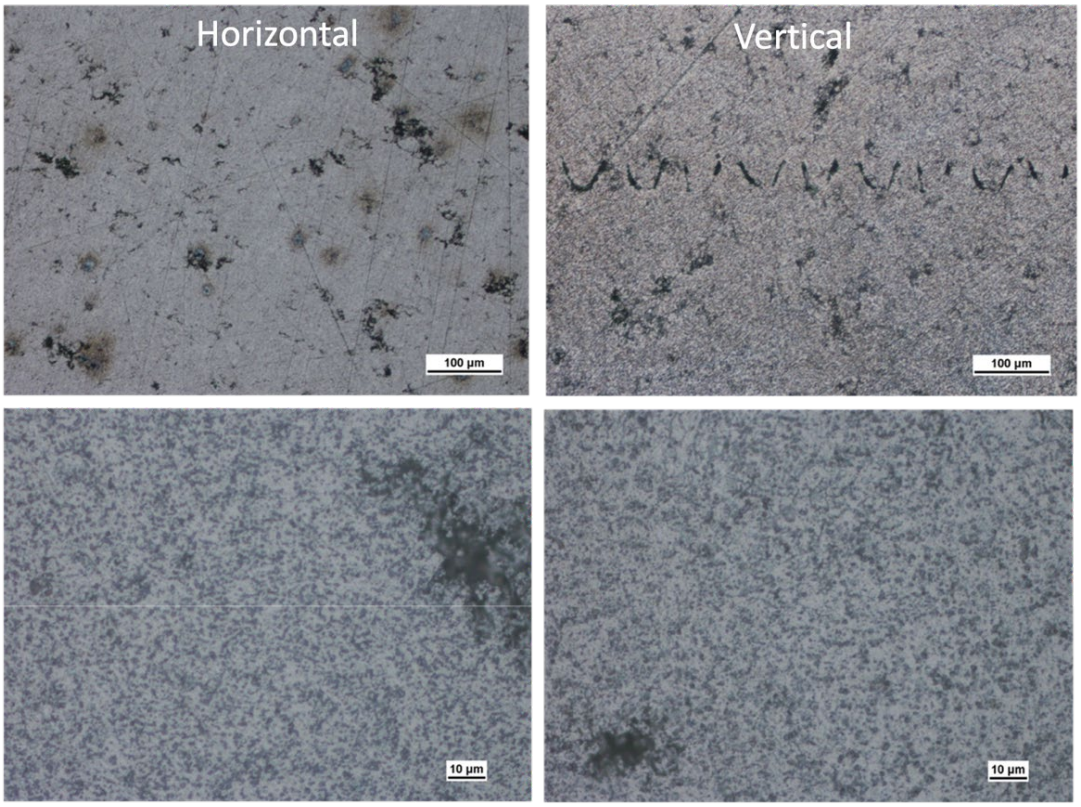

Top Left: Horizontally printed sample. Taken at 10x magnification. Top Right: Vertically printed sample taken at 10x magnification. Both horizontal (XY) and vertical (Z) printed specimens show indications of voids and cracks in various locations. Bottom Left: Horizontally printed sample taken at 50x magnification. Bottom Right: Vertically printed sample taken at 50x magnification. Both horizontal (XY) and vertical (Z) printed specimens indicate an evenly distributed microstructure.

Figure 38. Optical Microscope Images of As-Printed Horizontally and Vertically Printed Tensile Specimens

Pore analysis of the horizontally printed and vertically printed samples showed a smaller mean size of pores in the horizontally printed samples (32µm- 11.2µm STD) compared to the vertically printed samples (50µm- 20.6µm STD). Additionally, the horizontally printed samples showed a smaller maximum pore size (85µm) than the vertically printed samples (158µm). However, a crack of 237 microns was observed in the horizontal sample. Figure 39 illustrates the pores (dark areas) compared to the solid Al-4008 (white area) samples.

Pinholes have been identified in other studies from liquid metal aluminum disposition. Meda et al. observed this phenomenon with Al4043 after being deposited onto

a solid substrate [30]. They concluded there is less pinholes, with small diameters when a hotter solid substrate is used rather than on at room temperature. In this case, the build plate maintains 475°C, but the observed voids were embedded within higher areas from the build plate. It is possible the surface which the Al-4008 droplets are being deposited are cool enough to influence these voids.

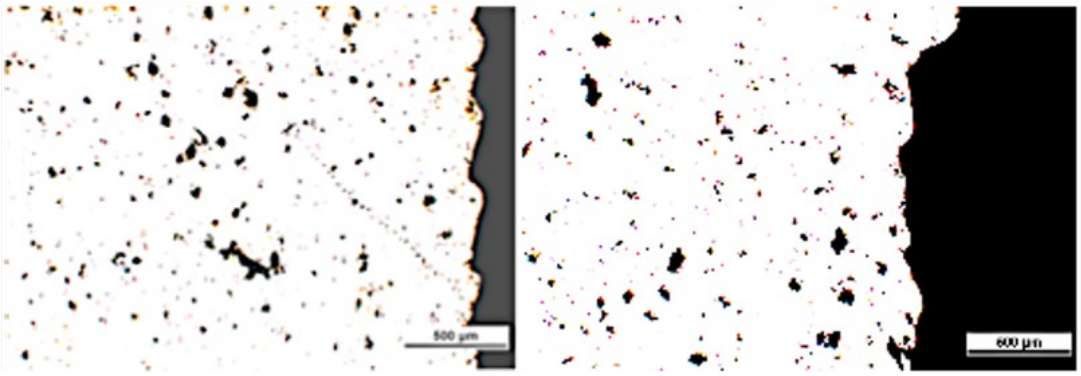

Figure 39. Pore Analysis of As-Printed Tensile Specimens

An increase in porosity has been linked to reduced performance characteristics in A356. Ran et al. state that one percentage (1%) of volume fraction porosity can lead to a reduction of 50% of the fatigue life and 20% of the endurance limit compared with the same alloy with a similar microstructure [31].

B. SAMPLES WITH POST PRINT PROCESSING: COMPARING HEAT TREATMENT AND SURFACE REFINEMENT

This section covers the samples that printed as tensile specimens to identify effects of T6 heat treatment and surface roughness reduction via sand blasting compared to the same samples printed without any post printing treatments. Samples were only printed in the horizontal direction to reduce print time and to reduce the risk of print failure. The MIL-A-21180D: Military Specification for Aluminum Alloy Castings, High Strength [27] Class 1 and Class 3 minimum standard are indicated on each graph.

1. Visual Inspection

The samples which were sand blasted were much smoother than before the surface treatment. Nearly all splatter and partially attached droplets were removed, including the first layer brims. The surface had a more matte finish than the as-printed samples as the reflective sheen was removed during the sand blasting process.

The heat-treated samples appeared stain with darker discolorations throughout the surface. The post print processes can be seen on the surfaces of the samples in Figure 40.

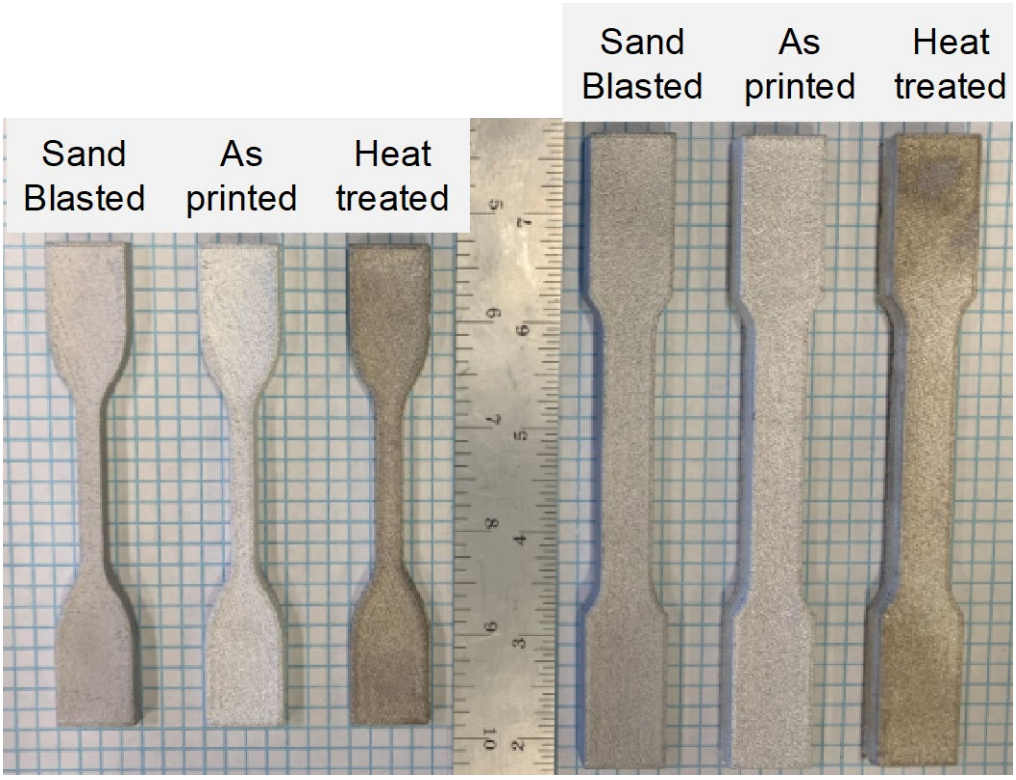

Figure 40. Surface Appearance: Post Print Processed Samples

2. Tensile Test Results

This section will discuss the tensile test results of the horizontally printed tensile specimens which were sand blasted or heat treated to the T6 heat treatment requirements. Table 4 highlights the material properties observed during the tensile test of the as-printed tensile specimens with post-print processing.

Table 4. Material Properties: Al-4008 Samples with Post-Print Treatments

	Type I: As Printed [MPa]	Type I: Sand Blasted [MPa]	Type I: Heat Treated [MPa]	Type IV: As Printed [MPa]	Type IV: Sand Blasted [MPa]	Type IV: Heat Treated [MPa]	As Cast A356.0 [MPa]	Class 1 MIL-A-21180D [MPa]	Class 3 MIL-A-21180D [MPa]
UTS	160.87	162.80	266.20	164.20	164.78	265.07	160	260	310
YS	50.3	55.2	158.6	75.3	82.3	152.0	70	195	235
EL%	26.8	25.3	22.2	22.6	19.8	16.2	6	5	3

a. Ultimate Tensile Strength

Ultimate tensile strength was nearly identical in the as-printed tensile specimens and the samples which were sand blasted to remove surface roughness for both specimen geometries. There was an increase of 1.2% in the Type-I (big) tensile specimens when the surfaces were sand blasted. The Type IV (small) tensile specimens had an increase of 0.35% in ultimate tensile strength following sand blasting. The reduction in surface roughness had very little impact on the ultimate tensile strength.

The samples that underwent the T6 Heat Treatment Process showed a much larger increase in Ultimate Tensile Strength. The Type-I had an increase of 65.47%, while the Type-IV samples increased 61.43%. In both geometries, the ultimate tensile strength increased to meet the MIL-A-21180D Class 1 minimum for A356. Class 1 and Class 3 are material strength classifications defined in MIL-A-21180D to distinguish higher material properties of the material for specific, often critical, applications. Figure 41 illustrates the effects of post-print heat treatment and sand blasting of the printed samples on their ultimate tensile strength.

Both Type-I and Type-IV heat treated samples exceeded the UTS of 230 MPa expected of A356-T6 samples [32].

Figure 41. Ultimate Tensile Strength: Heat Treated and Sand Blasted Printed Tensile Specimens

b. Yield Strength

There was roughly a 10% increase in yield strength to samples which were sand blasted versus those that were not sand blasted. In the Type-I (big) samples a 9.7% increase from 50.3 MPa (as printed) to 55.2 MPa (sandblasted) was observed. Additionally, in the Type-IV samples, a 9.3% increase from 75.3 MPa to 82.3MPa was observed (see Table 4). These observations indicate removal of surface roughness from 3D printed Al-4008, albeit small (sandblasting) will increase the yield strength. This is likely due to the reduction of stress concentrators on the surface of the sample. This could lead to a more visible indication of plastic deformation of the material due to material fatigue in the parts prior to catastrophic failure.

Both the Type-I and Type-IV samples which were T6 heat treated showed a large increase of yield strength from 50.3 MPa to 158.6 MPa (Type-I) and 75.3 MPa to 152.0 MPa (Type-IV). This represents a yield strength increase of over 3-fold and 2-fold for the different size samples.

The T6 heat treatment greatly increased the yield strength of the additively manufactured samples. As mentioned with the sand blasted samples, the T6 heat treated are more likely to show fatigue and deformation prior to catastrophic failure than those without post-print processing. Figure 42 illustrates the effects of post-print heat treatment and sand blasting of the printed samples on their yield strength.

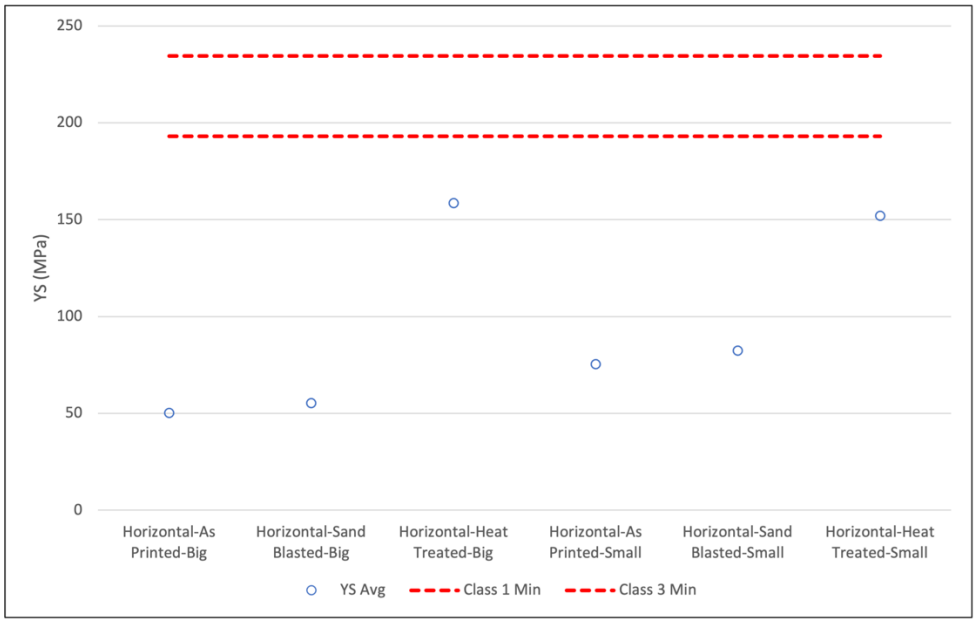

Figure 42. Yield Strength: Heat Treated and Sand Blasted Printed Tensile Specimens

c. Elongation Percentage

The elongation percentage of the as-printed tensile specimens was higher that the sand blasted samples and the T6 heat-treated tensile specimens. Sand blasted samples showed an average elongation percentage decrease from 26.8% to 25.3% for the large (Type-I) specimens and a decrease from 22.6% to 19.8% for the small (Type-IV) specimens. The T6 heat treated specimens showed a further decrease from 26.8% to 22.2% (Type-I) and 22.6% to 16.2% (Type-IV) in elongation percentage. The decrease in elongation percentage is due to the decrease in ductility of the heat-treated specimens. While the specimens increased in ultimate tensile strength after undergoing heat treatment, they also became less ductile. Barba et al. also reported the size difference in the tensile

specimens relating to the elongation percentages. The smaller the tensile specimen's cross-sectional area, the smaller the elongation percentage [20]. Figure 43 illustrates the effects of post-print heat treatment and sand blasting of the horizontally printed samples on their elongation percentage.

Despite the decrease in elongation percentage when the samples underwent a post-print process, all samples maintained an elongation percentage which exceeded Class 1 and Class 3 requirements as defined in MIL-A-21180D.

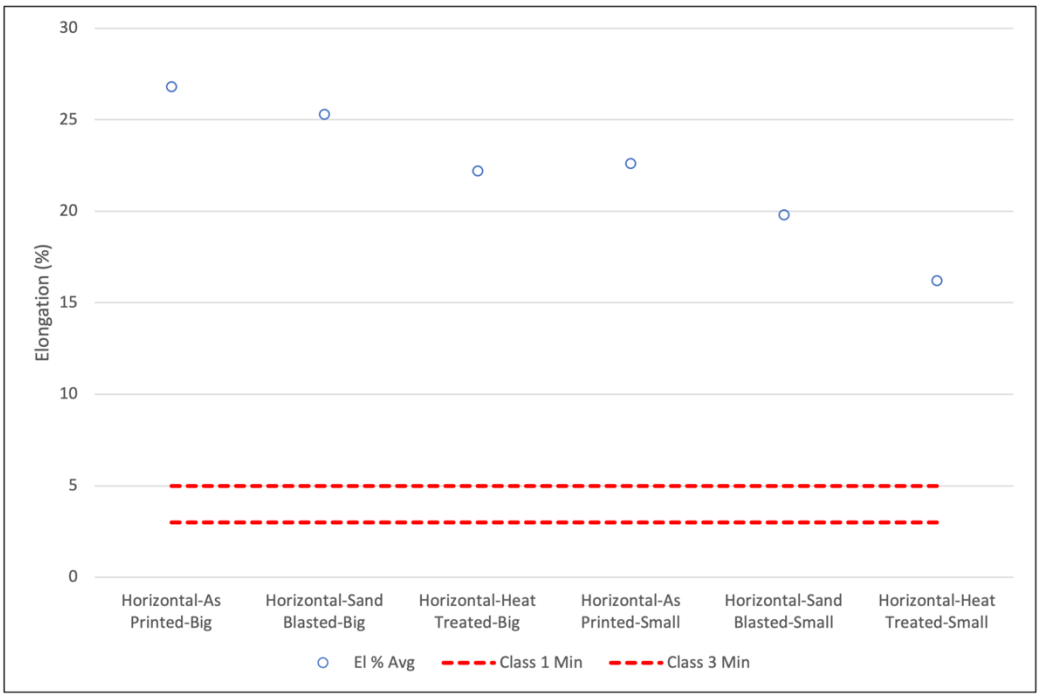

Figure 43. Elongation Percentage: Heat Treated and Sand Blasted Printed Tensile Specimens

3. Microhardness Results

This section discusses the microhardness analysis of the as-printed tensile specimens which underwent a T6 heat treatment. Samples which were sand blasted were not analyzed for microhardness because the samples were cut and polished to a flat, smooth surface prior to measuring microhardness which would negate any influence of the surface condition.

The samples which underwent a T6 heat treatment had an appreciable increase in microhardness compared to those which were left untreated. Vickers Hardness increased 86.02% from an average of 54.24 HV (1.06 STD) to an average of 100.9 HV (4.72 STD). Figure 44 illustrates those changes.

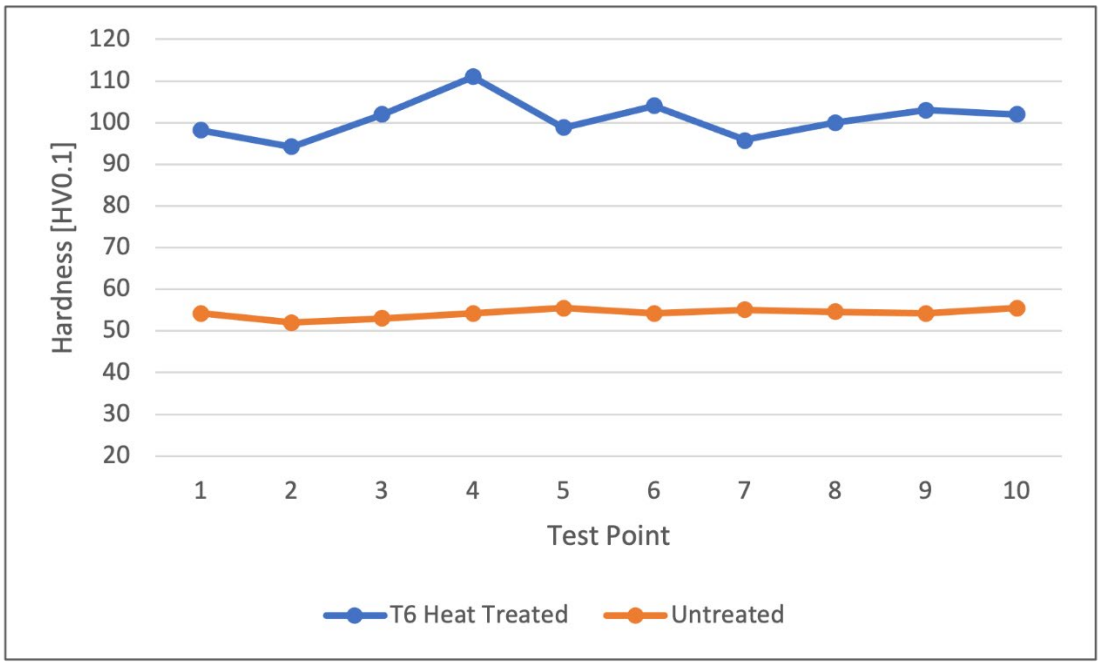

Figure 44. Vickers Hardness of T6 Heat Treated Tensile Specimens

4. Optical Microscopy

This section discusses the optical microscopy observations from the T6 heat treated printed tensile specimens. Since there was no change in microstructure of the Al-4008 due to sand blasting the surface, only the T6 heat treated samples were analyzed with the optical microscope.

Like the untreated specimens in section 1 of this chapter, the T6 heat treated samples also had areas of pores, cracks and internal defects. 0.5-5 µm voids were observed in the T6 heat treated samples. After the tensile tests, there were visible cracks connecting some of the pores, indicating high stress concentration areas and areas of reduced strength. Figure 45 highlights some of these observations. Some of these voids were in excess of

100 microns in diameter, which exceeded the size of the pores in the untreated samples. Despite larger pores in these samples, the ultimate tensile strength and yield strength were significantly higher in the T6 heat treated specimens compared to the untreated specimens.

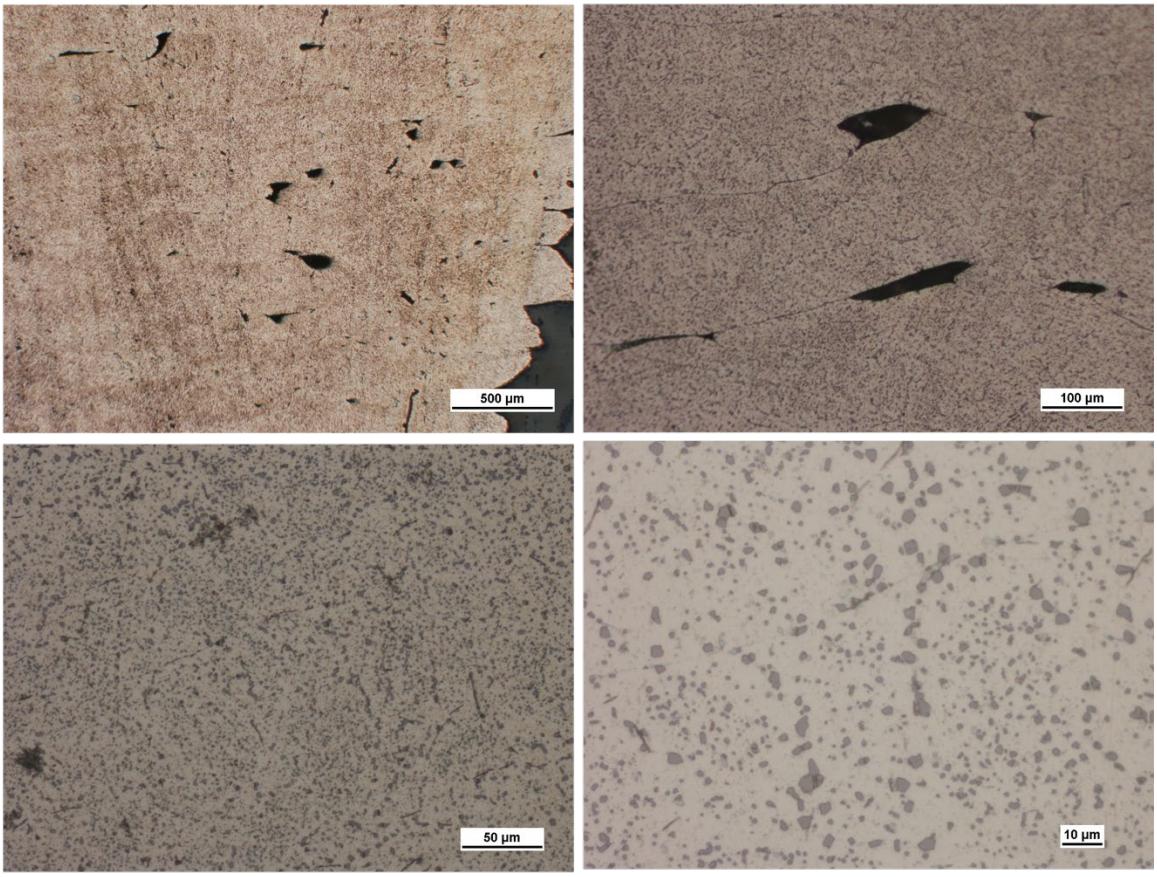

Figure 45. Optical Microscope Images of As-Printed Tensile Specimens with T6 Heat Treatment at Diverse Magnifications

The T6 heat treated specimens showed the α+Si and Mg_2Si phase at increased magnifications. This was expected after the precipitation hardening process in the T6 heat treatment. Additionally, the T6 heat treated samples had larger Silicon grains than present in the untreated samples. Figure 46 highlights the presence of these phases in the non-treated sample and a T6 heat treated sample. The Mg_2Si grains are the light-brown areas, while the Si grains are the darker brown areas. The α-Al is represented by the light tan area (background) that encompasses most of the sample.

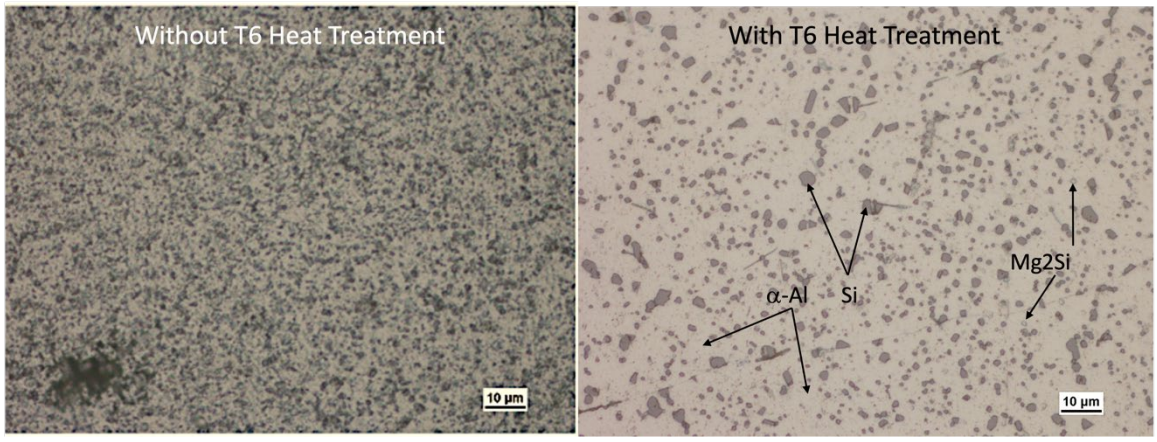

Figure 46. Optical Microscopic Images without T6 Heat Treatment and with T6 Heat Treatment with 50x Magnification

Silicon Phase grain sizes in the T6 heat treated samples were 1–5 microns, compared to >1 micron silicon grain sizes that were observed in the untreated samples.

5. X-Ray Diffraction

This section analyzes the XRD results from a printed tensile specimen that was T6 heat treated to that of an untreated sample.

Figure 47 highlights the 2-theta spectrum from 39.5 2-theta to 41.0 2-theta of an untreated printed sample and a sample which has complete only the solution treatment portion of the T6 heat treatment. The presence of the Mg_2Si phase is observed in the untreated sample and is absent following the solution treatment process. As observed in the optical microscopy analysis, the Mg_2Si phase is reconstituted during the precipitation hardening phases of the T6 heat treatment process.

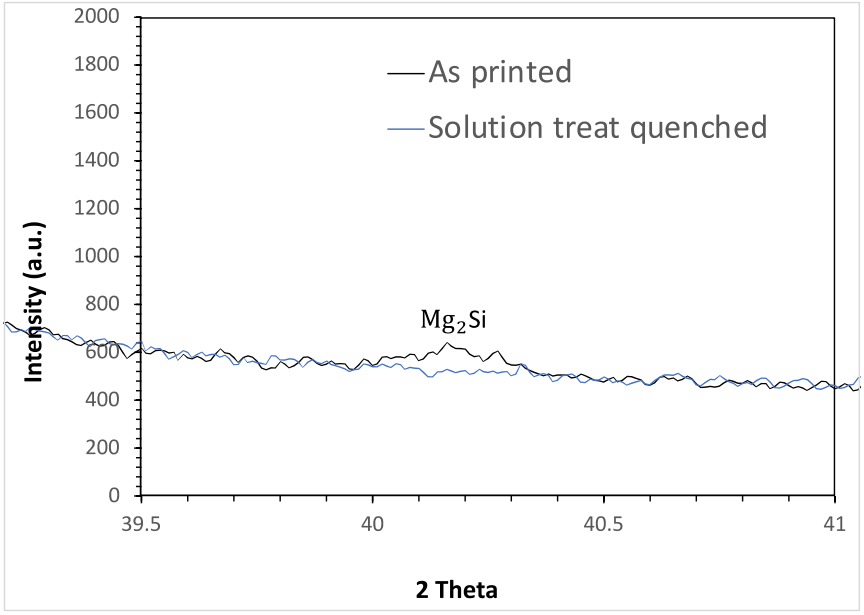

Figure 47. XRD Analysis Showing Presence of Mg_2Si in the As-Printed Sample

This is consistent with the expected phases present in the pseudo-binary phase diagram of AlSi7Mg0.3 [11] shown in Figure 48. The expected composition of Silicon is 7%wt +/- 0.5%wt in Al-4008. The vertical dashed line in Figure 48 shows the expected phases of the printed Al-4008 alloy as it is printed (825°C) and solidified/cooled to 475°C (heated print bed temperature).

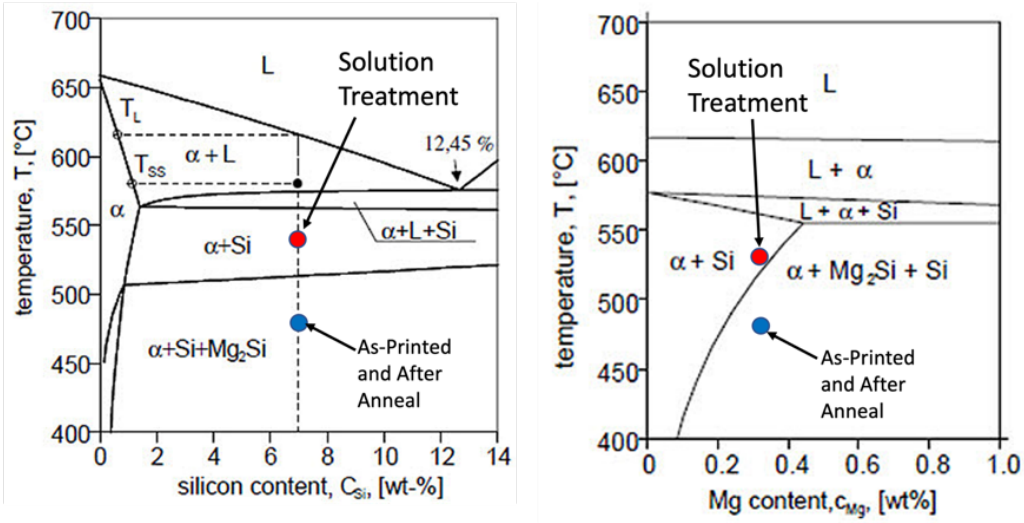

Figure 48. Pseudo-Binary Sections of the System AlSiMg0.3 Showing Phases Present During T6 Heat Treatment Process. Source [11].

During the solution treatment process, the samples were heated to 538°C and subsequently quenched, therefore the only stable phases following the solution treatment portion of the process are the α+Si phases. Thus, once solution treated, there is an absence of the Mg_2Si phase. This is consistent with the observed results of the XRD analysis. The reconstitution of the Mg_2Si phase occurs during the precipitation hardening process of the T6 heat treatment.

THIS PAGE INTENTIONALLY LEFT BLANK

IV. RESULTS: CIRCULAR CROSS-SECTION MACHINED TENSILE SPECIMENS

This section covers the testing results from the specimens which were printed as blocks in the vertical and horizontal positions, then underwent a T6 heat treatment before being machined into circular cross-sectioned tensile specimens. The industry standard is to machine the surface to minimize surface roughness effects and to have a uniform cross-section along the axis under tension.

The T6 heat treatment conducted on all these blocks was done to compare the material properties of the Al-4008 printed blocks to the ASTM standard equivalent of A356-T6. Each block was machined into three samples for a total of 24 test specimens. An outline of this chapter is in Figure 49.

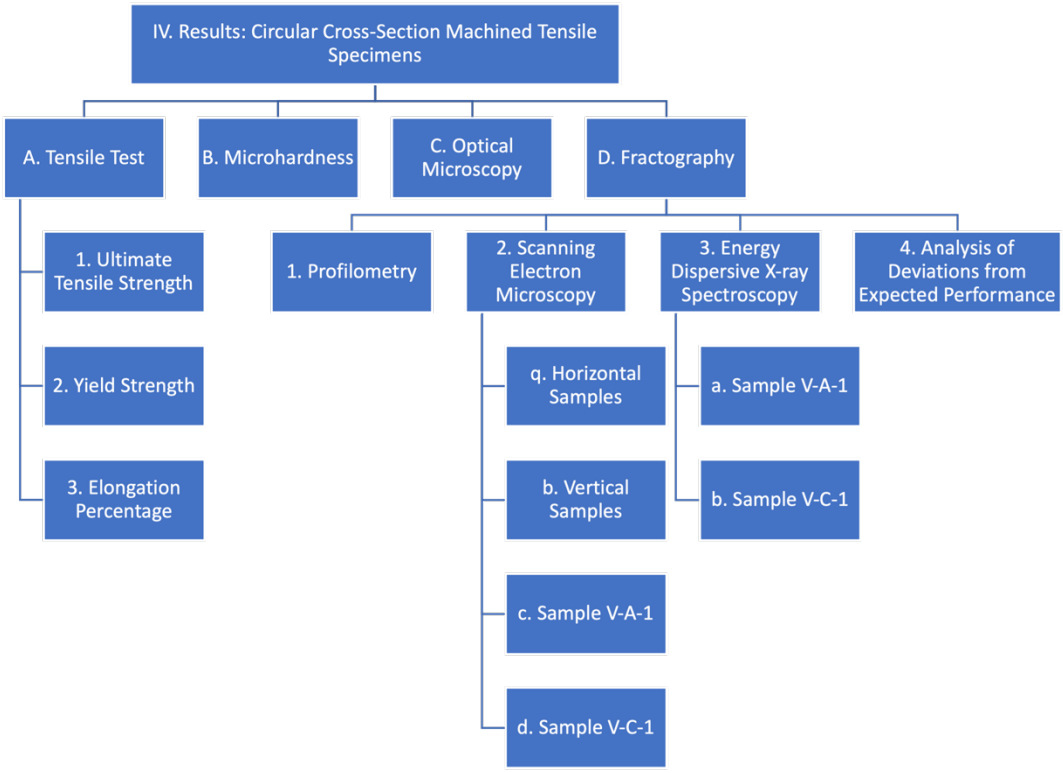

Figure 49. Circular Cross-Section Machined Tensile Specimens Results Chapter Outline

A. TENSILE TEST RESULTS

This section will discuss the Ultimate Tensile Strength, Yield Strength, and Elongation Percentage from the 24 tensile specimens which were machined from printed blocks in the horizontal and vertical print directions. Table 5 highlights the material properties observed during the tensile test of the T6 heat treated machined blocks.

Table 5. Material Properties: Samples Machined from Blocks with T6 Heat Treatment

	Hor: Block A [MPa]	Hor: Block B [MPa]	Hor: Block C [MPa]	Hor: Block D [MPa]	Vert: Block A [MPa]	Vert: Block B [MPa]	Vert: Block C [MPa]	Vert: Block D [MPa]	Class 1 MIL-A-21180D	Class 3 MIL-A-21180D
UTS (STD)	313.9 (4.15)	320.8 (1.73)	321.7 (2.21)	317.6 (4.09)	273.0 (17.4)	290.5 (1.19)	270.5 (24.7)	288.9 (1.31)	260	310
YS (STD)	217.4 (4.84)	228.4 (5.21)	227.9 (6.40)	219.7 (2.30)	209.6 (4.77)	211.9 (1.59)	209.3 (4.89)	220.7 (0.57)	195	235
EL% (STD)	14.3 (0.81)	14.8 (1.06)	15.5 (0.15)	16.4 (1.37)	4.9 (3.00)	7.2 (0.55)	4.9 (3.36)	6.2 (0.25)	5	3

Standard Deviations are in parenthesis.

1. Ultimate Tensile Strength

As observed in the as-printed samples, the samples machined from the horizontally (XY) printed blocks had a higher ultimate tensile strength than the samples machined from the vertically (Z) printed blocks. Overall, 22 of 24 samples machined (91.6%) met the MIL-A-21180D Class 1 minimum standard of 262.0 MPa (38 ksi) for ultimate tensile strength. 10 of 12 (83.3%) of the samples machined from vertically printed blocks met the MIL-A-21180D Class 1 standard while all the horizontal samples met the Class 1, including meeting the Class 3 minimum of 310.3 MPa (45 ksi). None of the 12 vertical samples met Class 3 minimum standard for ultimate tensile strength. This trend would indicate that only Al-4008 parts that are additively manufactured which are subjected to a tensile load parallel to the print direction would meet the Class 3 strength requirements. Parts experiencing a tensile load perpendicular to the print direction have shown to meet only the Class 1 requirements. B. Yang et al. had similar UTS results when testing A356-T6 under tension

[33]. Yang used the same geometry tensile specimen that was used in this research for the testing of A356-T6. Higher than cast UTS for additively manufactured A356 has also been observed in selective laser melting (SLM) processes. Kimura and Nakamoto reported the UTS of A356 in excess of 400 MPa due to the density of A356 following the process [34]. Like SLM, liquid metal printing has shown higher densities compared to cast A356. Using ImageJ, we found the density of the T6 heat treated blocks to be 99.80% (0.09% STD). The density Xerox® Elem™ Additive Solutions has measured the relative density of the liquid metal printed specimens as 99.73% (0.15% STD) using Archimedes method [35].

Figure 50 illustrates the effect of print direction on ultimate tensile strength. The standard deviation in these sample is less than 3 MPa except for vertical blocks A and C, which were the two blocks which had samples that failed to meet the MIL-A-21180D Class 1 minimum. The average UTS for all horizontal samples was 318.5 MPa (4.22 STD), while the vertical sample average UTS was 280.9 MPa (16.05 STD).

The two samples which failed to meet the MIL-A-21180D Class 1 minimum standards for ultimate tensile strength were further analyzed for cause of deviation from expected performance. This analysis will be discussed in future sections.

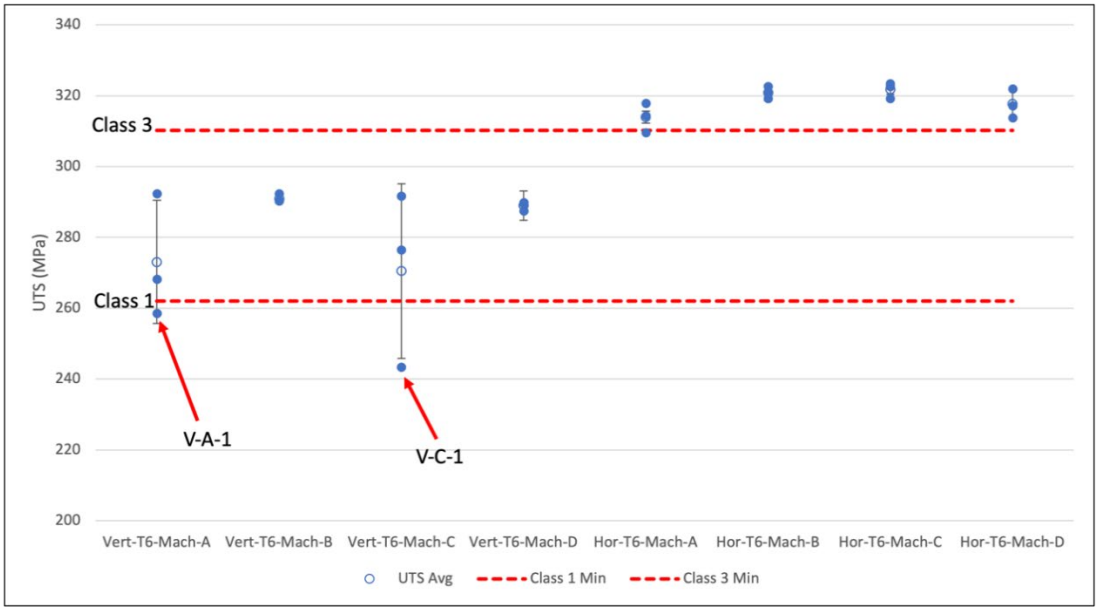

Figure 50. Ultimate Tensile Strength: T6 Heat-Treated Machined Blocks

2. Yield Strength

Yield strength in all 24 samples met the MIL-A-21180D Class 1 minimum standard of 193.1 MPa (28 ksi), but only 1 sample in the horizontal block C met the MIL-A-21180D Class 3 minimum standard of 234.4 MPa (34 ksi) for yield strength. The average yield strength for all of the horizontal samples was 223.3 MPa (6.57 STD) while the vertical samples had an average yield strength of 212.9 MPa (5.66 STD). Overall, there was a 4.88% increase in yield strength from machined samples in the horizontal position compared to the samples machined from vertical blocks. Figure 51 shows the yield strengths of the printed blocks, and the small standard deviations between the blocks.

As mentioned in the ultimate tensile strength section of this chapter, there were two vertical samples that failed to meet the MIL-A-21180D Class 1 minimum for UTS, however, both of those samples were within the MIL-A-21180D Class 1 minimum for yield strength.

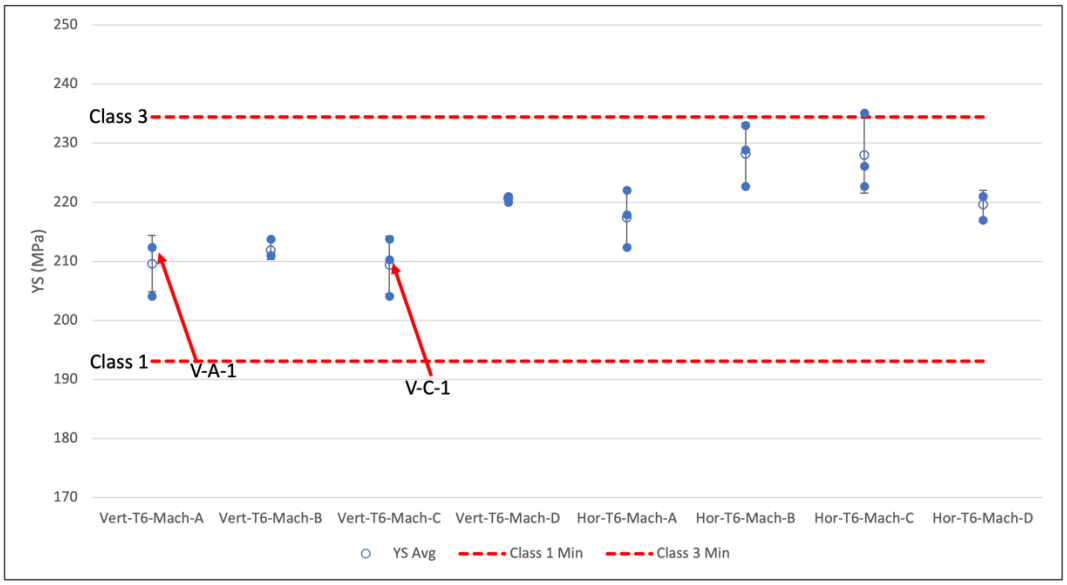

Figure 51. Yield Strength: T6 Heat-Treated Machined Blocks

3. Elongation Percentage

Elongation percentage varied greatly between the samples machined from horizontally and vertically printed blocks. Horizontal samples had more than double the percent elongation than the vertical samples. All 12 horizontal samples exceeded the MIL-A-21180D Class 3 minimum standard of 5% for elongation percentage. 8 of 12 of the vertical samples met the Class 3 minimum while 10 of 12 met the class 1 minimum of 3%. Figure 52 shows the breakdown of Percent Elongation amongst the printed blocks. Of the 4 samples that failed to meet the Class 3 minimum, 2 of the samples were from vertical block A and C each. As mentioned in the Ultimate Tensile Strength section, these blocks had samples which were below the Class 1 minimums for UTS and will be further analyze in future sections.

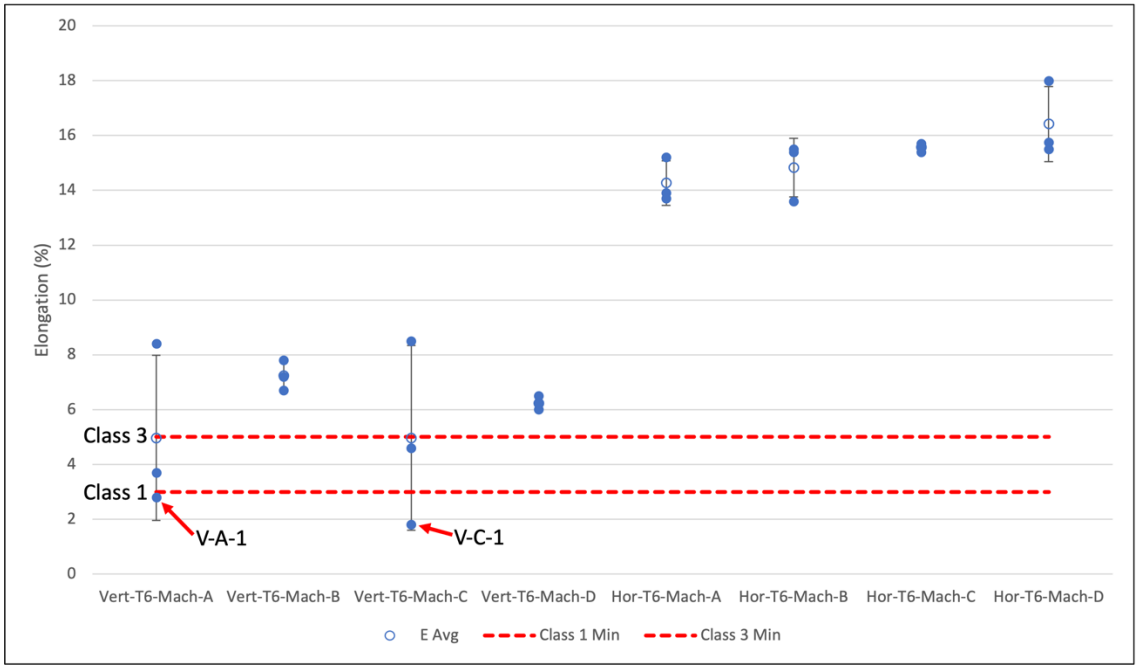

Figure 52. Elongation Percentage: T6 Heat-Treated Machined Blocks

B. MICROHARDNESS RESULTS

Microhardness was tested from vertical blocks and horizontal blocks after T6 heat treatments. Both horizontal and vertical samples had an average Vickers Hardness of 103

HV. Figure 53 highlights the similarity in microhardness between the two print positions. The standard deviation for the horizonal samples was 3.82 while the standard deviation for the vertical samples was 3.74. There was a consistency in microhardness throughout various locations within the sample.

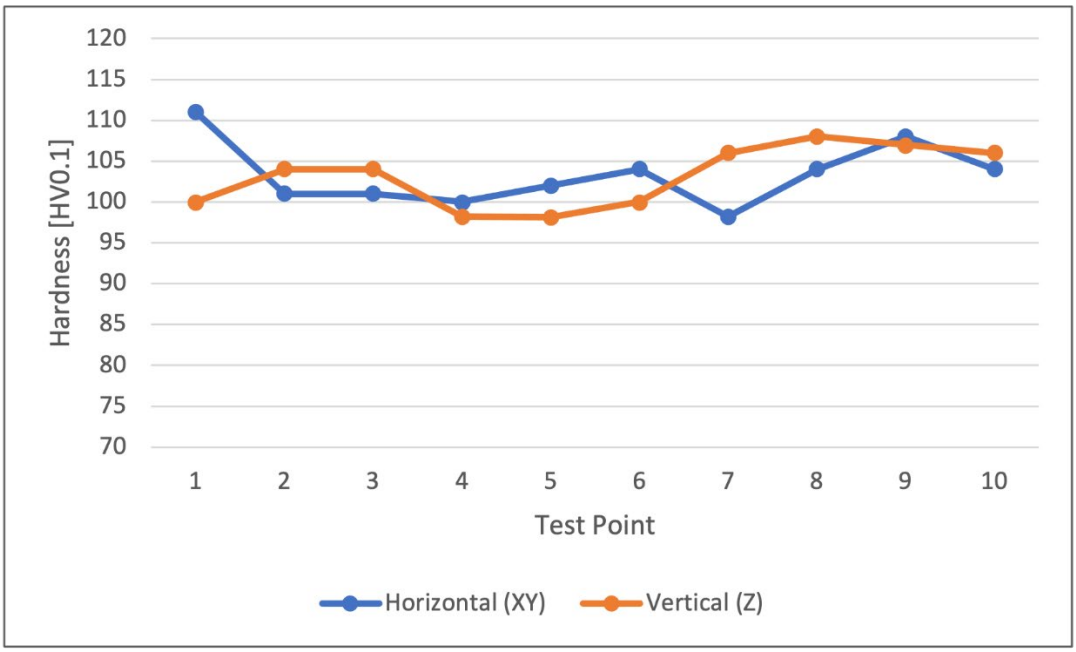

Figure 53. Vickers Hardness: Machined T6 Blocks

C. OPTICAL MICROSCOPY

This section discusses the results of the optical microscopy conducted on the samples which were machined form the T6 heat treated printed blocks. Additional, focused analysis was conducted on the two samples (V-A-1 and V-C-1) which fell below the MIL-A-21180D Class 1 minimum for ultimate tensile strength.

Similarly, to the as-printed samples, there was a presence of voids, cracks, and other defects throughout the samples in both the horizontal and vertical printing directions. However, there was a smaller concentration of defects in the majority of samples. Figure 53 shows images of a horizontal sample, vertical sample, and V-A-1 and V-C-1 at 2.5x

magnification. A uniform dispersion of phases is visible throughout the samples. The lack of fusion along the droplet edges can be easily observed in the V-C-1 sample.

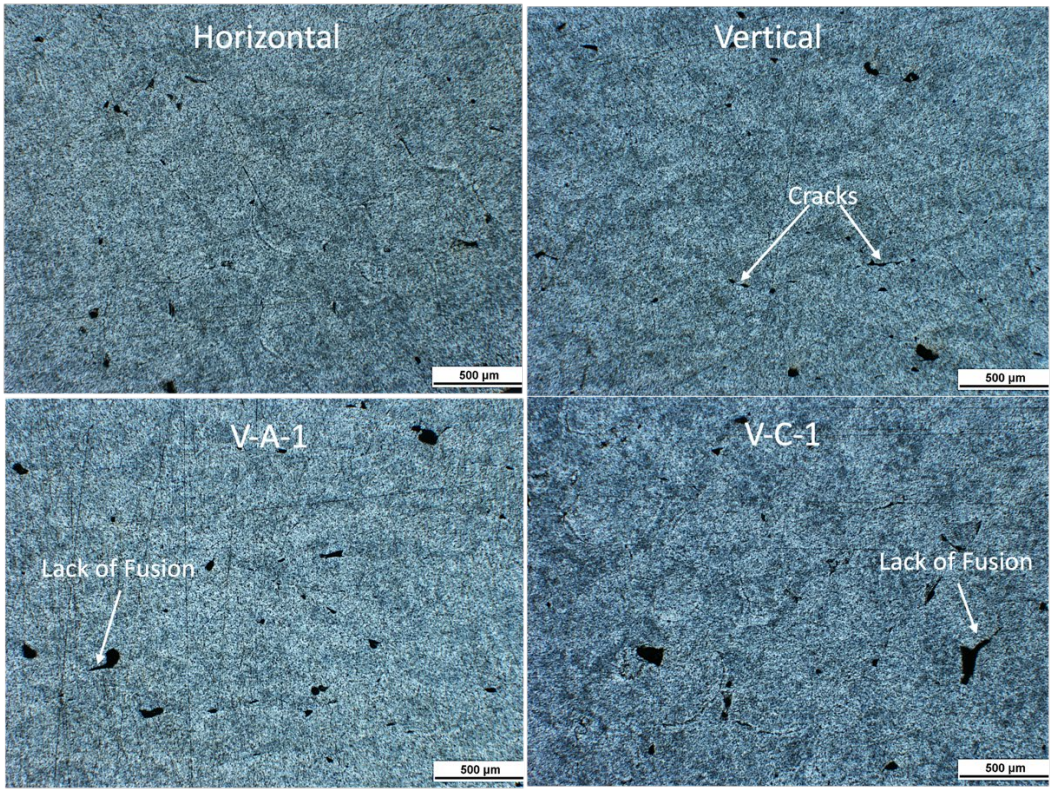

Figure 54. OM 2.5X: Machined Block Samples

As we increase magnification to 50x the observance on needle-like structures appears in both the horizontal and vertical samples. Research conducted by Mikolajczak explained these structures to be the β-Al5FeSi phase [36]. These structures were also observed by Xerox [37]. The targeted amount of Fe in the Al-4008 alloy is <0.09 wt%. Figure 55 highlights these needle-like structures. The horizontal sample has a much larger concentration of these β-Al5FeSi structures, appearing to interconnect like cracks. These structures start and/or stop at the silicon phase of the microstructure. Neither the concentration of these structures nor their lengths have any direct relation to the reduction in material properties as the horizontal and vertical samples shown to have more and longer needle-like structures than V-A-1 and V-C-1 which has lower mechanical properties.

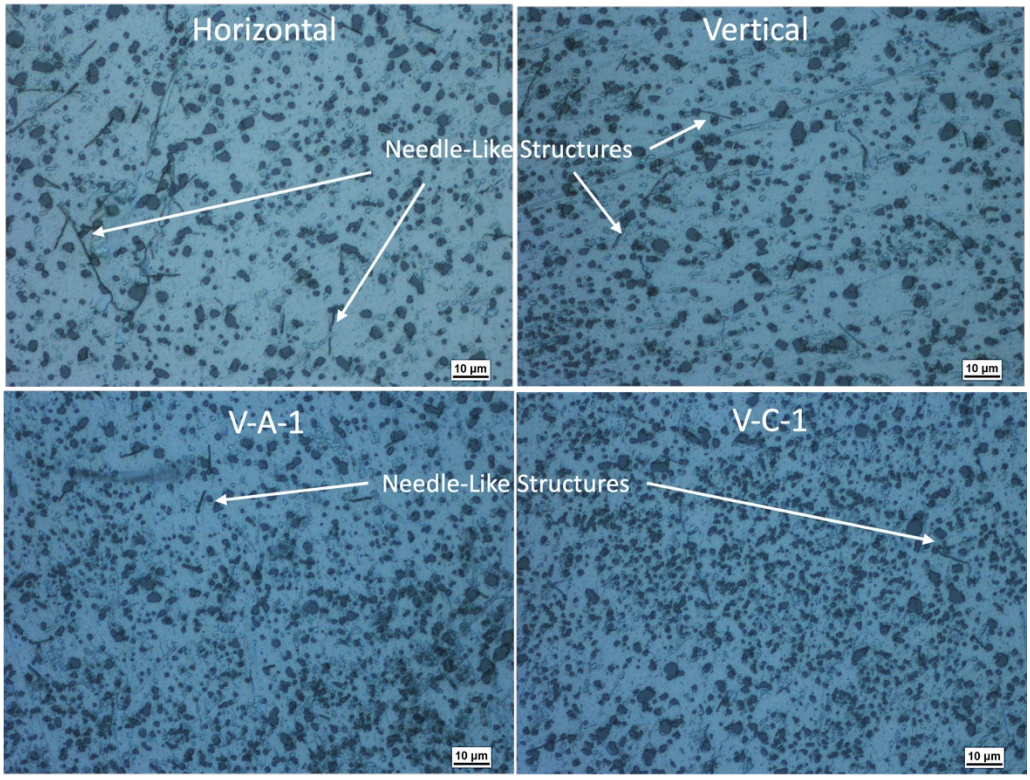

Figure 55. OM 50X: Machined Block Samples

Further increasing the magnification to 100x highlights the α+Si phases which dominate the microstructure and chemical composition. The Mg_2Si is also more visible at the higher magnification. Figure 56 outlines the phases present. The size difference in the silicon phase between the horizontal and vertical samples and V-A-1 and V-C-1 can also be observed. V-A-1 and V-C-1 both have a denser concentration of silicon phase, composing primarily of grains 2–3µm in diameter, while the horizontal and vertical samples have larger, more spread-out silicon grains 3–5µm in diameter. The needle-like structures appear to be multidirectional and randomly dispersed within the samples.

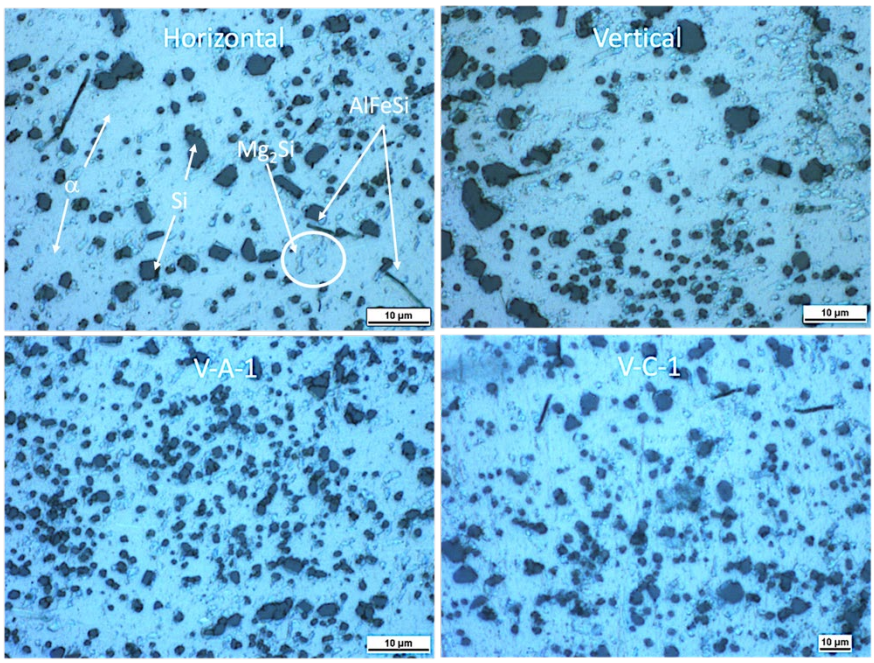

Figure 56. OM 100X: Machined Block Samples

Overall, there was very little differences between the horizontal and vertical samples. Both had areas of very uniform microstructures; however, both had a few areas with cracks, lack of fusion and voids. The needle-like structures appeared in both the horizontal and vertical samples.

The 2 samples whose ultimate tensile strengths were below the MIL-A-21180D Class 1 minimum standards showed slightly different density of silicon within the microstructures and contained larger voids and areas with lack of fusion compared to the samples that met the MIL-A-21180D standards.

The presence of α+Si+Mg_2Si phases was widely present as expected from samples that have undergone a T6 heat treatment process.

D. FRACTOGRAPHY

This section details the results and finding from fractographic analysis conducted on horizontal and vertical test specimens as well as the two samples which failed to meet the MIL-A-21180D Class 1 minimum standards for ultimate tensile strength, V-A-1 and V-C-1. Using profilometry, scanning electron microscopy (SEM) and Energy-Dispersive

X-ray Spectroscopy (EDS) we were able to identify probable causes for fracture promulgation which occurred prior to expected ultimate tensile strength in samples V-A-1 and V-C-1.

1. Profilometry

Profilometry images were provided by Xerox® Elem™ Additive Solutions [35]. Profilometry of the vertical samples showed a relatively smooth profile which verified the sample separated between printing layers, unlike the horizontal samples. Further analysis of the images shows a discoloration, almost stain-like spots that appear on V-A-1 (see Figure 57) and V-C-1 (see Figure 58). These spots do not show up on any other samples within the sample printed blocks. These stained spots correlate to the locations that will be identified in the SEM section as the areas of foreign material. Figures 57–58 also show the profilometry maps of the vertical samples fractured surfaces. It is believed that such defects were caused by inconsistencies in the jetting conditions, called ‘sputtering” at the printer at the time of the part fabrication [35].

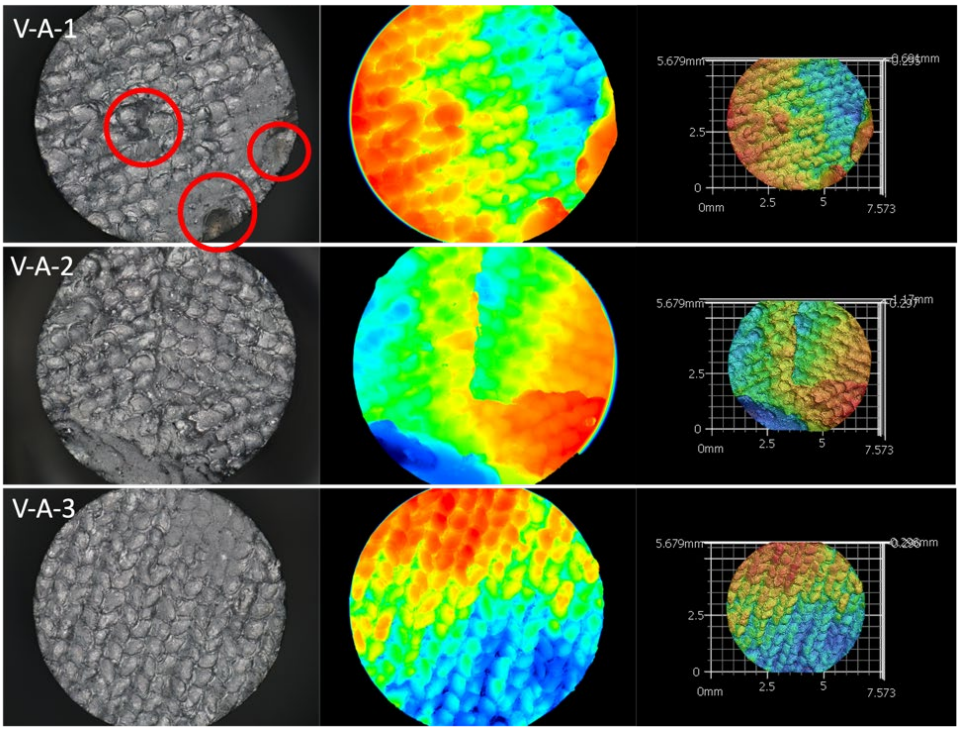

Figure 57. Profilometry of Sample V-A-1, SampleV-A-2, and Sample V-A-3

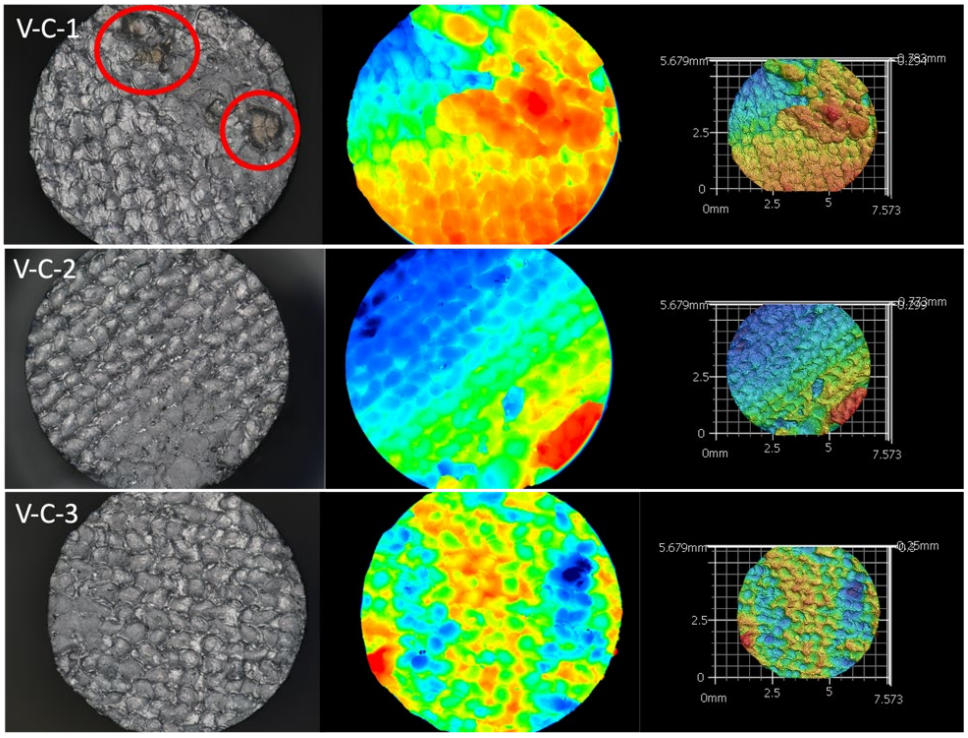

Figure 58. Profilometry of Sample V-C-1, Sample V-C-2, and Sample V-C-3

2. Scanning Electron Microscopy

This section details the results from the analysis conducted using the scanning electron microscope (SEM). The fracture surface of samples V-A-1 and V-C-1 were analyzed to aid in determination of the causes of failure which were pre-mature when compared to the other samples printed in the same conditions.

a. Horizontal Samples

The fracture surface from tensile testing on the horizontal samples showed the print layers during manufacturing. In all samples, there were layers that could be observed showing lack of fusion and delamination from the tensile testing process. Figure 59 (left) highlights the print layers from a horizontal sample, with several layers showing gaps between layers. Some of these gaps are due to delamination during the tensile testing,

however others, see Figure 59 (right) show lack of fusion between layers during the printing process.

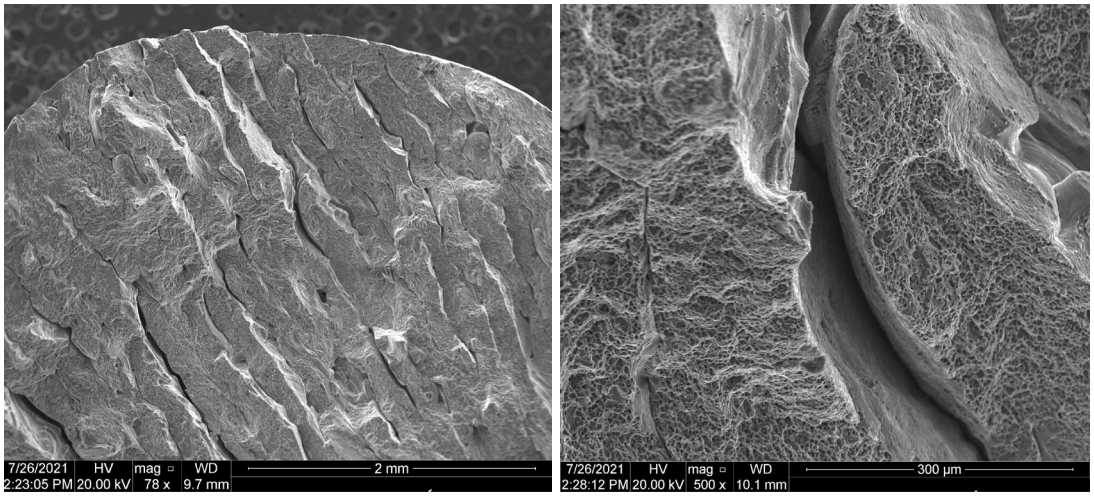

Left: The layers can be observed as well as areas where there is lack of fusion between the layers. Right: Lack of fusion was observed between some of the layers.

Figure 59. Fracture Surface: Horizontal Block Sample

The fractured surfaces on the horizontal samples were all very rough and jagged in texture (see Figure 59) due to every layer having to be broken to complete the fracture. In these samples, the fracture surfaces are dominated by cup and cone fractures which are indicative of ductile fractures, see Figure 60. In Figure 61, the cup and cone markings can be seen around the void in the left photo while the photo on the right shows an un-adhered droplet in a pocket of lack of fusion.

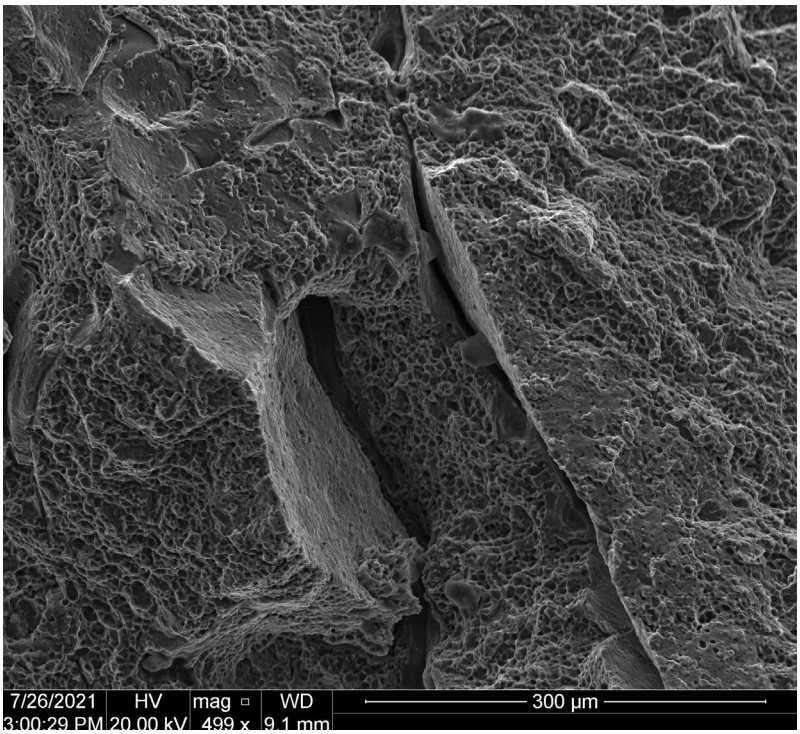

The cup and cone formations dominate the fractured surface area.

Figure 60. Fracture Surface: Horizontal Block Sample

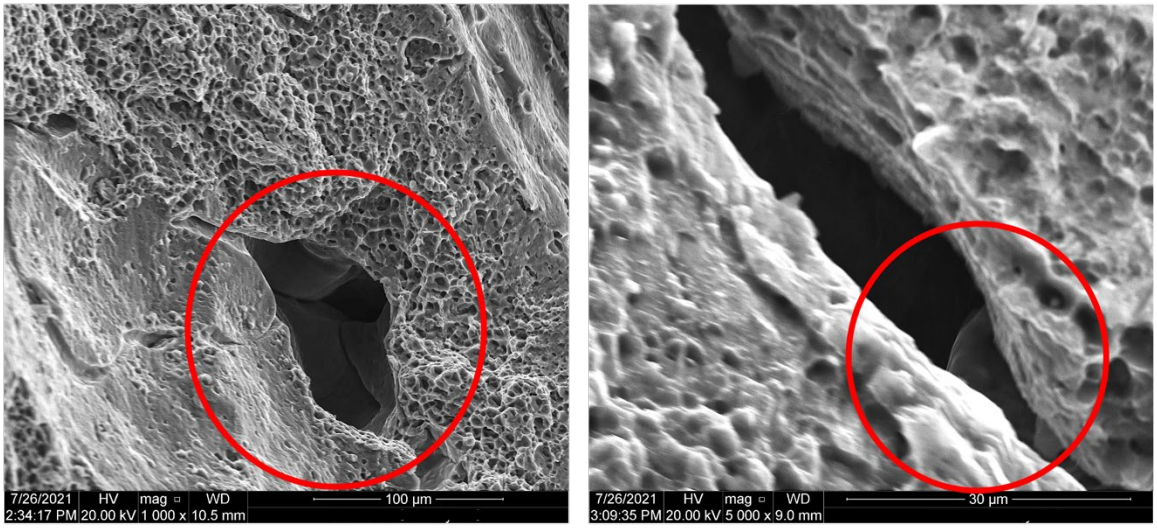

Left: Porosity up to 50µm x100µm can be observed in the sample. Right: A non-adhered droplet can be observed between layers.

Figure 61. Horizontal Sample A: Porosity and Non-Adhered Droplets

b. Vertical Samples

The fractured surface on the vertical samples however were quite different from the horizontal samples. These samples all had a relatively smooth fractured surface, always fracturing between two layers. The smooth fractured surface had indications of brittle fracture. In each vertical sample, the droplet overlay within each print layer can be observed on the fractured surface. This cellular microstructure on the fracture surface can be seen in Figure 62 and has been observed in other aluminum alloys in the SLM additive manufacturing process [38]. Additionally, lack of fusion between droplets can be observed in multiple locations throughout the fractured surfaces.

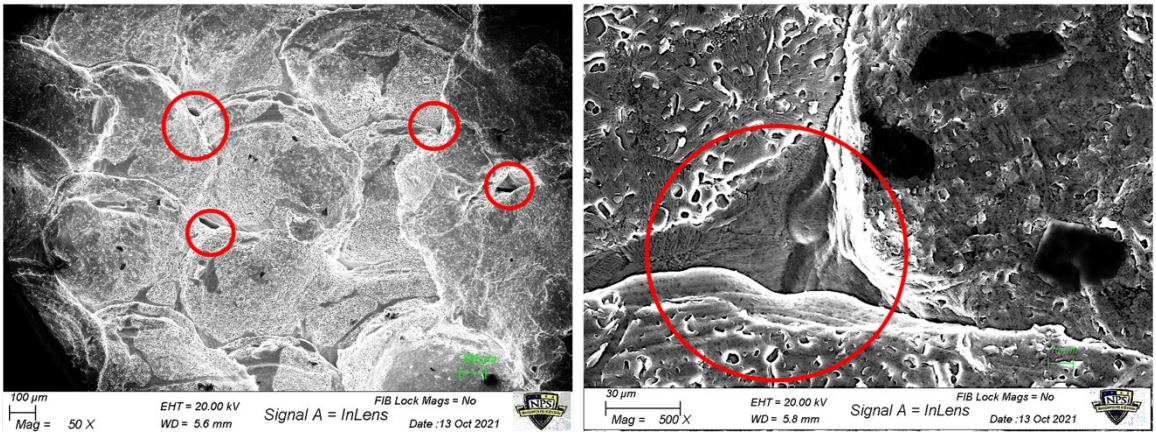

Figure 62. Fractured Surface: Vertical Machined Block

c. Sample V-A-1

Sample V-A-1 had a smooth fractured surface, consistent with other vertical samples, however an abundance of impurities were observed to be distributed within the outermost layer on the fracture surface. A high concentration of these impurities were located at and around the fracture initiation location, as can be observed in Figure 63. These impurities hadn't been observed in any other samples before.

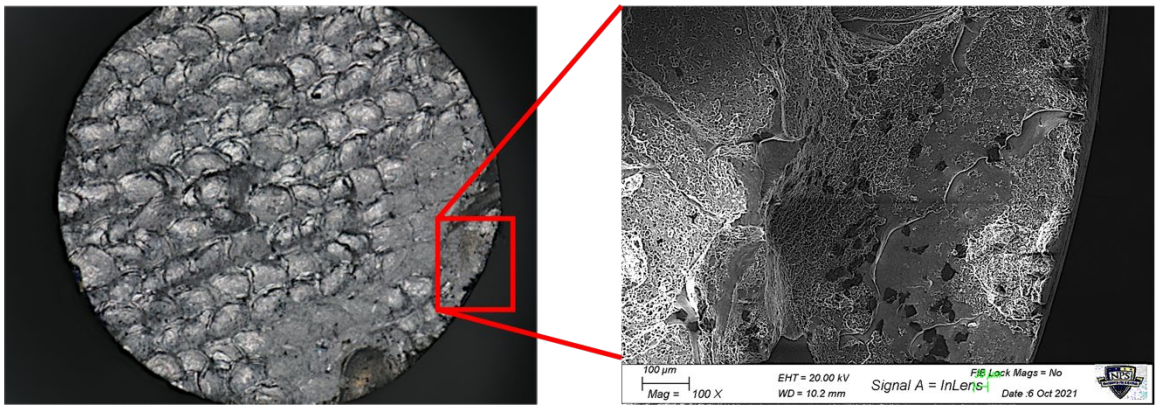

Figure 63. Vertical Sample V-A-1 with Sectors of Impurities

These impurities ranged in size between 20–40µm and had defined edges to them. Unlike the samples we have observed before which contained porosity or had areas of lack of fusion, this sample contained a foreign material, and well concentrated in the area of fracture initiation. These impurities were found in 3 areas on the fractured surface of sample V-1-A, but were most dense in the area surrounding the failure initiation spot. Figure 64 shows the impurities near the edge of the tensile specimen and their proximity to the fracture initiation area.

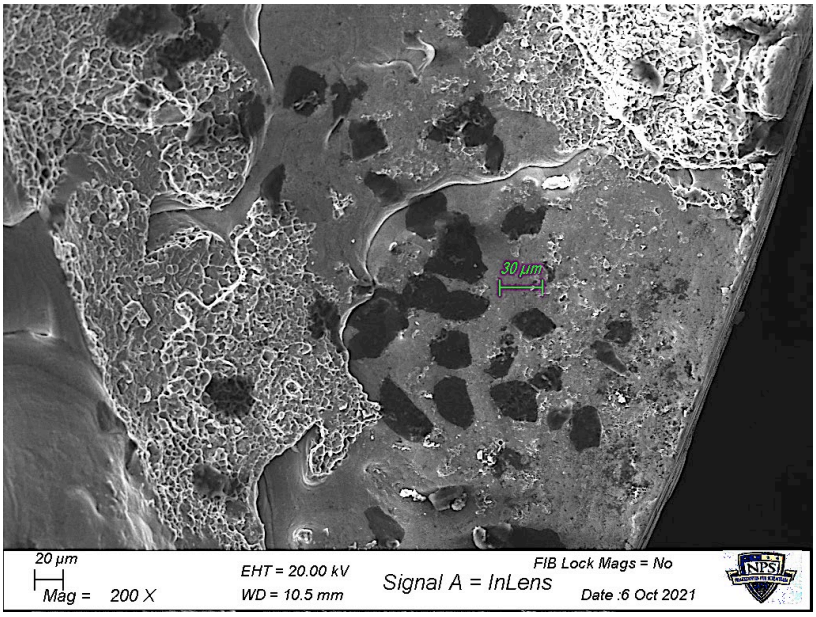

Figure 64. Sample V-A-1 with Concentrated Impurities

d. Sample V-C-1

Like sample V-A-1, sample V-C-1 also contained the similar looking impurities on the fractured surface. Although the concentration of these impurities was significantly less than those present on V-A-1, the size of the impurities observed on this sample were much larger (up to 90µm in length). The impurities in sample V-C-1 can be seen in Figure 65.

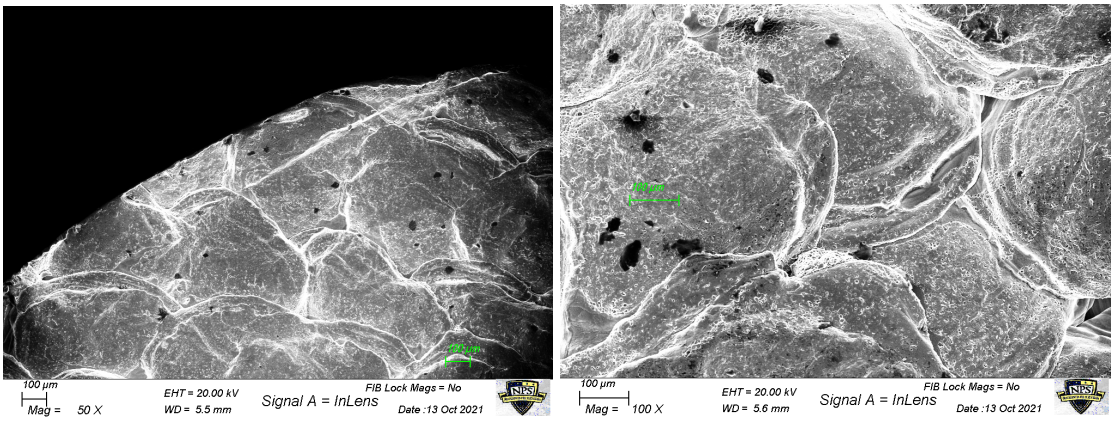

Figure 65. V-C-1 Fracture Surface

3. Energy-Dispersive X-ray Spectroscopy

Energy-dispersive X-ray spectroscopy (EDS) was used aid in identification of the impurities discovered in samples V-A-1 and V-C-1. Different spots were analyzed in each sample to compare the dark impurities from the base material.

a. Sample V-A-1

There were five total spots analyzed with EDS to determine elemental composition of the local areas in sample V-A-1. Figure 66 illustrates the spot selection for the EDS analysis.

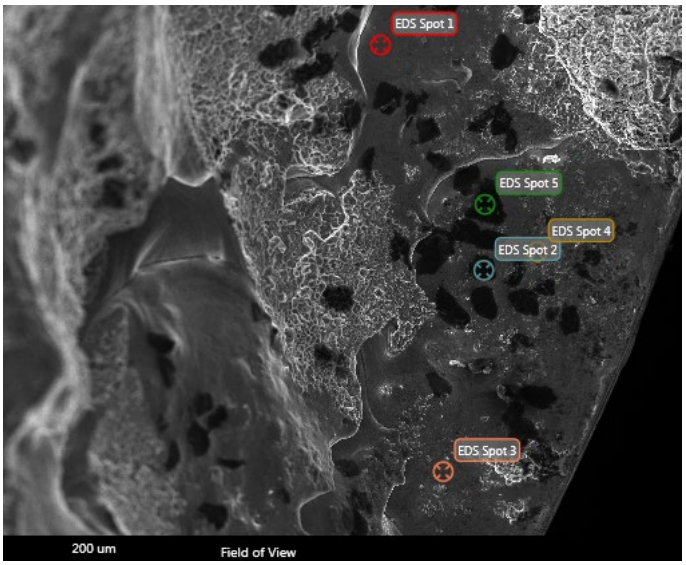

Figure 66. V-A-1 EDS Spot Sample Locations

Spot 1 was chosen because it represented and area of the based material and would provide a baseline of the non-impurity-based material. This location's spectrum provided expected compositional results as it consisted mainly of aluminum, silicon, and magnesium. These are the primary element in the composition of Al-4008, see Table 1 in chapter 1. There were no other elements detected in this localized area.

Spots 2–5 were selected because they were one of the many dark impurities observed in the SEM analysis. The spectrums of these location had the expected aluminum, silicon, and magnesium elements, but also contained carbon, oxygen, and nitrogen peaks. These additional elements are not expected to be found in the composition of Al-4008. Additionally, Spot 3 and Spot 5 had larger than expected quantities of silicon. The spectrums for Spots 1–5 can be seen in Figure 67.

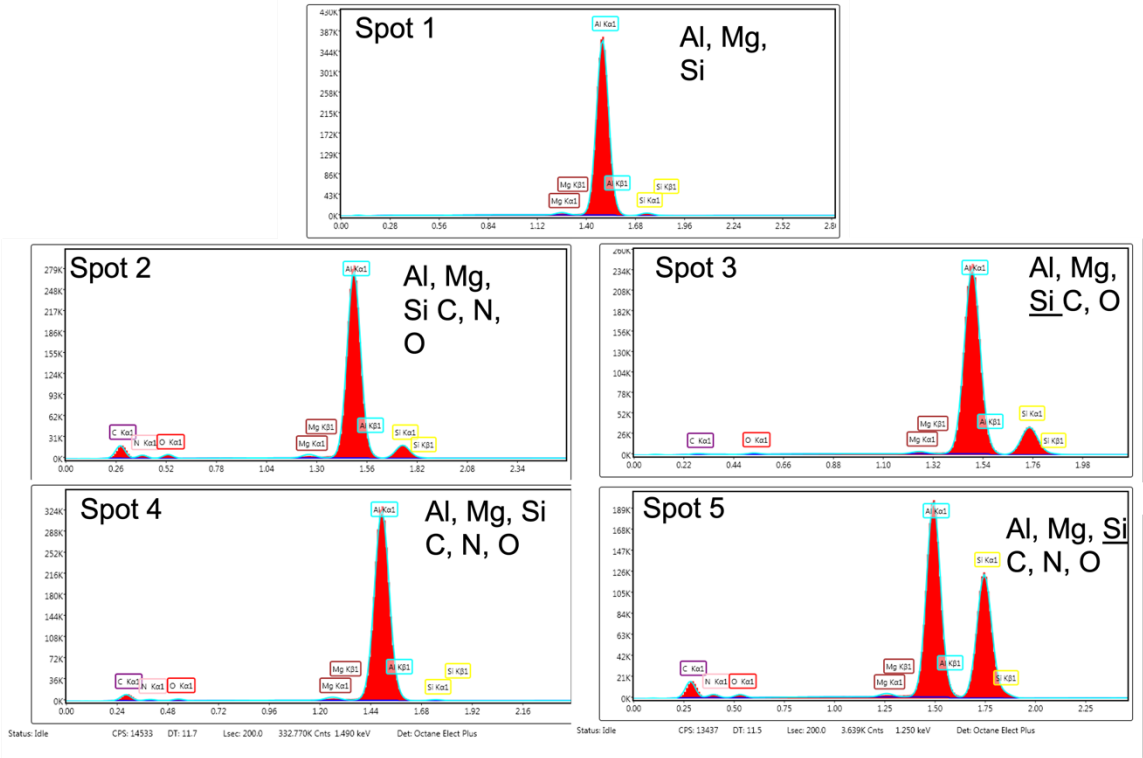

Figure 67. V-A-1 EDS Spot Analysis

Overall, it was determined the dark impurities that had been observed on the fractured surface of V-A-1 were comprised of carbon, nitrogen, oxygen, and increased amounts of silicon. These elements are foreign to the filler metal and not expected to be present in the printed block. Section 4 will further discuss the likely contribution of these elements. The likely cause of failure with this sample, lower than the other samples machined from the same block, is due to these impurities in combination with the lack of fusion and pores within the fractured surface. This combination with the concentration of these impurities in a localized area, imposed areas of higher stress concentration causing failure.

b. Sample V-C-1

A total of 7 spots were chosen to analyze the impurities located in sample V-C-1, which failed to meet the ASTM Class 1 minimum standard for ultimate tensile strength. Figure 68 illustrates the spot selection for the EDS analysis.

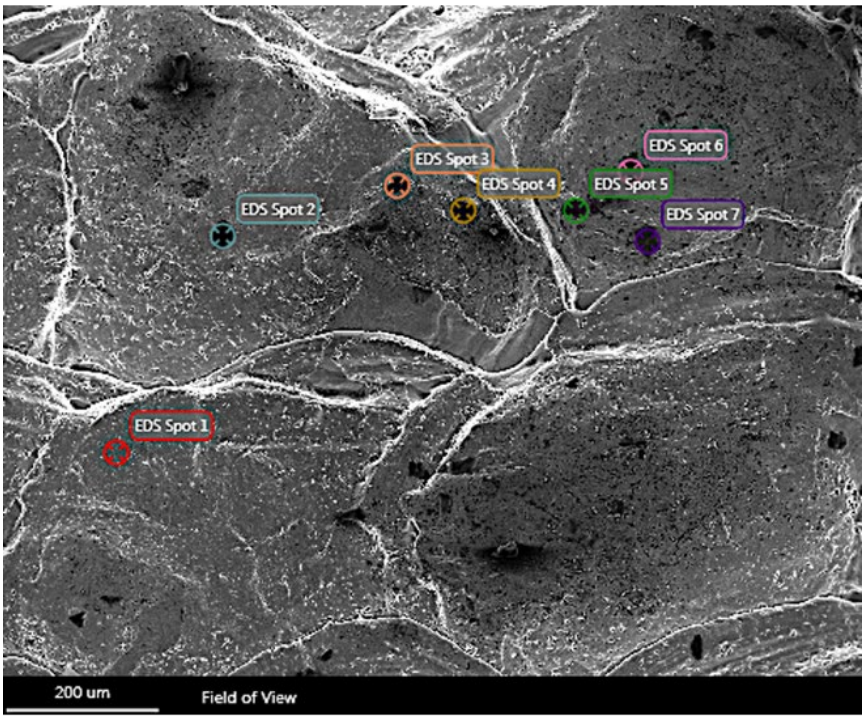

Figure 68. V-C-1 EDS Spot Sample Locations

The location of spot 1 was selected as a representation of the base material of the samples. As expected, the presence of Aluminum, Silicon, and Magnesium dominated the EDS spectrum, and no other elements were detected at this location. Spots 2–7 were taken at locations with visible inclusions. Like sample V-A-1, carbon, nitrogen, and oxygen were observed in nearly every location. In addition to those elements, we also observed chlorine and sodium in spots 3, 6, and 7. This is the first observation of those elements within any printed specimen. From Table 1, we know these elements are not native to the Al-4008 alloy. Further analysis in section 4 will help to identify a potential source for these elements. The spectrums for Spots 1–7 can be seen in Figure 69.

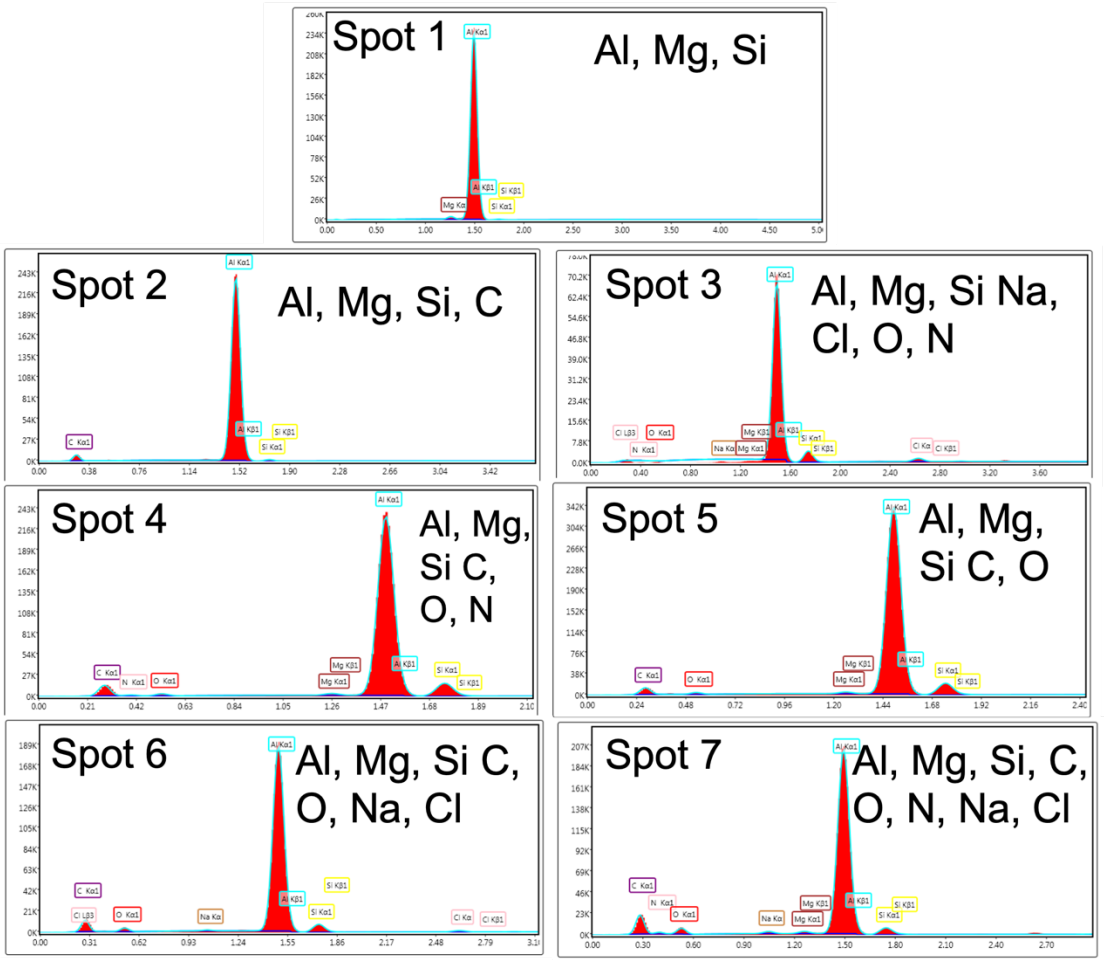

Figure 69. V-C-1 EDS Spot Analysis

Overall, there was a similar trend within each of the chosen dark spots-the presence of carbon, oxygen, and nitrogen. These elements were not observed within the base material nor are the expected in Al-4008. Like sample V-A-1, only the dark spot had these additional elements and only these 2 samples had the presence of this dark impurities peppered throughout the fractured surface. This sample is a from a vertically printed block, which as discussed prior, separate within the print layer when under tension. The presence of these impurities within a print layer, further reduces the bonding strength between the layers and causes earlier than expected failure compared to the other two samples (V-C-2 and V-C-3) produced from the same block. Further explanation of the introduction of these elements will be discussed in the next section.

4. Analysis of Impurities

As discussed in the fractography of samples V-A-1 and V-C-1, there was a presence of carbon, oxygen, and nitrogen within these samples. Oxygen and nitrogen introduction is believed to be a product of the atmosphere within the printing enclosure. Although argon is used as a shielding gas to the molten aluminum, the enclosure isn't completely sealed. In fact, the top of the enclosure is openly vented to the surrounding space. While the argon shields the molten Al-4008 in the nozzle, and the droplets as they are extruded from the nozzle, the print bed is a dynamically moving platform that doesn't stay under the protection of the argon shield. The surrounding air is the most likely candidate for the nitrogen and oxygen introduction to the printed material.

However, this doesn't account for the presence of the carbon. The mostly likely introduction of the carbon is from the graphite (carbon) nozzle. As mentioned in the introduction, one of the limiting factors for the size of the print capacity for the ElemX^{TM} printer is the mass of the print, not specifically the length, width, and height, dimensions. Although there are physical size limitations due to the print bed size, the primary printing limitation is the mass of the component being printed. This is due to the wear and tear of the nozzle orifice. Over time, the extrusion of the liquid metal droplets erodes the nozzle causing a change in the nozzle diameter and Lorentz forces, thus impacting droplet consistency and overall reducing print quality. These graphite nozzles are consumable and meant to be replaced frequently, usually each day, or within the same day if completing many prints.

Therefore, the nozzle and more specifically the filler metal within a used nozzle was analyzed for composition to compare to the impurities found in sample V-A-1 and V-C-1. The nozzle observed in this section was not used to manufacture the blocks which were machined into the tensile specimens; however, it was used in a 7-hour print for another project. Figures 70 and 71 show SEM images of a used nozzle tip with the melted, then resolidified Al-4008 filler material inside. Within the filler metal, several of the same impurities observed in sample V-A-1 and V-C-1 are observed.

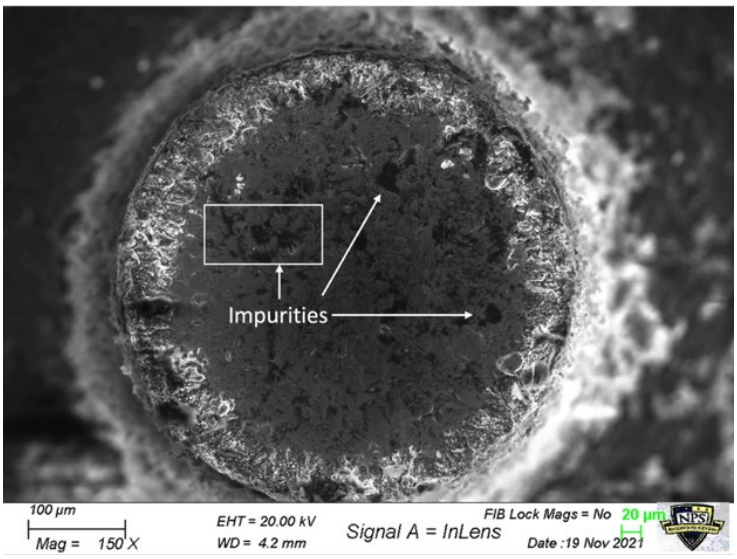

Figure 70. Used Nozzle with Al-4008 Filler Material Inside

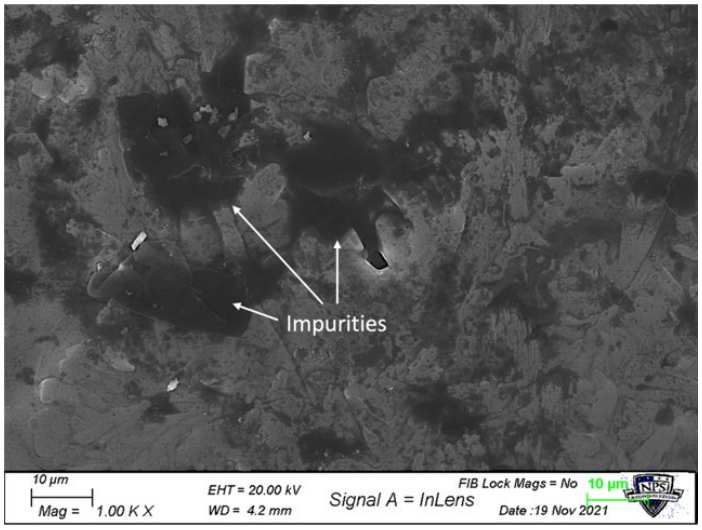

Figure 71. Impurities Found in Filler Material Within the Nozzle

EDS analysis was conducted on this area to determine the elemental composition of the area [39]. The areas of visible impurities showed consistent composition from the observed impurities located within samples V-A-1 and V-C-1. Figure 72 shows the EDS map of the local area, highlighting the presence of carbon in the specific dark areas, as well as oxygen and nitrogen, which could be observed in multiple locations within the mapped area.

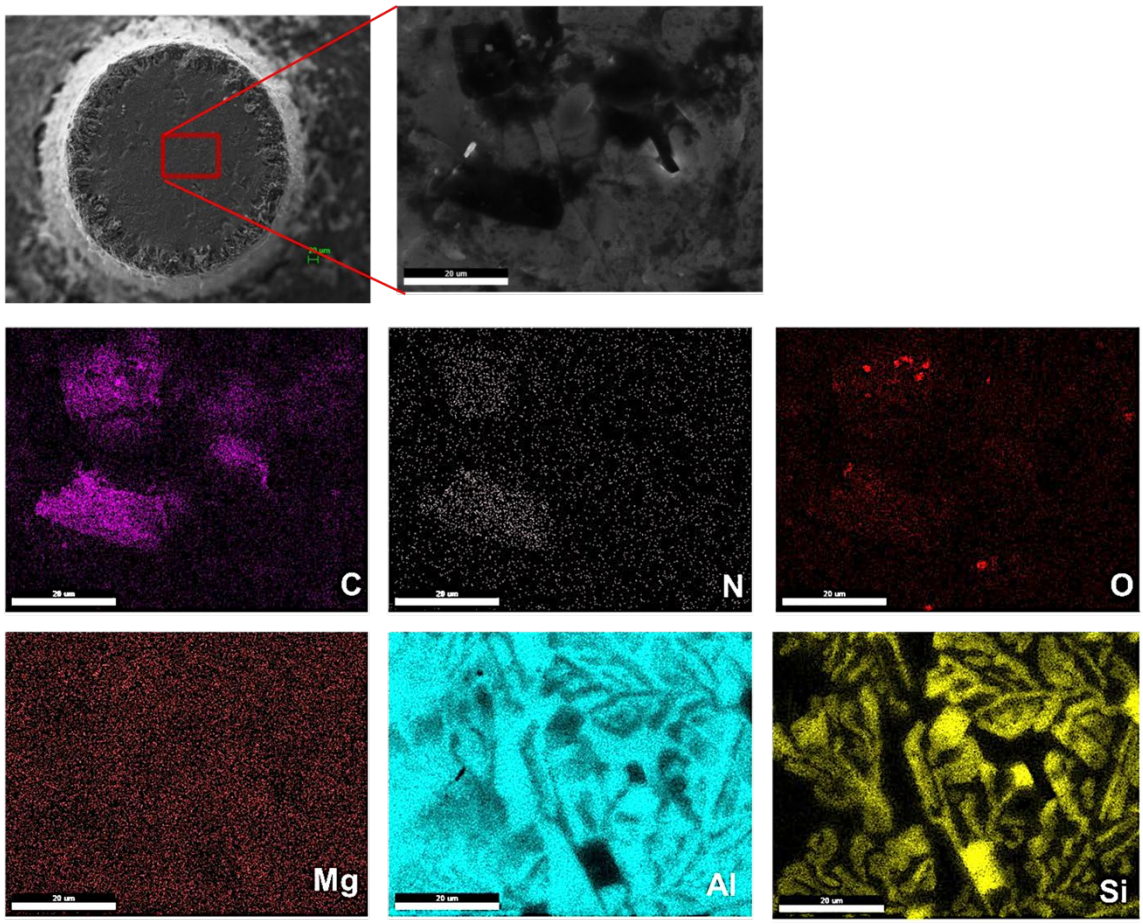

Figure 72. EDS Analysis of Melted and Re-Solidified Al-4008 Filler Material Within the Nozzle

The concentrated areas of carbon, oxygen, and nitrogen within the melted filler material inside the used nozzle are consistent with the observed impurities in samples V-A-1 and V-C-1. The graphite (carbon) nozzle, which is known to erode under the high temperature of the molten AL-4008, is mixed with the liquid metal prior to disposition. Meaning, the addition of carbon occurred during the manufacturing process while the filler material was liquified in the nozzle, then embedded into the printed specimens when the contaminated droplets were extruded.

Though it is understood the nozzles can only be used for a limited time before droplet performance is compromised, further testing and examination would need to be done to determine at what point erosion of the nozzle impacts the quality of the filler

material. There is a strong correlation between the presence of these impurities and a negative impact on the material properties of the additively manufactured Al-4008 components. Samples without these carbon deposits from the nozzle met or exceeded the MIL-A-21180D Class 1 standards. Both samples which failed to meet these standards contained the carbon impurities.

Additional analysis was conducted on the sandpaper used to remove the plasma treatment from the surface of the nozzle during pre-print set up procedures. The sandpaper used was a Norton Black Ice Waterproof SiC sandpaper, 1000 grit (6.8-9 µm).

EDS analysis confirmed the presents of carbon and silicon on the abrasive surface of the paper as well as both sodium and chlorine. It is possible that some of the inclusions could have come from the sandpaper. If so, the SiC on the sandpaper, which has a very similar geometry to the impurities found within the fractured surfaces of sample V-A-1 and sample V-C-1, could explain the brittle nature in which they fractured. It would also explain the potential source of the sodium and chlorine found in sample V-C-1. Figure 73 highlights the spectrum of elements found in the sandpaper.

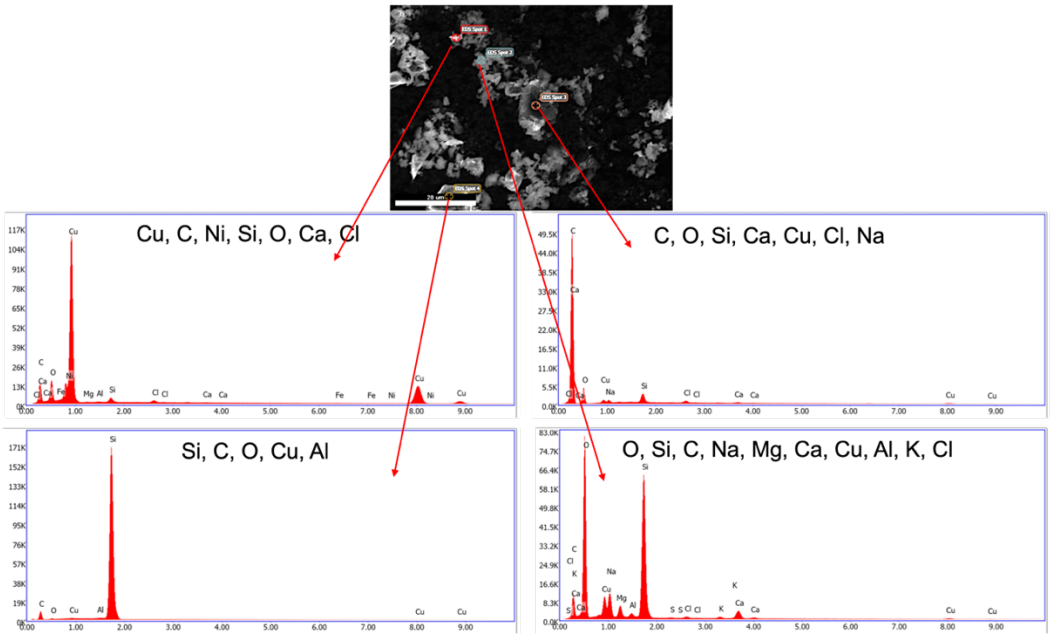

Figure 73. EDS Analysis of Sandpaper Used in Plasma Treatment of the Nozzle

V. CONCLUSION

This research focused on four primary goals. The results of each of these goals will be summarized in this section. The four objectives of this research were as follows:

- Evaluate the mechanical properties of the additively manufactured parts using Al-4008 filament and compare them to the established material property standards of MIL-A-21180D: Military Specification for Aluminum Alloy Castings, High Strength of comparable A356 Cast Aluminum.
- Understand the impact of post-process heat treatment on the additively manufactured components material properties.
- Understand the impact of build direction (horizontal and vertical) on the additively manufactured components material properties.
- Identify causes of premature failure and propose process changes, configuration changes, and methods to improve print quality and decrease material defects that could lead to premature failure.

A. EVALUATION OF MECHANICAL PROPERTIES COMPARED TO A356

The as-printed samples additively manufactured by liquid metal printing that were not heat treated had expected mechanical properties present in the as-cast A356.0 metal. Ultimate tensile strength, yield strength, elongation percentage and microhardness were all comparable to as-cast A356.0. After the T6 heat treatment all the horizontal (XY-print direction) samples met the MIL-A-21180D Class 3 requirements for ultimate tensile strength, while 83.3% of the vertical (Z-print direction) met the Class 1 requirements. All horizontal and vertical samples met the Class 1 requirements for yield strength. All horizontal samples met the Class 3 requirements for elongation percentage and 66.6% of the vertical samples met the Class 1 requirement.

B. IMPACT OF POST PROCESS HEAT TREATMENT

LMP samples that underwent a T6 heat treatment had an increase of 65.47% (Type-I) and 61.43% (Type-IV) in ultimate tensile strength. Additionally, there was a 2x (Type-I) and 3x (Type-IV) increase in yield strength. T6 heat treated specimens also had a reduction in percent elongation, as expected, from 26.8% to 22.2% (Type I) and 22.6% to 16.2% (Type IV).

Sand blasted samples showed improvement in the Al-4008 samples' UTS and YS as well but was much less than the improvements shown in the T6 heat treated samples. There was a 1.2% increase in UTS when the surfaces were sand blasted to remove surface roughness. Sand blasted samples had an 9.7% and 9.3% improvement YS for the Type-I and Type-IV respectively. Sand blasted samples also showed an average elongation percentage decrease from 26.8% to 25.3% for the large (Type-I) specimens and a decrease from 22.6% to 19.8% for the small (Type-IV) specimens.

The T6 Heat treating of the Al-4008 specimens resulted in much higher mechanical properties that would be sought after to replace high strength A356 components. Without heat treatment, the mechanical properties are reduced and do not favor the mechanical properties of A356-T6 in accordance with MIL-A-21180D. Sand blasting, however, did improve the mechanical properties due to the removal of surface defects. For components in which a T6 heat treatment isn't possible, sand blasting the surface could help to improve the mechanical properties of the as-printed component.

In addition to the Ultimate Tensile Strength, Yield Strength, and Elongation Percentage impacts, the T6 heat treatment greatly increased the liquid metal printed Al-4008 microhardness from an average of 54.24 HV to an average of 99.9 HV. Furthermore, the relative density was determined to be 99.80%, similar to that produced by SLM [40].

C. PRINT ORIENTATION EFFECTS ON MECHANICAL PROPERTIES

LMP samples printed in the horizontal direction had a 13.38% higher ultimate tensile strength and 4.88% higher yield strength than the samples printed in the vertical direction. This was found to be consistent regardless of heat treatment or not. The increase in strength in the horizontal print direction is due to the interlayer bonds within each layer.

The vertical prints rely on the bonding between different layers when in axial tension. These bonds are much weaker that the interlayer bonds of each droplet within the same layer. The presence of voids, cracks, and lack of fusion can also exacerbate the interlayer adhesion. Furthermore, the presence of these defects is concentrated along a single plane (along the vertical axis). The average UTS for all horizontal samples was 318.5 MPa (4.22 STD), while the vertical sample average UTS was 280.9 MPa (16.05 STD).

D. CAUSES OF PRE-MATURE FAILURE IN TESTING SAMPLES

There were two samples which failed to meet the MIL-A-21180D: Military Specification for Aluminum Alloy Castings, High Strength Class 1 standards for ultimate tensile strength as well as elongation percentage; sample V-A-1 and sample V-C-1. Both samples were analyzed to determine cause of failure. In both cases, foreign debris, specifically carbon deposits, were found embedded in the fractured layer's surface.

Upon investigation, it was determined the likely source of the carbon was from the graphite (carbon) nozzle and/or the sandpaper used in the plasma treatment process. The same carbon particles were observed in a used nozzle with solidified molten Al-4008. The high temperature of the molten Al-4008 erodes the nozzle during extrusion of the metal droplets. These carbon particles are mixed into the molten Al-4008 and extruded into the component being printed. This phenomenon has been referred to as 'sputtering', a jetting issue observed irregularly during printing [35]. Evidence of the carbon was found in the molten Al-4008 prior to extrusion.

The concentration of these particles within a single sample and not affecting the other samples machined from the same blocks suggests that this is an irregular occurrence, although critical to mechanical strength.

E. FUTURE WORK

Currently only the Al-4008 filler metal is used as a filament in the manufacturing process. Expanding the envelope of filler materials to other aluminum alloys would provide a more robust material selection options and more possibilities for additive manufacturing application. A similar approach as used in this research to determine the material properties

and applicable usages would help provide industries with the needed information to supplement traditionally manufactured parts with additively manufactured parts.

Another focus could be to study the lifespan of the graphite nozzle in terms of print duration, and/or investigate other materials than can be used as the nozzle to improve print quality and reduce or eliminate the erosion-based carbon impurities that are introduced to the filler metal inside the nozzle. This could also help to increase print volume within the same print bed dimensions.

DOD has expressed interest in the possibility to include additively manufacturing practices into repair and initial usage components [41]. Using these machines in a real-world environment such as onboard ships/submarines and in the forward deployed stations throughout the world would provide the most logical and realistic printing results. If the primary usage of the machines will be in initial production of a product, then a manufacturing building would provide the most logical installation location. However, if it is desired to be used to improve self-sufficiency and provide and optional manufacturing method for repair parts, then the machines would likely be installed and used in a more robust environment. Whether that be the in desert in a Conex box with hot, sandy, and arid environmental conditions, or onboard an aircraft carrier operating in humid, sea-salt dense environment, testing of the capabilities of these machines in their end usage locations would be beneficial.

Expanding on installation conditions, adding a machine and testing the print qualities onboard a ship which doesn't remain level would be beneficial. The dynamic motion of the ship could provide a challenge to the printer functionality due to the metal droplet extrusion method. The molten droplets are extruded downward as directed from the g-code. If there is a list on a ship, or the rocking motion of the ship would alter the angle of droplet extrusion, which could affect droplet precision. Exploring stabilization methods, weather a gyroscopic base or other products to combat the motion of the ship could help to provide a consistent print quality that would be expected on a level, land-based machine.

As this research was integrated as part of the Beta Testing of the ElemX^{TM} Liquid Metal Printer, the printing and testing process was recurring throughout the study. As

Xerox® received feedback, hardware and software updates were completed in an effort to improve print quality and material properties. The results represented in Chapter III for the as-printed tensile specimens were conducted in the earlier phases of this Beta Testing and prior to the completion of all software updates and hardware modifications. It would be beneficial to repeat these tests and analysis on as-printed tensile specimens, since at that point only printed blocks were analyzed, to compare the mechanical properties that can be expected of components in their as-printed additively manufactured Al-4008 parts.

THIS PAGE INTENTIONALLY LEFT BLANK

LIST OF REFERENCES

[1] M. Herrmann, "Additive Manufacturing Critical to DOD's Future," 11 January 2022. [Online]. Available: https://rooseveltdc.com/2022/01/11/additive-manufacturing-critical-to-dods-future/. [Accessed 2022 April 20].

[2] (ODASD(SE)), Office of the Deputy Assistant Secretary of Defense for Systems Engineering, "Department of Defense additive manufacturing stragety," January 2021. [Online]. Available: https://www.cto.mil/wp-content/uploads/2021/01/dod-additive-manufacturing-strategy.pdf.

[3] Deputy Assistant Secretary of the Navy Research, Development, Test and Evaluation (DASN RDT&E), "Department of the Navy(DON) Additive Manufacturing (AM) Implementation Plan V2.0 (2017)," 04 May 2017. [Online]. Available: https://apps.dtic.mil/sti/pdfs/AD1041527.pdf. [Accessed 25 March 2021].

[4] Z. Chen, C. Han, M. Gao, S. Y. Kandukuri and K. Zhou, "A review on qualification and certification for metal additive manufacturing," *Virtual and Physical Prototyping,* vol. 17, no. 2, pp. 382–405, 2022.

[5] N. Babich, "Everything You Need to Know About Beta Testing," Adobe, 11 October 2019. [Online]. Available: https://xd.adobe.com/ideas/process/user-testing/everything-you-need-to-know-about-beta-testing/. [Accessed 2021 April 13].

[6] Xerox, "Xerox-Additive Manufacturing-Insights," Xerox, 2021. [Online]. Available: https://www.xerox.com/en-us/innovation/insights/additive-manufacturing-3d-printing. [Accessed 3 August 2021].

[7] A. Elliot, "Advancing Liquid Metal Jet Printing," Oak Ridge National Laboratory, U.S. Department of Energy, Oak Ridge, 2019.

[8] Xerox Corporation, "Xerox ElemX 3D Printer Operator Manual," 2021.

[9] Weldtool Technologies Inc, "Aluminum A356-AMS 4181-Welding Wire," 2017. [Online]. Available: https://www.weldtool.com/products/aerospace-welding-materials/ams-grade-aluminum-welding-wire-rods/ams-4181-aluminum-a356-welding-wire-7-0si-0-38mg-0-10ti/. [Accessed 03 March 2021].

[10] "Al-4008 (A356) Data Sheet," United States Welding Corporation, [Online]. Available: https://www.usweldingcorp.net/TDS/tds4181.pdf. [Accessed 1 April 2021].

[11] Total Materia, "AlMgSi Alloys," Total Materia, October 2014. [Online]. Available: https://www.totalmateria.com/page.aspx?ID=CheckArticle&site=ktn&NM=348. [Accessed 18 May 2021].

[12] S. Farooqi, "One Drop at a Time: Xerox 3D Prints with Liquid Metal," engineering.com, 11 February 2021. [Online]. Available: https://www.engineering.com/story/one-drop-at-a-time-xerox-3d-prints-with-liquid-metal. [Accessed 6 June 2021].

[13] B. Gerdes, "Analysis of the metallic structure of microspheres produced by printing of aluminum alloys from the liquid melt," *Materials Research Express,* vol. 6, 2019.

[14] V. Sukhotskiy, P. Vishnoi, I. H. Karampelas, S. Vader, Z. Vader and E. P. Furlani, "Magnetohydrodynamic Drop-on-Demand Liquid Metal Additive Manufacturing: System Overview and Modelling," *Proceedings of the %th International Conference of Fluid Flow, Heat and Mass Transfer,* no. 155, pp. 1–6, 2018.

[15] T. Y. Ansell, "Current Status of Liquid Metal Printing," *Manufacturing and Materials Processing,* vol. 5, no. 31, 2021.

[16] "Standard Practice for Heat Treatment of Aluminum-Alloy Casting from All Processes," *ASTM B917/B917M,* 2020.

[17] Milwaukee Precision Casting Inc, "A356 Aluminum Casting & Treatments," [Online]. Available: https://www.milwaukeeprec.com/a356.html. [Accessed 14 10 2021].

[18] P. D. Bates and T. Robertson, "Safety Considerations for Additive Manufacturing and 3-D Printing," Underwriter Labratories, 4 February 2020. [Online]. Available: https://www.ul.com/news/safety-considerations-additive-manufacturing-and-3-d-printing. [Accessed 3 January 2022].

[19] "Standard Test Method for Tension Testing of Metallic Materials," *ASTM Standard E8/E8M,* 2021.

[20] D. Barba, C. Alabort, Y. T. Tang, M. J. Viscasillas, R. C. Reed and E. Alabort, "On the size and orientation effect in additive manufactured Ti-6Al-4V," *Materials & Design,* vol. 186, no. 108235, 2020.

[21] W. C. Smith and R. W. Dean, “Structural characteristics of fused deposition modeling polycarbonate material,” *Polymer Testing,* vol. 32, no. 8, pp. 1306–1312, 2013.

[22] A. Fabrizi, S. Capuzzi, A. De Mori and G. Timelli, “Effect of T6 Heat Treatment on the Microstructure and Hardness of Secondary AlSi9Cu3(fe) Alloy Produced by Semi-Solid SEED Process,” *Metals,* vol. 8, no. 750, pp. 1–18, 2018.

[23] L&L Special Furnance Co, Inc., “Aluminum Heat Treatment: Precipitation Hardening,” L&L Special Furnance Co, Inc., 23 July 2020. [Online]. Available: https://llfurnace.com/blog/aluminum-heat-treatment-precipitation-hardening/. [Accessed 14 05 2022].

[24] P. P. Seth, O. Parkash and D. Kumar, “Structure and mechanical behavior of in situ developed Mg2Si phase in magnesium and aluminum alloys-a review,” *Royal Society of Chemistry,* vol. 10, pp. 37327-37345, 2020.

[25] E. H. Dix and F. Keller, “Keller’s reagent,” *Mining and Metallurgy,* vol. 9, no. 327, 1929.

[26] Make It From, “A356.0-F Cast Aluminum,” Make It From, 5 May 2020. [Online]. Available: https://www.makeitfrom.com/material-properties/A356.0-F-Cast-Aluminum. [Accessed 11 November 2021].

[27] “Military Specification Aluminum-Alloy Castings, High Strength,” *MIL-A-21180D,* 1984.

[28] V. Sukhotshiy, I. H. Karampelas, G. Garg, A. Verma, M. Tong, S. Vader, Z. Vader and E. P. Furlani, “Liquid Metal 3D Printing,” Flow-3D, [Online]. Available: https://www.flow3d.com/liquid-metal-3d-printing/. [Accessed 27 February 2022].

[29] N. Ishak, M. S. Salleh, S. H. Yahaya, E. Mohamad and M. A. Sulaiman, “The Effect of Equal Channel Angular Pressing (ECAP) on the Microstructure and Hardness of A356 Aluminum Alloy,” *Journal of Advanced Manufacuring Technology,* vol. 11, no. 2, pp. 47–58, 2017.

[30] M. Meda, V. Sukhotskiy and D. Cormier, “Pinhole Formation in Printed Electron Traces Fabricated via Molten Metal Droplet Jetting,” *Electronics,* vol. 10, no. 1568, 2021.

[31] G. Ran, “Metallographic characterization of porosity in a cast aluminum alloy A356-T6,” *Materials Science Forum,* Vols. 546–549, p. 989, 2007.

[32] Hadleigh Casting, “A356.0 Aluminum Casting Alloy,” Hadleigh Castings, [Online]. Available: https://ahead4-hadleigh-castings.s3.eu-west-2.amazonaws.com/content/9be6417437c62c701d950454bd4d7756.pdf. [Accessed 14 Oct 2021].

[33] B. Yang, H. Song, S. Wang, S. Chen and S. Zhang, “Tension-compression mechanical behavior and corresponding microstructure evolution of cast A356-T6 aluminum alloy,” *Materials Science & Engineering A,* vol. 821, 2021.

[34] T. Kimura and T. Nakamoto, “Microstrustures and mechanical properties of A356 (AlSi7Mg0.3) aluminum alloy fabricated by selective laser melting,” *Materials & Design,* vol. 89, pp. 1294–1301, 2016.

[35] M. Moschel, *Scientist II / Metallurgist,* Cary,NC: Xerox Corporation, 2022.

[36] P. Mikolajczak, “Microstructural Evolution in AlMgSi Alloys during Solidification under Electromagnetic Stirring,” *Metals,* vol. 7, no. 89, 2017.

[37] C. Fletcher, “Metallography Guide for Xerox 4008 Aluminum Wire,” Xerox, 2021.

[38] F. Alghamdi and M. Haghshenas, “Microstructural and small-scale characterization of additive manufactured AlSi10Mg alloy,” *SN Applied Science,* vol. 10, no. 1007, 2019.

[39] B. D. Cullity and S. R. Stock, Elements of X-Ray Diffraction, 3rd ed., Harlow, Essex, United Kingdom: Pearson Education Limited, 2014.

[40] Inside Metal Addive Manufacturing, “Mechanical Properties of as-built A356 aluminum alloy processedby Selective Laser Melting,” Inside Metal Addive Manufacturing, 11 January 2015. [Online]. Available: https://www.insidemetaladditivemanufacturing.com/blog/-mechanical-properties-of-as-built-a356-aluminium-alloy-processed-by-selective-laser-melting. [Accessed 19 November 2021].

[41] C. E. Scheck, J. N. Wolk, W. E. Fraizier, B. T. Mahoney, B. T. Morris, R. Kestler and A. Bagchi, “Naval Additive Manufacturing: Improving Rapid Response to the Warfighter,” *Naval Engineers Journal,* Vols. 128–1, pp. 71–75, 2016.

INITIAL DISTRIBUTION LIST

1. Defense Technical Information Center
   Ft. Belvoir, Virginia

2. Dudley Knox Library
   Naval Postgraduate School
   Monterey, California